Characterization and evaluation of amphipathic, cationic peptides for small interfering RNA delivery

by

Baoling Chen

A thesis
presented to the University of Waterloo
in fulfillment of the
thesis requirement for the degree of
Doctor of Philosophy
in
Chemical Engineering

Waterloo, Ontario, Canada, 2015

AUTHOR'S DECLARATION

This thesis consists of material all of which I authored or co-authored: see Statement of Contributions included in the thesis. This is a true copy of the thesis, including any required final revisions, as accepted by my examiners.

I understand that my thesis may be made electronically available to the public.

STATEMENT OF CONTRIBUTIONS

Chapter 3 of this thesis is adapted from a manuscript "B. Chen, K. Yoo, W. Xu, R. Pan, X. Han, X. Ouyang, X. Qiu, P. Chen, A Histidine-containing, Amphipathic, Amino Acid Pairing Peptide mediated siRNA Delivery *In Vitro*".

Chapter 4 of this thesis is adapted from a paper "B. Chen, W. Xu, R. Pan, P. Chen. Design and Characterization of A New Peptide Vector for Short Interfering RNA Delivery. Journal of Nanobiotechnology, 2015, accepted."

Chapter 5 of this thesis is adapted from a manuscript "B. Chen, Y. Wu, W. Xu, Y. Yuan, P. Chen. GL1 Peptide mediated siRNA Delivery in Multicellular Tumor Spheroids and Therapeutic Effects *In Vivo*."

Chapter 6 of this thesis is adapted from a paper "B. Chen, R. Pan, D. Askhatova, P. Chen. Effective Small Interfering RNA Delivery *In Vitro* via A New Stearylated Cationic Peptide. International Journal of Nanomedicine, 2015, 10:1-12."

Abstract

RNA interference (RNAi) is a highly efficient and specific posttranscriptional gene silencing process, which can be triggered by small interfering RNA. The efficiency and specificity of this process makes siRNA a powerful tool for gene therapy. However, the use of siRNA is hampered by its rapid degradation and poor cellular uptake. A variety of carriers for example, virus, lipid, polymer, peptides, and nanoparticles, have been developed to protect siRNA and maximize its therapeutic effects. Among these carriers, peptides have emerged as a promising candidate due to their intrinsically rapid and highly efficient internalization and their typically low toxicity.

The amphipathic, cationic peptide C6 (sequence: Ac-RLLRLLLRLWRRLLRLLR-NH2) was previously designed and studied in our group. C6 achieved significant siRNA cellular uptake but induced low gene silencing, possibly due to siRNA entrapment in endosomes. In order to enhance endosomal release of siRNA, two strategies were incorporated to design a new peptide: (1) adding more pore-formation moieties, such as tryptophan; (2) including pH-sensitive moieties, such as histidine. The resulting peptide C6M3 (sequence: Ac-RL**WH**LL**W**RLWRRL**H**RLLR-NH_2) incorporated three tryptophan residues and two histidine residues that could induce the so called "proton sponge effect". Similar to C6, C6M3 could encapsulate all the free siRNA (siRNA: 5 μM) at minimal molar ratio 10/1. Moreover, C6M3 alone adopted a defined structure-α-helical secondary structure that could enhance peptide-cell membrane interaction, while C6 could not form a secondary structure. C6M3-siRNA complexes displayed a particle diameter of 80-100 nm, which was smaller than that of C6-siRNA complexes. Compared to C6 (K_a: $9.23x10^6$ M^{-1}), C6M3 had stronger binding affinity with siRNA (K_a: $8.59x10^8$ M^{-1}) in water at room temperature, which was confirmed by isothermal titration calorimetry (ITC). Moreover, in CHO-K1 monolayer cell culture, the GAPDH gene silencing efficiency induced by C6M3-siRNA complexes was significant (68% ±2). Effective in vivo RNAi was achieved in a human non-small lung tumor xenograft model through intratumoral injection of the C6M3-Bcl-2 siRNA complexes

(molar ratio: 60/1). This treatment induced a marked tumor suppression, with an inhibition rate of 55%±3, through suppression of antiapoptotic Bcl-2 protein in mice.

CADY (sequence: Ac-GLWRALWRLLRSLWRLLWRA-cysteamide), a reported amphipathic peptide, has been shown to deliver nucleic acids, peptides, and proteins into various cells. The high potency of this peptide is strongly related to its tryptophan rich property, helical conformation, and amphipathic character. The segment GLWRA seems to play a role in the potency of CADY. This information, associated with the sequence of C6M3, and also alanine amino acid being reported to facilitate helical conformation, led to the design of GL family peptides. After pre-screening for transfection activity, a promising candidate GL1 was identified and selected for further evaluation. Compared to C6M3, GL1 (sequence: Ac-**GLWRA**WLWKAFLASNWRRLLRLLR-NH_2) included a higher amount of tryptophan (4 vs. 3) to enhance peptide-membrane interaction, and three alanine (A) amino acids to contribute to helical conformation. GL1 could encapsulate all the siRNA (siRNA: 5 μM) at minimal molar ratio 15/1, displaying a spherical shape with a particle diameter of 80-100 nm. GL1 adopted α-helical secondary structure in water and exhibited strong binding affinity with siRNA (K_a: $4.47x10^8$ M^{-1}) confirmed by circular dichroism (CD) spectroscopy and ITC respectively. In monolayer culture of CHO-K1 cells, GL1 could deliver siRNA to 95% of the cells even at molar ratio 20/1 (siRNA: 50 nM), while C6M3 required a higher molar ratio (40/1) to achieve the same result. This difference may be due to the higher amount of tryptophan and the GLWRAW segment in the GL1 sequence. Interestingly, GL1 induced a lower GAPDH gene silencing efficiency (49% ±2) than C6M3, possibly because of lack of efficient endosomal release of siRNA. Both GL1 and C6M3 achieved minimal cytotoxicity (<10% ±2) with siRNA concentration of 50 nM. As monolayer cell culture lacks the 3D features of an in vivo model, multicellular tumor spheroids (MCTS), an intermediate model between traditional monolayer cell culture and in vivo model, are developed. CHO-K1 MCTS were established utilizing a hanging drop method and used for investigating the efficacy of GL1-siRNA complexes. This approach induced markedly suppression of GAPDH gene expression (50%±2) with minimal cytotoxicity (<5%±2). Following procedures of in vivo studies mentioned above, GL1-Bcl-2 siRNA complexes (molar ratio:

60/1) caused a tumor inhibition rate of 54%±4 through downregulation of antiapoptotic Bcl-2 protein, which was similar to that of C6M3-Bcl-2 siRNA complexes.

Recently, stearylation has proven to be successful in increasing the transfection efficiency of cell penetrating peptides (CPPs) for DNA delivery or that of polyethyleneimine (PEI) for siRNA delivery. A stearyl moiety is believed to play an essential role in enhancing compaction of DNA, cellular uptake, and endosomal escape. Therefore, a new design strategy incorporating stearic acid conjugation in peptide sequence was applied. STR-HK (sequence: C_{18}–HHHPKPKRKV-NH_2) consisted of a stearyl moiety enhancing peptide-siRNA/cell membrane interaction, three histidine inducing "proton sponge effect", a cytoplasm localization sequence (PKPKRKV) contributing to cytoplasma localization of the complexes, and the cationic amino acids (K & R) facilitating the peptide-siRNA binding through electrostatic interaction. STR-HK required minimal molar ratio 15/1 to fully encapsulate siRNA (siRNA: 5 μM) and the complexes displayed a spherical shape with a size distribution of 80-140 nm in diameter. Note that STR-HK adopted ß sheet secondary structure in water and exhibited strong binding affinity with siRNA (K_a: $3.73x10^5$ M^{-1}) confirmed by CD and ITC respectively. Interestingly, at molar ratio 20/1 (siRNA: 50 nM), STR-HK could deliver siRNA to ~20% of the CHO-K1 cells, which was significantly lower than that of C6M3 and GL1. Increasing the molar ratio to 40/1, STR-HK achieved similar cellular uptake as C6M3. The possible reason was that a high amount of stearyl moieties could enhance cellular uptake. In monolayer culture of CHO-K1 cells, STR-HK achieved higher GAPDH gene silencing efficiency (75%±2) than C6M3 and GL1 with minimal cytotoxicity (<10%±2). Following similar procedures of in vivo treatment mentioned above, STR-HK-Bcl-2 siRNA complexes (molar ratio: 60/1) resulted in a tumor inhibition rate of 63%±3 via downregulation of Bcl-2 protein in mice. This tumor inhibition rate was higher than that of C6M3/GL1-Bcl-2siRNA complexes.

This thesis focuses on characterization and evaluation of the three newly designed peptides as potential siRNA delivery systems. These three peptides were designed according to the following strategies: (1) modification of the amphipathic, cationic peptide C6 with tryptophan and histidine in the sequence; (2) adoption of parts of peptides CADY and C6M3

along with addition of an amphipilic segment; (3) conjugation of a stearyl moiety to peptide sequence. Among the three peptides, C6M3 could encapsulate all the free siRNA (siRNA at 5 μM) with the lowest molar ratio (10/1) and exhibited the strongest binding affinity with siRNA (K_a: $8.59x10^8$ M^{-1}). The three peptides adopted secondary structures: C6M3 and GL1 adopted helical structure and STR-HK adopted ß sheet structure. The peptide-siRNA complexes all assumed a spherical shape and induced minimal cytotoxicity in CHO-K1 cells (<10%±3). To achieve optimum gene silencing efficiency, the peptide/siRNA molar ratio needed to be optimized. STR-HK-siRNA complexes at molar ratio 60/1 achieved the highest GAPDH gene silencing efficiency (75%±2) in monolayer culture of CHO-K1 cells. In the human non-small cell lung tumor xenograft model, the STR-HK-siRNA complexes induced the highest tumor inhibition rate (63%±3). These data indicated the advantage of the peptide STR-HK. However, the potency of these three peptides could be further evaluated in other cell lines and in vivo models through systemic administration of the peptide-siRNA complexes.

Acknowledgements

In the best four years of my life, I have met many wonderful people and received tremendous help from them. Now it is the best timing for me to express my sincere thanks to all of them.

Firstly, I would like to thank Dr. Pu Chen, who offered me the opportunity to do my PhD study in the University of Waterloo. His frankness and encouragement has motivated me to enhance my communication skills through professional training and participating different associations on campus. His patience and guidance has helped me make a big progress in scientific writing proven through patents and research publications. His scientific vision and valuable advisory has assisted me in leveraging my research during my PhD study. As a supervisor, besides research, Dr. Chen strongly supported me to explore other professional skills for my future career, such as teaching. Fortunately, I have received the certificate in University Teaching. In a word, without him, I would not accomplish so much in the past few years.

Secondly, I would like to thank my committee members, Dr. Michael C. Tam, Dr. Frank Gu, Dr. Juewen Liu, and xxx for their time and valuable comments and advices on my thesis.

Thirdly, I am thankful for the following individuals contributing to the experiments, discussion, and suggestions during my PhD study. I truly acknowledge Mishi Savulescu from Biology department and Cameron Postnikoff from System Design Engieering for carrying out flow cytometry analysis experiments for me. Thanks to our collaborator Dr. Yongfang Yuan from Shanghai Jiao Tong University School of Medicine and her students, I have obtained the in vivo data.

My next acknowledgements go to our group members. Thanks to Tatiana Sheinin, who taught me how to use KDalert Kit for the peptide library screening and initiated the 3D cell culture project; Xiaoxia Han and Nita Modi for their help on western blot experiment; Wen Xu for training me cell culture, FACS, and qRT-PCR. I also want to give my special thanks to Ran Pan, Dafeng Chu, Mousa Jafari, Dr. Parisa Sadatmousavi, Mohammad Ali Shekholeslam, Yong Ding, Sheng Lu, and Dr. Denise Gosselink for their support during my

PhD program. Additionally, I received great help from the undergraduate and co-op students Kimoon Yoo, Diana Askhatova, Claudia Wang, and Xiaonan Cai in my research.

I would like to thank all my great friends in Waterloo who have supported me in every possible way. Hassan Khorami, a great partner, has always been supporting me and comforting me. Thanks to his family, I have a second home in Canada. Dihua Wu, my roommate and close friend, who always cheers me up when I am down, I will remember every second we spent together and explore more with you in the future. Parinaz Akhlaghi, my gym buddy, I really miss the time we sweat, laughed, and taught each other our mother language. It made my life more colorful and enjoyable.

Last but not least, I would like to thank my family. My four sisters and younger brother who have been taking care of my parents so that I can focus on my research. My lovely mother Ronghua Guo teaches me persistence, patience, and optimism and my dear father Qingran Chen teaches me responsibility, braveness, and tolerance. Their love and support has inspired me to do things those I once thought were impossible.

Dedication

To my dear parents Ronghua and Qingran.

Table of Contents

List of Figures

List of Tables

Nomenclature

Acronym	Full Name
RNAi	RNA interference
dsRNAs	double-stranded RNAs
mRNA	messenger RNA
siRNA	small interfering RNA
miRNA	micro RNA
RISC	RNA-induced silencing complex
UTR	untranslated region
AGO2	Argonaute-2
PEI	polyethyleneimine
PLL	poly-L-lysine
PLGA	poly-D,L-lactide-co-glycolide
AD–PEG	adamantane–PEG
AD–PEG–Tf	adamantane–PEG–transferrin
PEG	Polyethylene glycol
RBP	retinol binding protein
DPCs	Dynamic PolyConjugates
ApoB	apolipoprotein B
ppara	proliferator-activated receptor alpha
ONPs	oligonucleotide nanoparticles

CPPs	cell penetrating peptides
PNA	peptide nucleic acids
CPP	cell penetrating peptide
CME	Clathrin-mediated endocytosis
CCVs	clathrin coated vesicles
PCI	photochemical internalization
DP	dendrimer-based photosensitizer
DPc	dendrimerphthalocyanine
AMPs	amphiphilic peptides
ITC	isothermal titration calorimetry
CD	circular dicroism
SEM	scanning electron microscopy
MR	molar ratio
NT	non-treated
Lipo	Lipofectamine 2000
FACS	fluorescence activated cell sorting
DLS	dynamic light scattering
PFA	paraformaldehyde
CHO-K1	Chinese hamster ovary
FBS	fetal bovine serum

PBS	phosphate buffered saline
MCTS	multicellular tumor spheroids
EPR	enhanced permeability and retention
EthD-1	ethidium homodimer
ATCC	American Type Culture Collection
GAPDH	glyceraldehyde-3-phosphate dehydrogenase
NC	nitrocellulose
ECM	extracellular matrix
N.T.	non-treated
CCK-8	cell couting kit-8
HPLC	high performance liquid chromatography
LC-MS	liquid chromatography-mass spectrometry
PC-3	Human prostate cancer cell line
TEM	transmission electron microscopy

Chapter 1
Introduction

1.1 Overview

The term RNA interference (RNAi) was first coined after the discovery in the nematode Caenorhabditis elegans that double-stranded RNAs (dsRNAs) can trigger silencing of complementary messenger RNA (mRNA) sequences[1]. The mechanism by which RNAi inhibits the conversion of mRNA into protein is briefly reviewed here. Small interfering RNA (siRNA) and micro RNA (miRNA) are central to RNA interference. Double-stranded RNA is recognized by an RNase type III enzyme, Dicer, and cleaved into small fragments of 21- 23 nucleotides called siRNAs. Each siRNA is unwound into a sense (passenger) strand and an antisense (guide) strand with respect to the target mRNA (Figure 1.1). siRNA binds to a protein complex called RNA-induced silencing complex (RISC) and the passenger strand is degraded, while the guide strand is directed to the 3' untranslated region (UTR) of the complementary target mRNA. A cleavage enzyme within RISC (argonaute 2) degrades the target mRNA, thus preventing translation. miRNAs also exist in cells and are pre-processed by a nuclear RNase III (Drosha) before export into the cytoplasm by nuclear transport receptor complexes. Due to limited complementarily to the target mRNA, miRNAs do not lead to the cleavage of mRNA with the RISC but, instead, result in translational suppression [2].

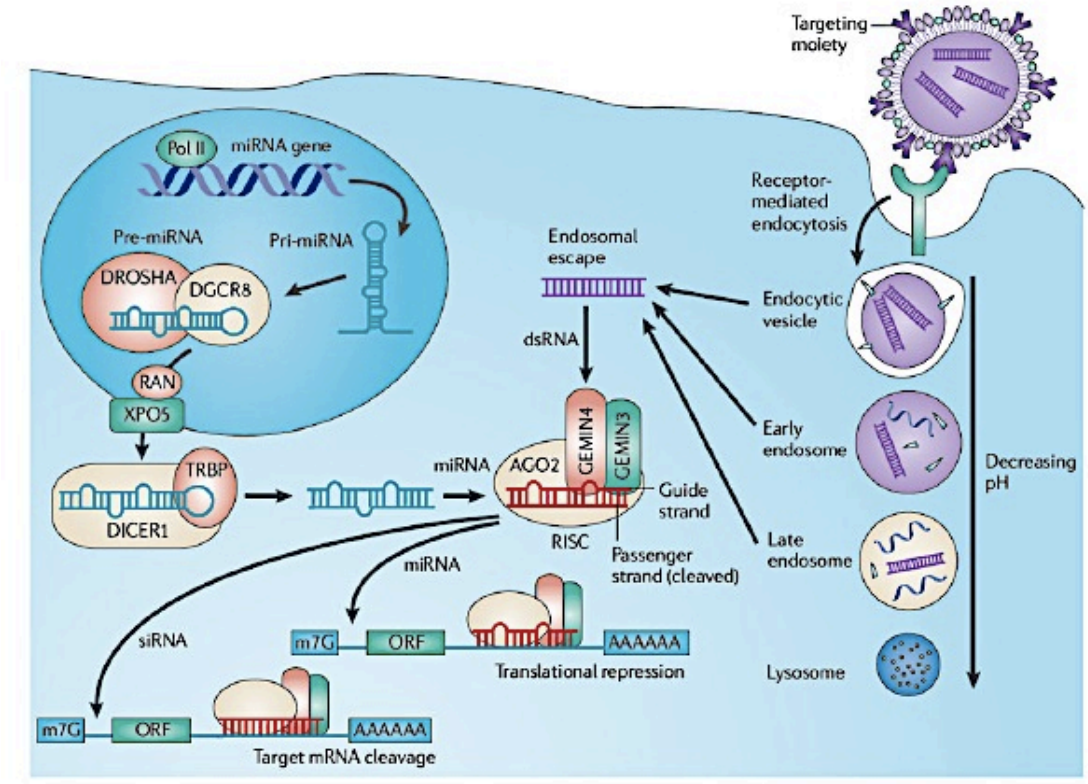

Figure 1.1. Mechanism of RNAi following intracellular dsRNA delivery. Adapted from[2]**. Reprinted with permission from Nature.**

Since the discovery of RNAi, there has been an explosion of interest in using this technology for basic and applied research and RNAi has been one of the most promising new approaches for disease therapy. The list of diseases that may be treated by RNAi is extensive, including cancers, Parkinson's disease [3], HIV infection [4], age-related macular degeneration [5], type 2 diabetes [6], obesity [7], hypercholesterolemia [8], and rheumatoid arthritis [9].

Despite this promising research, a number of problems remain in the realization of siRNA therapeutics. Although several human clinical trials are being conducted, most of these treatments are limited to local delivery of siRNAs, such as direct injection into the eye or skin. Targeting specific genes in tissues and organs is best facilitated with systemic delivery

during treatment. The main limitations in siRNA therapeutics are instability of naked siRNA under physiological conditions, rapid clearance from the blood stream, inability to cross targets cell membranes and gain access to the intracellular environment at the clinically relevant dose. These drawbacks are intrinsically related to some of the unfavorable physicochemical properties of siRNA molecules, including large molecule weight, negatively charged surface, hydrophilicity, sensitivity to nuclease degradation and short plasma half-life of less than ten minutes [10]. Thus, the development of siRNA therapeutics requires an efficient and safe delivery system.

In search for effective siRNA delivery systems, a number of materials have been attempted, including virus vectors, liposomes, lipoplexes, polymers, and peptides [11,12]. Among them, cell-penetrating peptides (CPPs) have been utilized for intracellular delivery of a variety of macromolecules, including proteins, peptide nucleic acids (PNA), and siRNAs [13].

In this research, three newly designed amphipathic, cationic peptides were characterized and their potential as a siRNA delivery system was evaluated. Biophysical, spectroscopic, thermodynamic, and microscopic techniques were used to characterize the interaction between peptide and siRNA. The uptake, gene silencing efficiency, and cytotoxicity of the designed peptides in complex with siRNA were investigated.

1.2 Research Objectives

The goal of this study was to develop an effective and safe peptide based siRNA delivery system. To achieve this goal, three newly designed peptides were investigated including their siRNA binding capacity, gene silencing efficiency, and cytotoxicity in mammalian cells and a xenograft mouse model. Compared to our group's previous work on peptide based siRNA delivery systems, this thesis presented different peptide design strategies to further enhance the peptide's delivery efficacy, developed a three dimensional (3D) culturing model, and evaluated the delivery efficacy of the peptide in this 3D model. The specific objectives of this thesis are listed as follows:

1. Screen the modified/designed amphipathic cationic peptides to evaluate their siRNA transfection efficiency and cytotoxicity.
2. Characterize the binding between peptides and siRNAs, the size, zeta potential, secondary structure, and morphology of peptide-siRNA complexes; evaluate the uptake, transfection efficiency of siRNA delivered by peptides and the cytotoxicity of peptide-siRNA complexes in traditional monolayer cell culture envrionment.
3. Establish a three dimensional cell culture model—multicellular tumor spheroids—to investigate the uptake gene silencing efficiency, and cytotoxicity of the peptide-siRNA complexes.
4. Evaluate the antitumor activity of the peptide-siRNA complexes in a mouse xenograft tumor model.

1.3 Outline of the Thesis

The thesis consists of seven chapters. The scope of each chapter is listed as follows:

Chapter 1 gives an in introduction to RNA interference process, siRNA therapeutics, gene delivery systems, and the potential of peptides as siRNA delivery systems. The research objectives and the outline of the thesis are also given.

Chapter 2 provides a review of siRNA therapeutics and current siRNA delivery systems. Uptake pathways and mechanisms of endosomal escape are also reviewd.

Chapter 3 introduces peptide C6M3, a modified version of our previously studied peptide C6. The modification strategy and physicochemical characteristics of C6M3 in complex with siRNA are discussed. The uptake, gene silencing efficiency, and cytotoxicity of the complexes are also reported.

Chapter 4 introduces peptide GL1. The design strategy and physicochemical properties of GL1 and the uptake, gene silencing efficiency, and cytotoxicity of the GL1-siRNA complexes are reported.

Chapter 5 investigates the potential of GL1 as a delivery system in multicellular tumor spheroids and the therapeutic effects of GL1-siRNA complexes in a tumor xenograft tumor model.

Chapter 6 introduces peptide STR-HK, which incorporated the conjugation of stearyl moiety in the sequence. The physicochemical properties of this peptide and the uptake, gene silencing efficiency, and cytotoxicity of the complexes are investigated.

Chapter 7 presents the original contributions of this research and recommendations for future work.

Chapter 2
Literature Review

2.1 RNA Interference

The term RNA interference (RNAi) was first coined after the discovery in the nematode Caenorhabditiselegans that double-stranded RNAs (dsRNAs) can trigger silencing of complementary messenger RNA (mRNA) sequences [1]. The mechanism by which RNAi inhibits the conversion of mRNA into protein is briefly reviewed here. Small interfering RNA (siRNA) and micro RNA (miRNA) are central to RNA interference. Double-stranded RNA is recognized by an RNase type III enzyme, Dicer, and cleaved into small fragments of 21 - 23 nucleotides called siRNAs. Each siRNA is unwound into a sense (passenger) strand and an antisense (guide) strand with respect to the target mRNA (Figure 2.1). siRNA binds to a protein complex called RNA-induced silencing complex (RISC) and the passenger strand is degraded, while the guide strand is directed to the 3' untranslated region (UTR) of the complementary target mRNA. A cleavage enzyme within RISC (argonaute 2) degrades the target mRNA, thus preventing translation. miRNAs also exist in cells and are pre-processed by a nuclear RNase III (Drosha) before export into the cytoplasm by nuclear transport receptor complexes. Due to limited complementarity to the target mRNA, miRNAs do not lead to the cleavage of mRNA with the RISC but, instead, result in translational suppression [2].

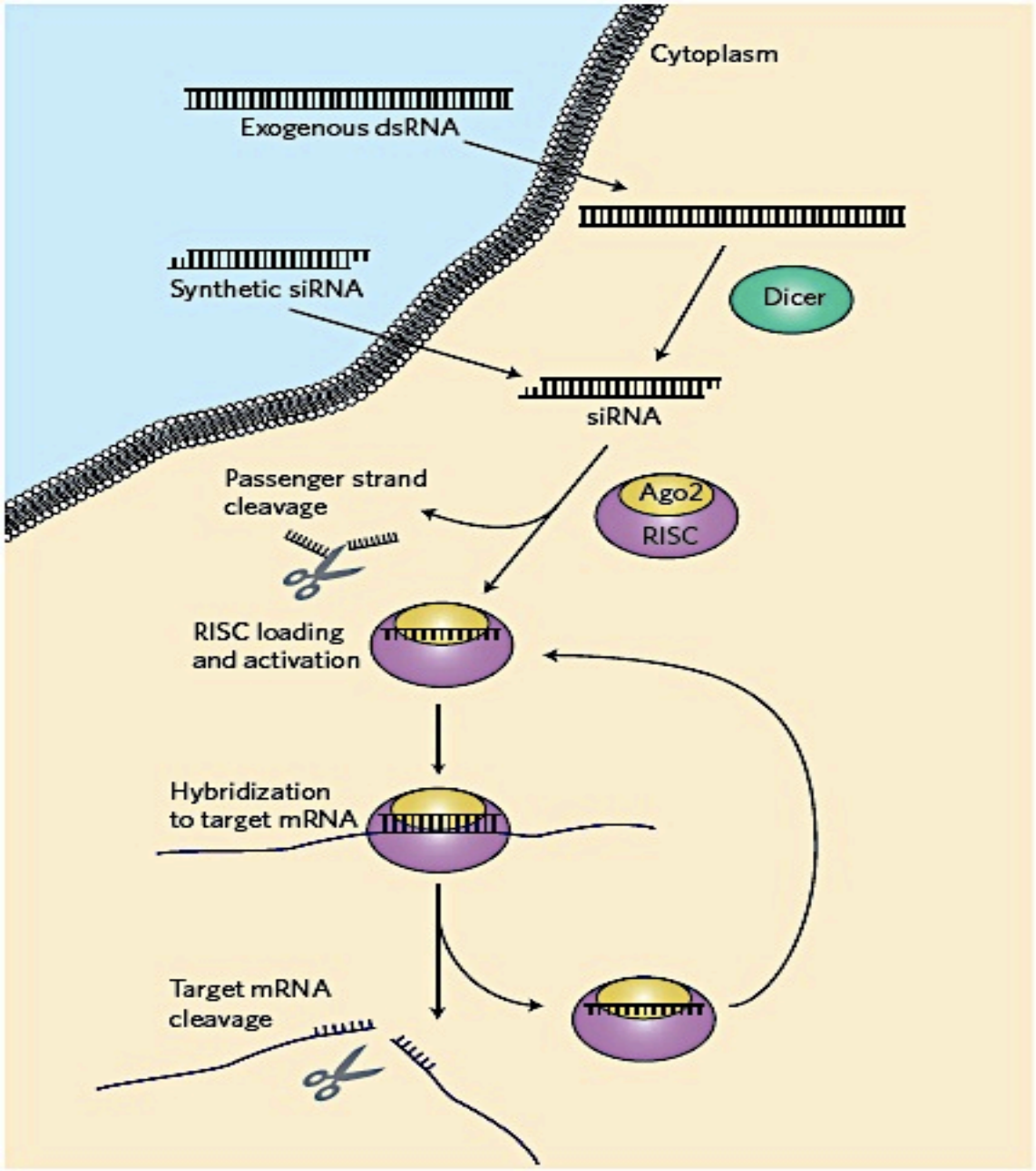

Figure 2.1. RNA interference. Long dsRNA introduced into the cytoplasm is processed by the enzyme Dicer into 22-nt pieces with 2-nt single-stranded overhangs on the 3' ends. The structure of synthetic siRNA mimics that of Dicer products. The siRNA guide strand is loaded into the RNA-induced silencing complex (RISC), and the passenger strand is cleaved by Argonaute-2 (AGO2). The activated RISC-guide-strand complex identifies and cleaves mRNA

that is complementary to the guide strand, preventing translation and thereby silencing gene expression. Adapted from reference[14]**. Reprinted with permission from Nature.**

Since the discovery of RNAi, there has been an explosion of interest in using this technology for basic and applied research and RNAi has been one of the most promising new approaches for disease therapy. The list of diseases that may be treated by RNAi is extensive, including cancers, Parkinson's disease [3], HIV infection[4], age-related macular degeneration[5], type 2 diabetes[6], obesity[7], hypercholesterolemia [8], and rheumatoid arthritis[9]. So far, more than 22 RNAi-based drugs have been tested in clinic (Table 1)[14], and many more are under exploration.

The cancer therapeutic siRNAs have been studied for silencing target molecules that are crucial for tumor-host interactions and tumor resistance to chemo- or radiotherapy and the silencing of critical cancer-associated target proteins by siRNAs has resulted in significant antiproliferative and/apoptotic effects[15]. Nevertheless, most approaches to RNAi-mediated gene silencing for cancer therapy have been tested in vitro in the laboratory and many challenges for translating siRNA therapeutics to the clinic due to delivery systems still remain.

The main limitations in siRNA therapeutics are instability of naked siRNA under physiological conditions, rapid clearance from the bloodstream, inability to cross target cell membranes and gain access to the intracellular environment at the clinically relevant dose. These drawbacks are intrinsically related to some of the unfavorable physicochemical properties of siRNA molecules, including negative charge, hydrophilicity, sensitivity to nuclease degradation and short plasma half-life of less than ten minutes[10]. Thus the development of siRNA therapeutics has focused on the design of a multifunctional delivery system that can improve siRNA stability and cancer cell specificity, involving minimal off-target and nonspecific immune stimulatory effects.

There has been a broad spectrum of nano-scale carriers, polymers, liposomes, conjugate delivery systems, cell penetrating peptides, and many others have shown unique biological

properties for siRNA delivery. Here, we review a variety of strategies for developing siRNA delivery systems for cancer therapy.

Table 2.1. RNAi-based drugs in clinical trials. Adapted from reference[14]. Reprinted with permission from Nature.

Drug	Target	Delivery system	Disease	Phase	Status	Company	ClinicalTrials.gov identifier
ALN-VSP02	KSP and VEGF	LNP	Solid tumours	I	Completed	Alnylam Pharmaceuticals	NCT01158079
siRNA-EphA2-DOPC	EphA2	LNP	Advanced cancers	I	Recruiting	MD Anderson Cancer Center	NCT01591356
Atu027	PKN3	LNP	Solid tumours	I	Completed	Silence Therapeutics	NCT00938574
TKM-080301	PLK1	LNP	Cancer	I	Recruiting	Tekmira Pharmaceutical	NCT01262235
TKM-100201	VP24, VP35, Zaire Ebola L-polymerase	LNP	Ebola-virus infection	I	Recruiting	Tekmira Pharmaceutical	NCT01518881
ALN-RSV01	RSV nucleocapsid	Naked siRNA	Respiratory syncytial virus infections	II	Completed	Alnylam Pharmaceuticals	NCT00658086
PRO-040201	ApoB	LNP	Hypercholesterolaemia	I	Terminated	Tekmira Pharmaceutical	NCT00927459
ALN-PCS02	PCSK9	LNP	Hypercholesterolaemia	I	Completed	Alnylam Pharmaceuticals	NCT01437059
ALN-TTR02	TTR	LNP	Transthyretin-mediated amyloidosis	II	Recruiting	Alnylam Pharmaceuticals	NCT01617967
CALAA-01	RRM2	Cyclodextrin NP	Solid tumours	I	Active	Calando Pharmaceuticals	NCT00689065
TD101	K6a (N171K mutation)	Naked siRNA	Pachyonychia congenita	I	Completed	Pachyonychia Congenita Project	NCT00716014
AGN211745	VEGFR1	Naked siRNA	Age-related macular degeneration, choroidal neovascularization	II	Terminated	Allergan	NCT00395057
QPI-1007	CASP2	Naked siRNA	Optic atrophy, non-arteritic anterior ischaemic optic neuropathy	I	Completed	Quark Pharmaceuticals	NCT01064505
I5NP	p53	Naked siRNA	Kidney injury, acute renal failure	I	Completed	Quark Pharmaceuticals	NCT00554359
			Delayed graft function, complications of kidney transplant	I, II	Recruiting	Quark Pharmaceuticals	NCT00802347

PF-655 (PF-04523655)	RTP801 (Proprietary target)	Naked siRNA	Choroidal neovascularization, diabetic retinopathy, diabetic macular oedema	II	Active	Quark Pharmaceuticals	NCT01445899
siG12D LODER	KRAS	LODER polymer	Pancreatic cancer	II	Recruiting	Silenseed	NCT01676259
Bevasiranib	VEGF	Naked siRNA	Diabetic macular oedema, macular degeneration	II	Completed	Opko Health	NCT00306904
SYL1001	TRPV1	Naked siRNA	Ocular pain, dry-eye syndrome	I, II	Recruiting	Sylentis	NCT01776658
SYL040012	ADRB2	Naked siRNA	Ocular hypertension, open-angle glaucoma	II	Recruiting	Sylentis	NCT01739244
CEQ508	CTNNB1	*Escherichia coli*-carrying shRNA	Familial adenomatous polyposis	I, II	Recruiting	Marina Biotech	Unknown
RXI-109	CTGF	Self-delivering RNAi compound	Cicatrix scar prevention	I	Recruiting	RXI Pharmaceuticals	NCT01780077
ALN-TTRsc	TTR	siRNA–GalNAc conjugate	Transthyretin-mediated amyloidosis	I	Recruiting	Alnylam Pharmaceuticals	NCT01814839
ARC-520	Conserved regions of HBV	DPC	HBV	I	Recruiting	Arrowhead Research	NCT01872065

DPC, dynamic polyconjugate; LNP, lipid nanoparticle; NP, nanoparticle; shRNA, short hairpin RNA.

2.2 Current siRNA Delivery Systems

2.2.1 Polymeric Carriers

Cationic polymers have been used for delivery of plasmid DNA since 1990 and, more recently, for siRNA delivery. The positively charged polymers interact with negatively charged phosphates of siRNA through electrostatic force forming the polyplexes. This process causes siRNA condensation and protects it from nuclease degradation. The ratio of the positive charges of cationic polymers to the number of phosphate groups of siRNA affects the size, surface charge, and structures of the polyplexes. Thus, optimization of the ratio, which is crucial for transfection efficiency, is required. A number of polymers, either synthetic or natural, such as branched or linear polyethyleneimine (PEI), poly-L-lysine (PLL), poly-D,L-lactide-co-glycolide(PLGA), poly(alkylcyanoacrylate), chitosan and gelatin have been studied. PLGA is the most extensively studied copolymer as a carrier for controlled release of siRNA, with lower toxicity than cationic lipids and cationic polymers. PLGA nano-capsules are used to stabilize siRNA and provide sustained release[16]. Recently, efforts have focused on modification of PLGA to get positively charged carriers to

increase cellular uptake. For instance, chitosan coated PLGA nanoparticles improved the cellular internalization of siRNA in cultured cells[17,18]. Incorporation of PEI into PLGA nanoparticles improved siRNA loading and activity. PEI-PLGA nanoparticles showed 100% siRNA loading, protected siRNA and resulted in higher gene silencing activity in cultured cells than PEI alone[18,19]. Intratumoral injection of PEI-PLGA microspheres of anti-VEGF siRNA also showed improved effect of tumor growth suppression[20].

Cyclodextrin polymer-based delivery system (Figure 2.2) was first used for plasmid DNA in 1999 and re-optimized for siRNA delivery years later[14,21–26]. Less than a decade after their introduction, cyclodextrin polymer-based nanoparticles entered clinical trials for siRNA delivery and they were the first targeting delivery systems that entered clinical trials for cancer[27]. Cyclodextrin polymers are polycationic oligomers ($n \approx 5$), which can efficiently condense the nucleic acids at nitrogen/phosphorous ratios as low as 3. End-capping of the polymer termini with imidazole functional groups can enhance endosomal escape[28], which improved the delivery efficacy of siRNA[22]. Although Cyclodextrin polymers could deliver siRNA efficiently in vitro, they still required additional formulation components such as adamantane–PEG (AD–PEG) and adamantane–PEG–transferrin (AD–PEG–Tf) for stabilization and efficacy in vivo. Adamantane, a hydrophobic molecule, can interact with the cyclic core of the cyclodextrin structure to form a stable complex. PEG shielding could decrease protein-induced aggregation in serum. However, PEGylation also decreased cellular uptake and silencing efficacy. In order to recover efficacy, the protein transferrin, which can bind to the CD71 transferrin receptor, was conjugated to the free end of AD-PEG to improve efficacy[29]. The therapeutic effects of the cyclodextrin polymer-siRNA delivery system have been proven in several animal models: a xenograft model for Ewing's sarcoma[22], targeting the oncogenic EWS–FLI1 fusion gene; a syngeneic subcutaneous mouse tumour model, targeting ribonucleotide reductase subunit 2[30]. In phase-I clinical trial of human melanoma patients, RNAi-specific gene inhibition targeting RRM2 gene was monitored by this delivery system, which showed its clinical potential. The low toxicity, facile condensation with nucleic acids, the steric stabilization through PEGylation, and the incorporation of a targeting ligand have made this delivery system promising in clinic.

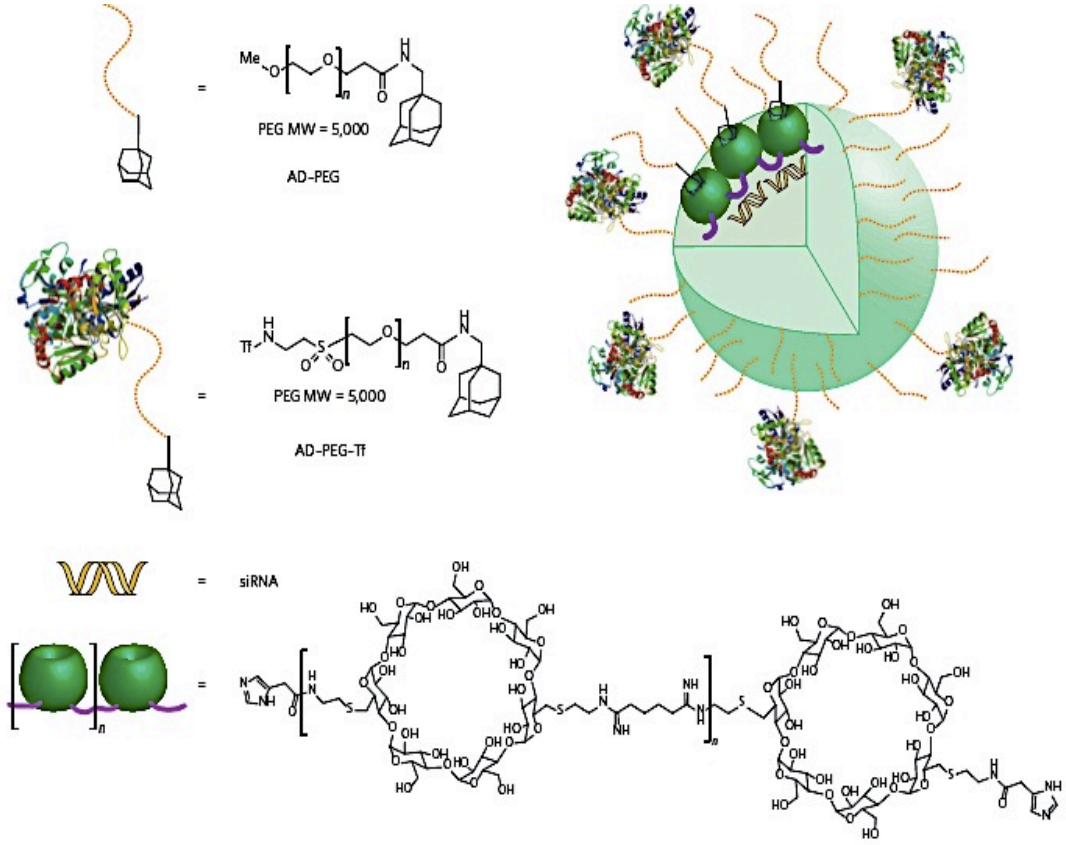

Figure 2.2. Cyclodextrin polymer nanoparticles. Composition of the cyclodextrin delivery systems developed in reference [27]**. MW: molecular weight. Adapted from reference**[14]**. Reprinted with permission from Nature.**

Dendrimers are repetitively branched molecules[31]. Dendrimers have been used as carriers of small molecule drugs and large biomolecules. Dendrimers with positively charged surface groups are used to deliver siRNA, and the precise core-shell nanostructures make it load siRNA by interior encapsulation, surface adsorption, or chemical conjugation. The biocompatibility of dendrimers depends on their structure, molecular size and surface charge[32]. Cytotoxicity and immunogenicity of dendrimers are related to their surface charge. Modifications are the main methods to improve their loading capacity and cellular uptake of siRNA.

2.2.2 Lipid-Based Carriers

Liposomes, microemulsions, solid lipid nanoparticles, and micelles are lipid-based siRNA delivery systems. Liposomes are globular vesicles, which comprise the phospholipid bilayer and an aqueous core. The amphipathic nature of liposomes allows the incorporation of both hydrophilic and hydrophobic drugs. The hydrophilic head groups of phospholipid bilayers show affinity to hydrophilic molecules, and the fatty acyl chains of the lipid bilayer tend to intercalate the hydrophobic molecules into it. Liposomes are divided into two categories: neutral liposomes and cationic liposomes. Though neutral liposomes have achieved some success in delivering siRNA both in vitro and in vivo, cationic lipids remain the crucial components of lipid-based siRNA carriers[12]. Up to now, a number of different lipid and lipid-like structures and formulation methods have been developed and several features are particularly effective for siRNA delivery systems, such as shielding lipids, cholesterol and targeting ligands.

Cationic lipids consist of three parts, a lipophilic tail group, a cationic head and a connecting linker. Lipophilic tail groups are usually made up of saturated or unsaturated alkyl chains (12-18 carbons in length) or cholesteryl groups. Cationic head groups consist of amidinium salt lipids, lipoamines, quaternary ammonium, and combinations of lipoamines and quaternary amines. Usually, esters and ethers, amides, or carbonates are used as linkers. The structure of the cationic head group, the carbon chain length of the tail group and the nature of the linker affect the transfection efficiency and the toxicity of siRNA carriers. It is known that lipids with small hydrophilic groups and bulky alkyl chains favor endosomal escape and enhance the transfection efficiency[33]. The cationic lipid condenses siRNA through electrostatic interaction and forms multilamellar structures. The ratio of lipid to siRNA can be optimized to generate a positive zeta potential for the lipoplex to help its interaction with the cell membrane and cellular internalization. A variety of cationic lipids have been investigated, and Lipofectamine 2000 is a commercialized formulation used for in vitro transfection.

Lipid-based carriers have been used to deliver siRNA successfully to target sites in the endothelium, RES organs, and solid tumors. For example, intraperitoneal injection of

cationic liposomal anti-TNF-alpha gene expression prevented the development of sepsis induced by a subsequent lipopolysaccharide injection[33]. However the toxicogenomics of cationic lipids including the initiation of immune response and changes in the expression of non-target genes limit the use of lipid in vivo.

Meanwhile, several studies have shown that ionizable lipids, whose charge depends on the pH of the surrounding environment is more efficacious[34] and less toxic than cationic lipids that have a net positive charge. Consequently, the focus of recent study is on the development of new ionizable lipids. Similarly, these lipids also include three parts: an amine head group, a linker group and hydrophobic tails (Figure 3a). In order to minimize toxicity, the pK_a of an ionizable lipid needs to be optimized as low enough to become unprotonated during circulation but high enough to be protonated in either the early or late endosome. At lipid transition temperature, lipid membranes will shift from the more stable lamellar phase to the less stable hexagonal phase (Figure 3d), which can improve the endosome escape of siRNA. The lower transition temperatures lipids have, the more readily their phases shift. Lipids with small polar head groups and large unsaturated hydrophobic tails (Figure 3b) are more likely to have low transition temperatures. The structure of a lipid's hydrophobic head and the linker of lipids also affect the in vivo efficacy, such as the lipid DLinDMA and DLin-KC2-DMA (Figure 3c)[35]. Most of the ionizable lipids are two tailed species with a single amine. However, ionizable lipids with multitails and abundant amines have also proved highly efficacious[14].

PEG (Polyethylene glycol), a common component in liposomes, can reduce particle size[36,37], prevent aggregation, increase circulation time and reduce unintended uptake by red blood cells and macrophages[36,38]. However, it also reduces cellular uptake by target cells and efficacy both in vitro and in vivo. There are two strategies to reduce these negative effects: incorporation of acid-sensitive bonds connecting PEG to the liposome86, the use of a pH-sensitive modified PEG[39].

Cholesterol is usually included in the liposomal formulations. The increase of cholesterol can lower the transition temperature of liposomal membranes that contain conical-shaped

lipids, which induced the phase change from lamellar to hexagonal. The incorporation of cholesterol has been shown to enhance the release of drugs from endosome.

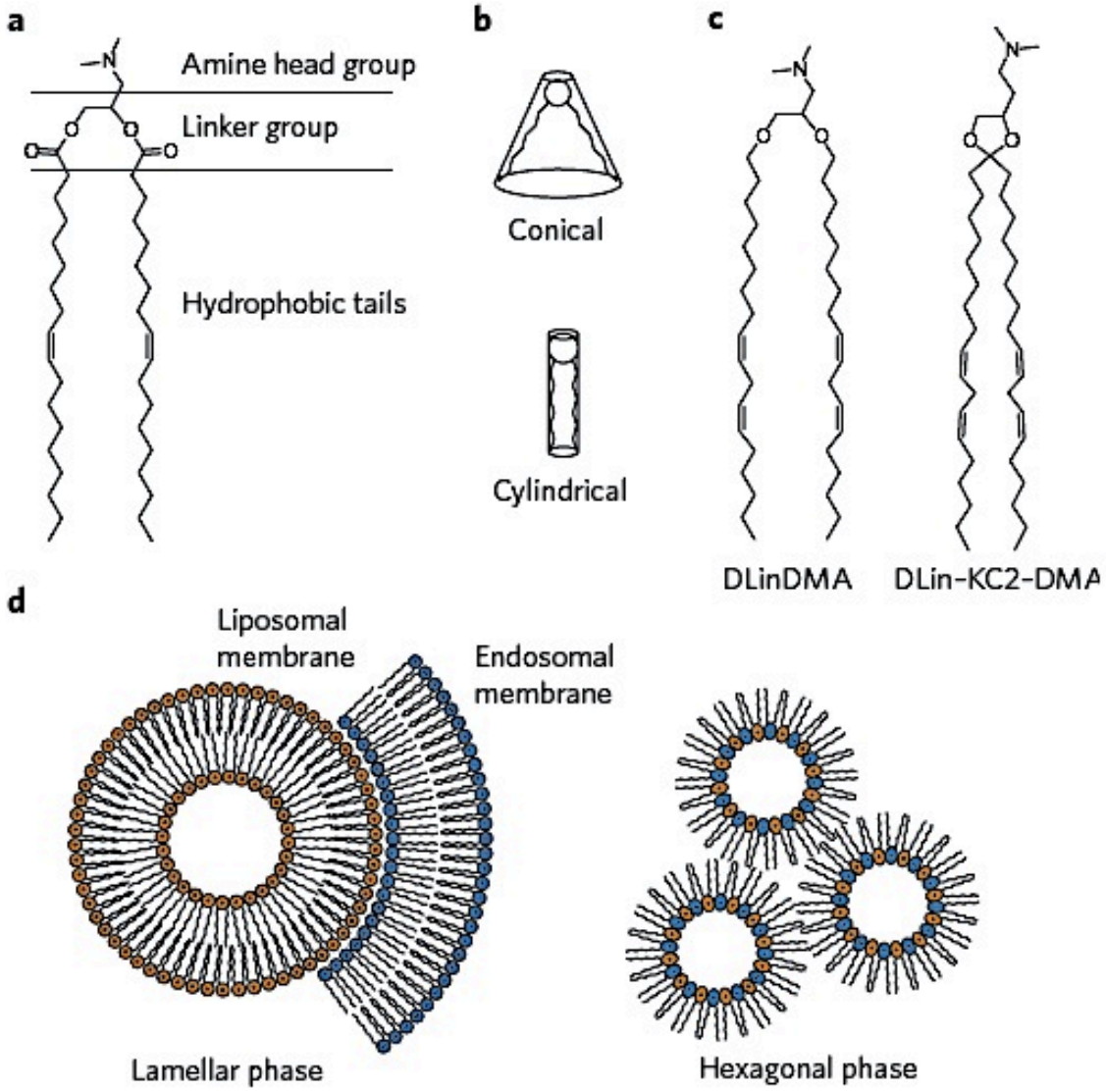

Figure 2.3. Lipid structures and shapes. (a) Ionizable lipids are composed of three sections: the amine head group, the linker group and the hydrophobic tails. (b) Lipids with a small head group and tails composed of unsaturated hydrocarbons tend to adopt a conical structure, whereas lipids with a large head group and saturated tails tend to adopt a cylindrical structure. (c) The structures of siRNA delivery lipids DLinDMA and DLin–KC2–DMA. (d) The mixing of

cationic (orange) and anionic (blue) lipids promotes the transition from the more stable lamellar phase to the less stable hexagonal phase, thus aiding fusion of the liposomal and endosomal membranes. Adapted from reference[14]**. Reprinted with permission from Nature.**

In order to improve the biodistribution of liposomes, targeting ligands are incorporated to liposomal formulation. There are two types of targeting ligands: endogenous and exogenous. Endogenous targeting ligands, often serum proteins, bind to the liposome during circulation and guide the particle to the ligand's natural cellular target. Lipoprotein ApoE and retinol binding protein (RBP) are two reported endogenous targeting ligands that have achieved success in improving the efficacy in vivo. Meanwhile, exogenous targeting ligands have also been examined, such as a small molecule GalNAc and folate. GalNAc can bind to the asialoglycoprotein receptor on the surface of the hepatocytes, which directs the target delivery to the liver[40]. Folate is usually used to target rapidly dividing cancer cells[41–43].

Although liposomes have been used for some 50 years, the number of lipids that have been used for creating them has been limited. Recently, by use of a high-throughput synthesis approach, thousands of new lipids[44–46] have been generated and screened for siRNA delivery. This enables the creation of promising liposomes that require lower amount of siRNA to achieve specific gene knockdown by three or four orders of magnitude.

2.2.3 Conjugate Delivery Systems

Conjugate delivery systems are developed by directly conjugating delivery materials to the siRNA cargo. To date, the delivery materials that have been used for conjugate delivery systems include cholesterol and other lipophilic molecules, polymers, peptides, antibodies, aptamers and small molecules. Two of the most-developed conjugate platforms are Dynamic PolyConjugates (DPCs) and GalNAc conjugates.

DPCs consist of several components: siRNA cargo, a membrane-disrupting polymer, PEG ligand and targeting ligand (Figure 2.4).[47] The DPCs system silenced apolipoprotein B (ApoB) and peroxisome proliferator-activated receptor alpha (ppara) effectively in the liver with intravenous administration. GalNAc ligand was essential for targeting liver cells. Newer

generations of DPCs are more homogenous achieved by the use of new synthesis methods. Hydrolysable bonds are incorporated into different positions of the polymer backbone and side chains to reduce cytotoxicity. More stable bonds between the membrane-active polymer and the PEG ligand are used to extend the circulation time. In order to target other tissues besides liver, many types of targeting ligands have been studied, such as peptides, small molecules, lectins, antibodies, glycans, and nucleic acids. It is reported that two different conjugate delivery systems were co-injected to target the same gene in the liver and this strategy is currently in phase-I clinical trials.

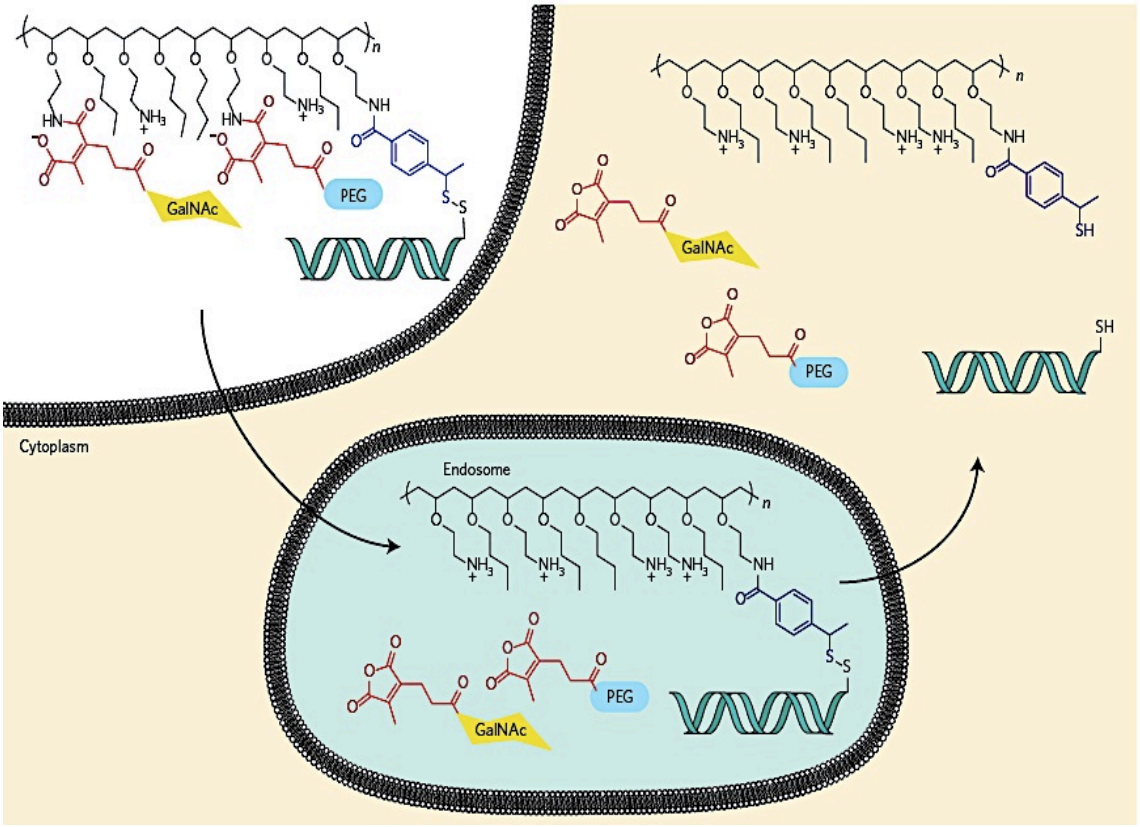

Figure 2.4. DPC conjugates. DPC materials are designed to respond to the acidic environment of the endosome and the reducing environment of the cytoplasm. In circulation, the membrane-disrupting PBAVE polymer (black) is shielded by PEG. After cell uptake, the PEG chains are shed as the pH of the endosome lowers, exposing the polymer and causing endosomal release. In the cytoplasm, the disulphide bond linking the siRNA to the polymer is reduced, freeing siRNA

to trigger RNAi. GalNAc is included in the formulation as a targeting ligand to aid uptake by hepatocytes. Adapted from reference[14]**. Reprinted with permission from Nature.**

GalNAc conjugates only include a chemically stabilized siRNA and a trivalent targeting ligand. In Alnylam Pharmaceuticals, three conjugates ALN-TTPsc, ALN-AT3, ALN-PCS are being examined for the treatment of transthyretin amyloidosis, haemophilia and hypercholesterolemia, respectively[48,49]. The structure of this type of conjugate is shown in Figure 2.5 [14]. This structure provides high affinity binding to its target ASGPR on hepatocytes. Study has shown that subcutaneous administration of this conjugate achieved better biodistribution of siNRA in the liver and higher gene silencing efficiency compared to intravenous administration. By changing the siRNA sequence, this conjugate can target different genes.

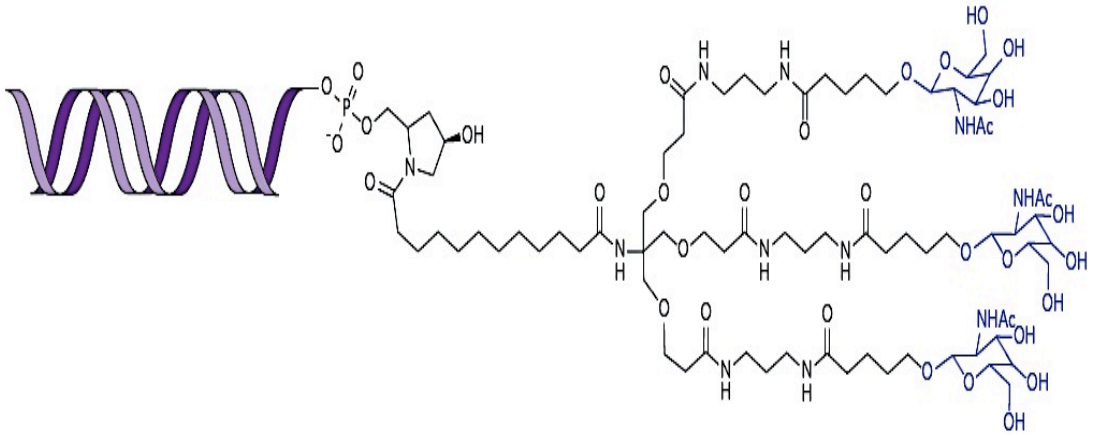

Figure 2.5. GalNAc–siRNA conjugates. Structure of the triantennary GalNAc–siRNA conjugate used in several drug candidates from Alnylam Pharmaceuticals. Adapted from reference[14]**. Reprinted with permission from Nature.**

Another newly developed conjugate system, oligonucleotide nanoparticles (ONPs), is based on nucleic acids. DNA self-assembly enabled the control over particle structure. ONPs

include complementary DNA fragments, chemically modified short interfering RNAs. Through unique overhang sequences, each particle could include six siRNA strands, each in certain position. The size of these nanoparticles is about 29 nm in diameter. These ONPs were further modified through conjugation with a targeting ligand, such as folate (Figure 2.6). The optimized number of folate ligands was three in order to achieve significant gene silencing. The optimized position of these three ligands was around one side of one vertex. However, the ligand position did not influence the cellular uptake efficiency. Folate-ONPs were evaluated in vivo and have gained merit. Other delivery strategies may benefit from the structure-function information of this delivery system[50].

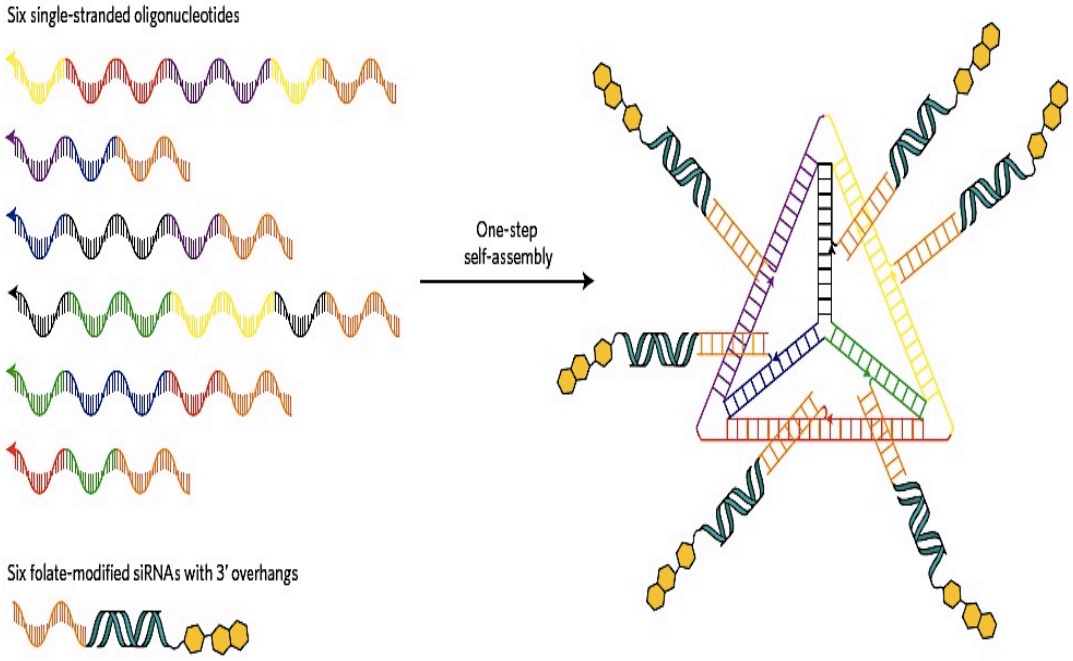

Figure 2.6 Self-assembly of oligonucleotide nanoparticles. DNA tetrahedra carrying six siRNAs were synthesized in a single step through hybridization of complementary strands[50]**. Positioning of each siRNA on the surface of the tetrahedron could be controlled by using unique sequences in each of the siRNA 3' overhangs. This precise synthesis method enabled the study of structure–function relationships , such as the effects of the number and spatial orientation of targeting folate ligands. Adapted from reference**[14]**. Reprinted with permission from Nature.**

2.2.4 Cell Penetrating Peptide-Based Carriers

Cell penetrating peptides (CPPs) have been utilized for the intracellular delivery of a variety of macromolecules, including peptides, proteins, peptide nucleic acids (PNA), plasmid DNA[51], and iron beads[52]. Cell penetrating peptide (CPP) mediated siRNA delivery systems can enter cells either through endocytic pathways or by directly crossing the cell membrane.

CPP can be conjugated to siRNA through covalent cross-links, such as disulfide bonds. Disulfide bonds are cleaved in cells to release siRNA into the cytoplasm, where RISC happens. For instance, covalent conjugation of CPP penetratin or transportan to thiol-containing siRNA via a disulfide bond shows equivalent or better gene knockdown effects compared to cationic liposome siRNA carriers in several mammalian cell types. Conjugation between siRNA and CPP affects cellular localization. For instance, conjugation of TAT-derived oligocarbanate or TAT peptide to siRNA through chemical cross-linking enhances cellular uptake of siRNA and the perinuclear localization of the conjugates, whereas the non-conjugated free TAT peptide is localized in the nucleus. Furthermore, the presence of the target mRNA and variations of the siRNA do not affect the subcellular localization of siRNA[13]. Only conjugation changed the localization of CPP [53], probably in lysosomes and endosomes that are localized perinuclearly.

CPP and siRNA can also form non-covalent complexes through electrostatic interactions. At the right molar and charge ratios, packaging of siRNA and CPP form the positively charged complexes aiding in cell membrane translocation. The advantages of this methodology include low cost of reagents, and easy preparation of CPP/siRNA complexes. MPG is a peptide derived from the hydrophobic fusion peptide domain of HIV-1 gp41 protein and the hydrophilic nuclear localization signal (NLS) of SV40 large T antigen (GALFLGFLGAAGSTMGAWSQPKKKRKV)[54]. siRNA can form a non-covalent complex with MPG. The complexes enter cells through endosome-independent pathways followed by entry into the nucleus. The nucleus localization requires the SV40 nuclear localization sequence; alterations to this sequence prevented nuclear delivery and caused the rapid release of siRNA into the cytoplasm[55].

To minimize the off-target effect of siRNA delivery, some peptides targeting specific cancer cells are incorporated. The evidenced ones are listed in Table 2.2[51].

Table 2.2. Some of the peptides evidenced to target specific tissues or cell types. Adapted from reference[51]. Reprinted with permission from Elsevier.

Peptide sequence	Length	Targeted tissue	Cellular target	Reference
TSPLNIHNGQKL	12	Human head and neck solid tumours	Unknown	[56]
CGKRK	5	Tumour neovasculature	Heparan sulfate	[57]
CGNKRTRGC	7[a]	Breast carcinoma	Unknown	[58]
SMSIARL	7	Prostate vasculature	Unknown	[59]
FQHPSFI	7	Hepatocellular carcinoma cell line	Unknown	[60]
RGD	3	Integrin receptor	$\alpha v\beta 3$ integrin	[61]
NGR	3	Tumour neovasculature	Amino-peptidase N	[62]
VHSPNKK	7	Endothelial VCAM-1 expressing cells	VCAM-1	[63]
RRPYIL	6	Adenocarcinoma cells	Neurotensin receptor	[64]
EDYELMDLLAYL	12	Various carcinoma	Unknown	[65]
LTVSPWY	7	Breast carcinoma	erbB2	[66]
ATWLPPR	7	Tumour neovasculature	VEGF receptor	[67]

a Excluding the cysteine residues used for peptide cyclization.

2.3 Uptake Pathways in Non-Viral Gene Delivery

Most non-viral gene vectors cannot cross the plasma membrane rapidly because of their hydrophilic nature and large size. Endocytosis has been established to be the main mechanism for the internalization of non-viral vectors into the cells[68,69]. As shown in Figure 2.7, endocytosis can also be divided into two broad categories: phagocytosis (the uptake of large particles) and pinocytosis (the uptake of fluid and solutes)[70]. They differ in the size of the detached vesicles, in the composition of the coat (if any), and in the fate of the internalized particles. Multiple mechanisms for endocytosis are summarized below.

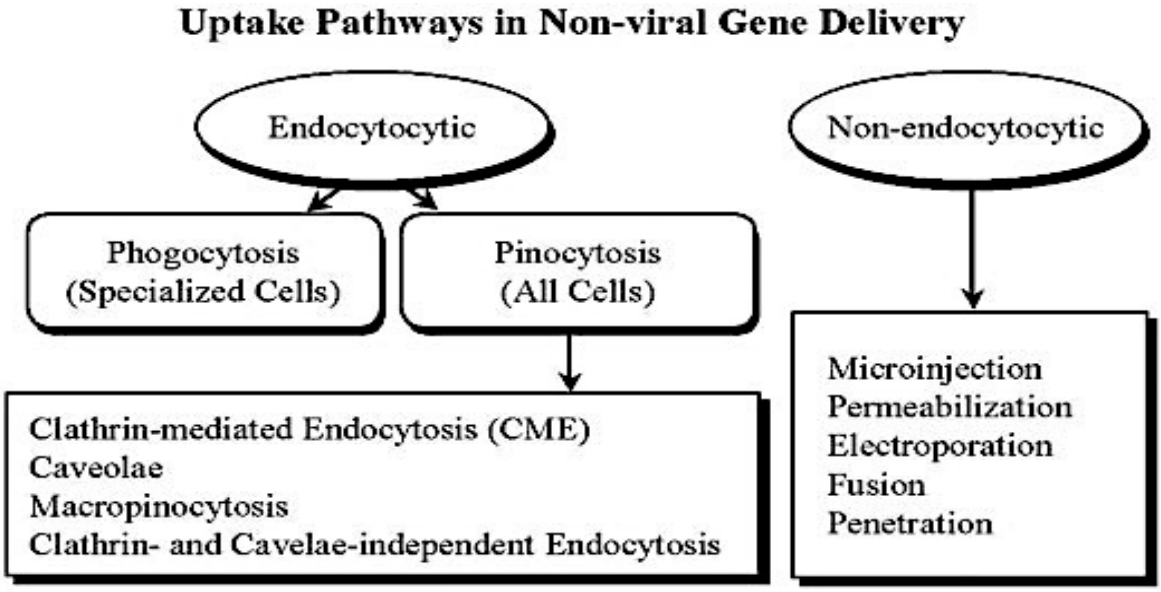

Figure 2.7. Different uptake pathways in non-viral gene delivery. Adapted from [71]**. Reprinted with permission from ASPET.**

- **Clathrin-Mediated Endocytosis**. Clathrin-mediated endocytosis (CME) is a highly regulated and energy-dependent process (Figure 2.8, 2.9). The ligand first binds to a specific cell surface receptor. As a result, the ligand-receptor complexes cluster in coated pits on the plasma membrane, and then, the coated pits invaginate and pinch off the plasma membrane, with the help of dynamin, to form intracellular clathrin coated vesicles (CCVs). CCVs carry concentrated receptor-ligand complexes into the

cells. They range in size from approximately 100 to 150 nm[72]. The clathrin coat then depolymerizes, resulting in early endosomes, which fuse with each other or with other preexisting endosomes to form late endosomes. Molecules entering cells by this pathway experience a drop in pH from neutral to pH 5.9 to 6 in the lumen of early endosomes, with a further reduction to pH 5 from late endosomes to lysosomes[73]. A receptor-rich region buds off to form a separate vesicle that recycles the receptors, and the vesicles then fuse with other late endosomes, which are eventually degraded in lysosomes. Therefore, a device that can enhance the release of the gene to the cytosol is essential.

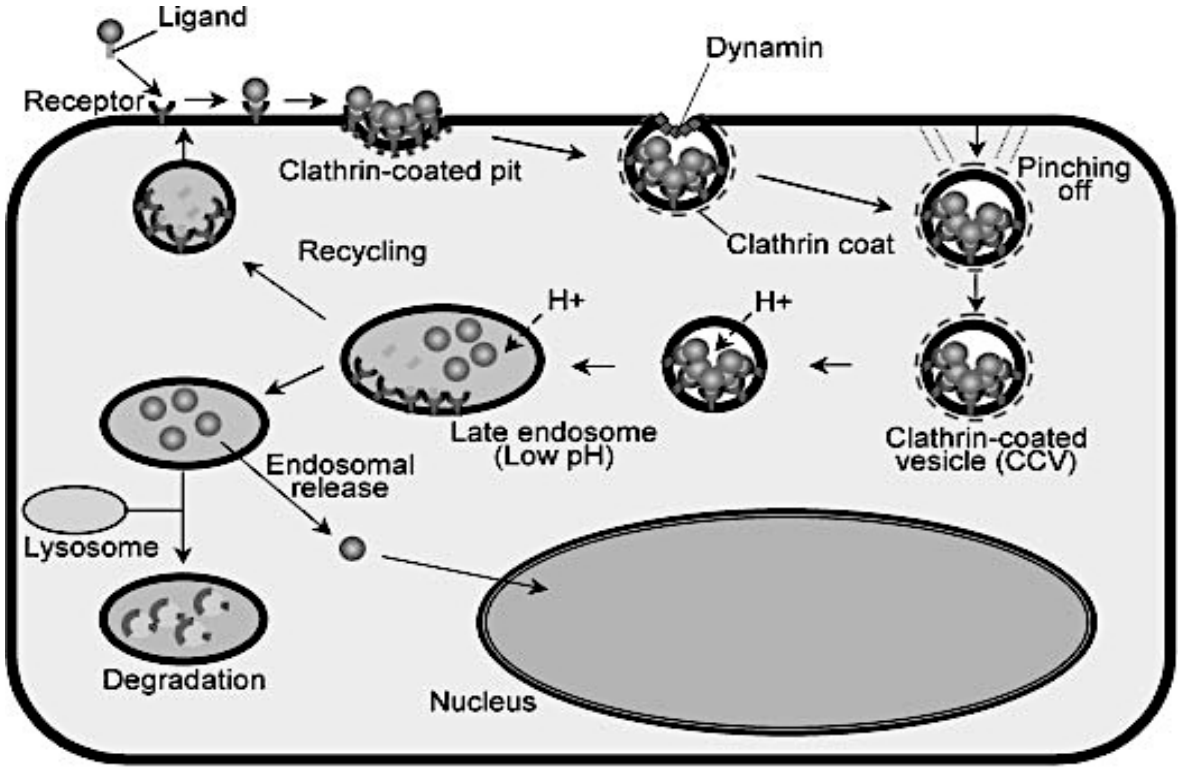

Figure 2.8. Receptor (clathrin) mediated endocytosis. Adapted from reference[71]**. Reprinted with permission from ASPET.**

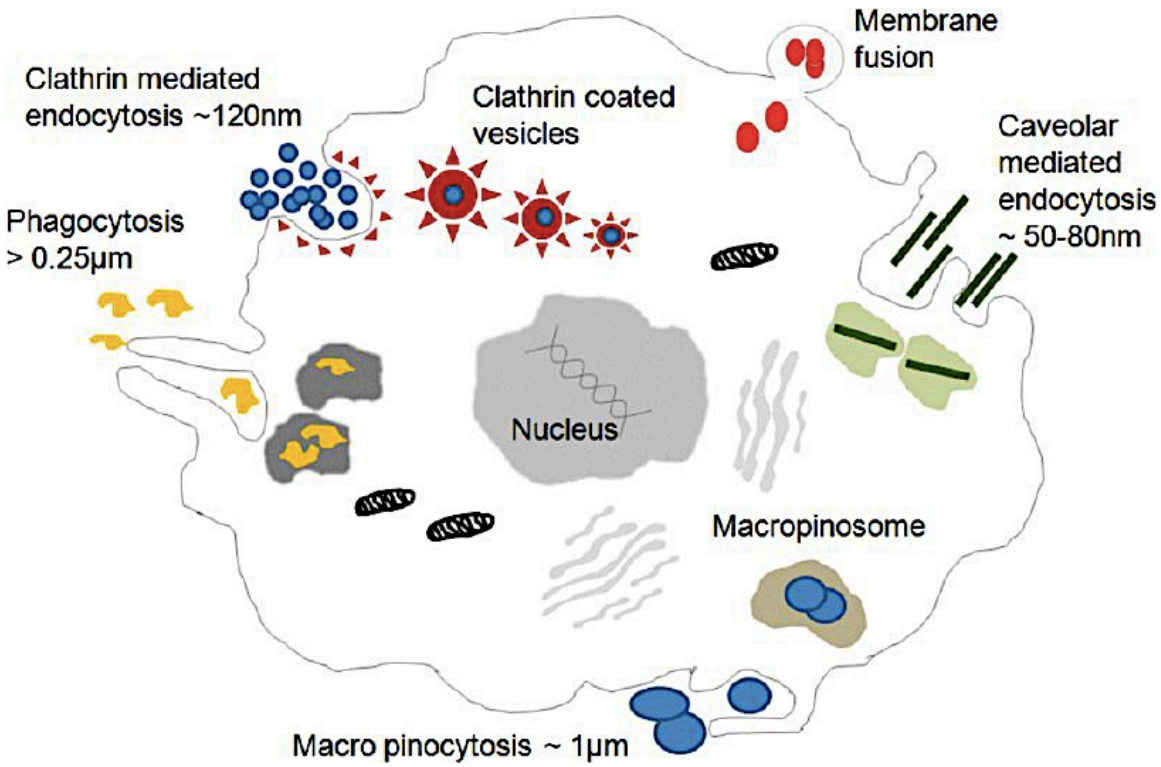

Figure 2.9. Different cell uptake pathways involved in nanoparticle uptake into cells. Adapted from reference[74]**. Reprinted with permission from ACS.**

- **Caveolae-Mediated Endocytosis**. Caveolae are small, hydrophobic membrane microdomains that are rich in cholesterol and glycosphingolipids[75], which are present in many cell types and are abundant in endothelial cells[70]. Generally, caveolae ranging in size from approximately 50 to 60nm are highly stable and slowly internalized, and caveolae uptake is a nonacidic and non-digestive route of internalization[76]. Caveolae-mediated endocytosis is still a promising approach especially if the internalization can be increased.

- **Macropinocytosis**. Macropinosoms, with irregular shape and larger size, sometimes as large as 5 μm in diameter, have no coat and do not concentrate receptors. As a result, macropinocytosis is used as an efficient route for the nonselective endocytosis of solute macromolecules[70].

- **Phagocytosis.** Primarily specialized cells, such as macrophages, monocytes, and neutrophils, conduct phagocytosis in mammalian cells. Hence, phagocytosis is not expected to play a significant role in gene delivery. However, a phagocytosis-like mechanism was proposed for the uptake of large cationic lipid-DNA complexes and PEI polyplexes [77]. This proposed mechanism is dependent on the actin cytoskeleton and can explain the uptake of large particles.

- **Receptor-Mediated Endocytosis**. CME is the main pathway for internalization of most receptors. However, other pinocytic pathways are capable of selective receptor-mediated endocytosis events. For instance, after clathrin-mediated endocytosis was disrupted, the internalization of interleukin-2 into lymphocytes was partially inhibited, indicating that a clathrin-independent mechanism contributes to the efficient internalization of interleukin-2 receptors[78]. The use of receptor-mediated endocytosis is a promising strategy for the introduction of gene therapy agents into defined cell populations. For example, hepatocytes exclusively express large numbers of high-affinity cell surface receptors that bind to and subsequently internalize asialogly - coproteins[79]. Another advantage of clathrin-independent endocytosis is that these uptake mechanisms are relatively unaffected by lysosomal degradation. Thus, exploring and targeting new receptors that can be internalized by clathrin-independent endocytosis will probably provide more efficient systems.

Other than endocytic pathways, there are several non-endocytic pathways, such as microinjection, permeabilization, electroporation, fusion, and penetration. However, the first three techniques are highly invasive and cannot be used for in vivo gene delivery.

2.4 Mechanisms of Endosomal Escape

The endocytic pathway is the most widely involved mechanism to deliver nano-medicines, such as siRNA. However, particles entering the cells via the endocytic pathway encounter problems, including endosomal entrapment and subsequent enzyme digestion in the lysosome. These problems result in low transfection efficiency and are the main obstacles for most non-viral delivery systems. Thus, several approaches have been investigated to

facilitate the early release of therapeutic cargos from the endosomal pathway into the cytosol, where RISC is located. These approaches include pore formation in the endosomal membrane; photochemical disruption of the endosomal membrane; conformational changes of enhancers facilitating endosomal escape and pH-buffering effect.

Fusogenic peptides are used in a variety of fusion systems to destabilize the endosomal membrane. Haemaglutinin is a peptide of the influenza virus coat, and acts as a fusogenic agent, which undergoes conformational changes from an anionic, hydrophilic coil at pH 7.4 to a hydrophobic helical conformation at the acidic endosomal pH. This conformational change leads to fusion of the viral membrane into the cellular membrane [81] .

Photochemical internalization (PCI) is another technique to disrupt the endosomal membrane and helps the therapeutic agents escape from the endosome. A number of photosensitizers such as $TPPS_4$, $TPPS_{2a}$, $AIPcS_{2a}$, and dendrimer-based photosensitizer (DP) (dendrimerphthalocyanine (DPc)) localize primarily in the membrane of the endosomes and lysosomes[82,83]. After exposure to light, the photostimulation of the photosensitizer triggers the generation of highly reactive singlet oxygen, which destroys the endosomal/lysosomal membrane, whereas the contents of the organelles remain intact and are released to the cytosol[84]. This strategy has been applied to the delivery of therapeutic complexes containing CPP. However, the use of photosensitizers with siRNA and CPP may not be suitable for therapeutic applications because the photosensitizers may exhibit a different distribution of CPP/siRNA from in vitro to in vivo.

Pore formation is another mechanism for endosomal escape. In general, pore formation is based on the interplay between a membrane tension that enlarges the pore and a line tension that closes the pore. The binding of some components such as cationic amphiphilic peptides (AMPs) to the lipid bilayers leads to internal stress or internal membrane tension that can be strong enough to form pores in the lipid membrane. Several models, for example, barrel-stave pores or toroidal channels [85,86], have been developed to describe these events.

The proton sponge effect, also called the pH-buffering effect, is mediated by components with a high buffering capacity and the flexibility to swell when protonated. Protonation

induces an extensive inflow of water and ions into the endosomal environment, thereby resulting in disruption of the endosomal membrane and release of the entrapped components. For example, histidine-rich molecules show a buffering effect based on protonation of the imidazole ring of histidine, leading to rupture of the endosomal membrane[87].

Chapter 3*

Peptide C6M3 mediated siRNA Delivery *In Vitro*

Abstract

Since its inception more than a decade ago, gene-silencing mediated by double-stranded small interfering RNA (siRNA) has been widely investigated as a potential therapeutic approach for a variety of diseases. However, the use of siRNA is hampered by its rapid degradation and poor cellular uptake in vitro and in vivo. Recently, peptide-based carriers have been applied to siRNA delivery, as an alternative to the traditional delivery systems. Here, a histidine-containing amphipathic amino acid pairing peptide, C6M3, which can form complexes with siRNA, was used as a new siRNA delivery system. This peptide exhibited a high affinity for siRNA and ability to efficiently deliver siRNA into the cells. The interaction of C6M3 with siRNA was investigated to determine the loading capacity of C6M3 at different peptide/siRNA molar ratios. A minimum C6M3/siRNA molar ratio of 10/1 was required to encapsulate all the free siRNA, as indicated by a gel electrophoretic assay and further confirmed by zeta potential analysis. The particle size distribution of the C6M3-siRNA complexes was studied using dynamic light scattering, which showed an intensity-based size distribution peaked approximately at 100 nm in RNase-free water and 220 nm in Opti-MEM C6M3 adopted a helical secondary structure in RNase-free water and became more so after forming complexes with siRNA. The interaction of siRNA with C6M3 is an entropy-driven spontaneous process, as determined by the results of isothermal titration calorimetry (ITC). The efficiency of cellular uptake of the siRNA complexes at different C6M3/siRNA molar ratios was evaluated, and the results indicated that the uptake efficiency was related to the molar ratio. Furthermore, a significant level of GAPDH gene silencing was achieved in CHO-K1 cells, with minimal cytotoxicity.

* This chapter is based on a manuscript. B. Chen, K. Yoo, W. Xu, R. Pan, X. Han, X. Ouyang, X. Qiu, P. Chen, A Histidine-containing, Amphipathic, Amino Acid Pairing Peptide mediated siRNA Delivery *In Vitro*.

3.1 Introduction

The term RNA interference (RNAi) was first coined after the discovery that double-stranded RNAs (dsRNAs) can trigger silencing of complementary messenger RNA (mRNA) sequences in the nematode Caenorhabditis elegans [88]. Since the discovery of RNAi, there has been an explosion of interest in using this technology for basic and applied research, including analysis of signaling pathways and gene functions, as well as in developing a therapeutic method to target disease-related mRNAs in the cytoplasm of cells [88–94]. In spite of the high therapeutic potential of small interfering RNAs (siRNAs), their negative charge has limited their ability to penetrate cell membranes, and naked siRNAs are easily degraded by nucleases [10].

To date, a number of materials have been used to develop siRNA delivery systems, including virus vectors, liposomes, lipoplexes, polymers, and peptides [11,12]. Among them, cell-penetrating peptides (CPPs) have been utilized for intracellular delivery of a variety of macromolecules, including proteins, peptide nucleic acids (PNA), and siRNAs [13].

CPPs can be conjugated to siRNA through covalent cross-links such as disulfide bonds. The disulfide bonds are cleaved in cells, releasing the siRNA into the cytoplasm, where the RNA-induced silencing complex (RISC) forms [13]. CPPs and siRNA can also form non-covalent complexes through electrostatic interactions. At certain molar or charge ratios, siRNA and CPPs form positively charged complexes that are translocated across the plasma membrane. The advantages of this methodology include the low cost of the reagents and the easy preparation of CPP-siRNA complexes [54,55].

CPP-siRNA complexes can enter cells either through endocytotic pathways or by directly crossing the cell membrane [71]. In our previous study, we reported that a new amphipathic, amino-acid pairing peptide, C6, formed complexes with siRNAs in a non-covalent manner and protected the siRNA from degradation [95]. Although its cellular uptake was highly efficient, we found that its gene silencing activity was not significantly high (not reported). Therefore, it was concluded that after entering cells, the C6-siRNA complexes were trapped in endosomes[95], which decreased their gene silencing efficiency. Strategies to induce the

membrane disruption are required. Tryptophan (W), because of its aromaticity, flat rigid shape, and π electronic structure, has a strong preference at the membrane interface and acts as an anchor to the cell membrane [96–99], thus enhances the peptide-membrane interaction. Histidine proves to enhance the endosomal membrane disruption through proton sponge effect [87,100,101]. Therefore, C6 (Ac-RLLRLLLRLWRRLLRLLR-NH2) was modified to C6M3 (Ac-RL**WH**LL**W**RLWRRL**H**RLLR-NH_2), where histidine and a higher amount of tryptophan were incorporated. In this study, the physicochemical properties, cytotoxicity, cellular uptake and gene silencing efficiency of C6M3-siRNA complexes were investigated.

3.2 Materials & Methods

3.2.1 Materials

Peptide C6M3 (Ac-RLWHLLWRLWRRLHRLLR-NH_2, MW=2621 g/mol) was synthesized by CanPeptide Inc (Quebec, CA) with a purity of >95%. siRNA targeting the glyceraldehyde 3-phosphate dehydrogenase (GAPDH) gene and Cy3-labeled GAPDH siRNA were purchased from Ambion (Silencer^{TM} GAPDH siRNA kit). The siRNA targeting sequence for eGFP, GCGACGUAAACGGCCACAAGU was purchased from Dharmacon. The antisense sequence is ACUUGUGGCCGUUUACGUCGC, and the sense sequence is GACGUAAACGGCCACAAGUUC. The negative control siRNA, which sets the threshold, is crucial for determining the transfection efficiency of an siRNA. The negative control siRNA used here was purchased from Ambion. Cell counting kit-8 (CCK-8) was used for cell viability test and was purchased from Dojindo Molecular Technologies.

3.2.2 Methods

3.2.2.1 Cell line

Chinese hamster ovary cells (CHO-K1) [purchased from American Type Culture Collection (ATCC CCL-61)] were grown in F-12K medium (Thermo Scientific, Ontario, CA) supplemented with 10% fetal bovine serum (FBS) (Sigma-Aldrich, Ontario, CA). The cells were incubated at 37^{o}C in 5% CO_2.

3.2.2.2 Preparation of siRNA complexes

For the cell treatments, the peptide/siRNA complexes were prepared in Opti-MEM (Invitrogen, California, USA). For the physicochemical characterization, the complexes were prepared in RNase-free water. The complexes were generally incubated at room temperature for 20 min immediately before transfection/measurements.

3.2.2.3 Agarose gel-shift assay

Samples containing 300 ng of eGFP siRNA were electrophoresed on a 1.2% wt/vol agarose gel in 1x TBE at 55 V for 1 h. The ethidium bromide-stained siRNA was visualized on a UV transilluminator equipped with a camera.

3.2.2.4 Isothermal titration calorimetry (ITC)

The isothermal titration calorimetry experiments were conducted using a Nano-ITC calorimeter (TA Instruments). A 250 μM C6M3 peptide solution and a 10 μM siRNA solution were both prepared in RNase-free water. All of the samples were degassed in a degassing station (TA Instruments) prior to the experiments. RNase-free water was placed in the ITC reference cell. For each titration, 2 μl of the peptide in a pipette rotating at 250 rpm was injected into the siRNA solution in the sample cell of the calorimeter, which was equilibrated to 25^{o}C, with an interval of 300 s between injections. The heat of dilution was measured by titrating the C6M3 solution into RNase-free water and was later subtracted from the sample measurement. The data were analyzed using NanoAnalyze software v.2.3.0.

3.2.2.5 Dynamic light scattering and zeta potential

Particle size measurements were conducted at 25^{o}C in transparent ZEN0040-disposable microcuvette cells (40 μl) using a Zetasizer Nano ZS (Malvern, UK) after the samples were allowed to stabilize for 20 min at peptide-siRNA molar ratios of 10/1, 20/1 or 40/1 with a final siRNA concentration of 100 nM in RNase-free water. At molar ratio 40/1, the particle size of peptide-siRNA complexes was also measured after incubation for 40 min and 90 min respectively. After the incubation of peptide-siRNA complexes (molar ratio: 40/1) for 20 min at 25^{o}C, the sample was further incubated at 37^{o}C and the particle sizes were measured after

incubation for 30 min and 60 min respectively. In order to study the effect of Opti-MEM culture medium on the particle size, the peptide-siRNA complexes (molar ratio 40/1) were prepared in Opti-MEM and incubated for 20 min at 25^{o}C following with size measurements. The zeta potentials of the peptide-siRNA complexes were measured using a Clear DTS1070-zeta dip cell.

3.2.2.6 Scanning electron microscopy (SEM)

SEM was used to characterize the morphology of C6M3-siRNA complexes at a molar ratio of 20/1 with siRNA concentration of 100 nM. Right after incubation for 20 min, 40 μl samples were allowed to dry at room temperature over substrates. The samples were coated with gold (10 nm in thickness) before taking images. The SEM images were taken with a LEO FESEM 1530 field-emission SEM.

3.2.2.7 Circular dichroism (CD) spectroscopy

Spectra at 250 to 190 nm with a spectral resolution and pitch of 1 nm and scan speed of 200 nm/min were recorded using a J-810 spectropolarimeter (Jasco, USA). Increasing amounts of siRNA were added to the peptide solution (30 μM), to obtain different molar ratios. The samples were transferred into 1-mm long quartz cells and maintained at 25^{o}C. The spectra presented here are the average of three measurements.

3.2.2.8 Cytotoxicity of peptide-siRNA complexes

CHO-K1 cells were seeded at 5,000 cells/well in clear, flat-bottomed, 96-well plates (Costar) 24 h before treatment. After washing the cells, the peptide-siRNA complexes or control samples prepared in 100 μl of Opti-MEM were added to the wells and incubated for 4 h. Thereafter, 50 μl of 30% serum containing medium was added, and the cytotoxicity of the relevant reagents was determined by the CCK-8 assay after 48 h. The reagent was added according to the manufacturer's instructions and the absorbance at 570 nm was measured with a plate reader (BMG, FLUOstar OPTIMA, Germany). The background absorbance of the multiwell plates at 690 nm was determined and subtracted from the 570 nm

measurement. The results obtained from triplicate wells were averaged and normalized to the value obtained from non-treated samples.

3.2.2.9 Cellular uptake

CHO-K1 cells were seeded in a 24 well plate 24 h before treatment. The cells were incubated with C6M3-Cy3-labeled GAPDH siRNA complexes at a molar ratio of 20/1 for 4 h. Thereafter, the cells were washed three times with PBS and then fixed by 4% paraformaldehyde (PFA). The nucleus of the cell was stained by DAPI. The image showing the intracellular localization of Cy3-labeled siRNA was taken with a fluorescence microscope.

The cellular uptake of Cy3-labeled siRNA was quantified using flow cytometry (BD Biosciences, BD FACSVantage SE Cell Sorter, USA). CHO-K1 cells (50,000) were incubated in 24-well plates for 24 h. The medium was replaced with Opti-MEM (Invitrogen) containing complexes or control samples with a final siRNA concentration of 100 nM. After incubating for 4 h, the cells were rinsed with PBS and then washed with heparin (10 U/ml). After washing the cells, trypsin-EDTA was added to detach them from the plate. The cells were re-suspended in 4% paraformaldehyde (PFA) and placed in FACS tubes for analysis.

3.2.2.10 In vitro gene-silencing efficiency

CHO-K1 cells were seeded at 3,5000 cells/well in 24-well plates and incubated for 24 h. Next, the cells were incubated with various complex formulations in Opti-MEM at 37^{o}C for 4 h. Then, the cells were incubated for an additional 48 h in complete culture medium. siRNA concentration was 100 nM.

For qRT-PCR analysis, the total RNA was extracted from the treated cells using the SV Total RNA Isolation System (Promega, CA, USA). A Nanodrop (Nanodrop spectrophotometer ND-1000, Thermo Scientific, Ottawa, CA) was used to determine the RNA concentrations. The RNA samples were reverse-transcribed into cDNA using a Bio-Rad iScript cDNA synthesis kit according to the manufacturer's protocol. After the cDNA was synthesized, PCR was performed with Brilliant II fast SYBR Green QPCR Master Mix

(Agilent Technologies, Wilmington, DE, USA) using an Mx3005P^{TM} real time PCR System (Agilent Technologies). The sequences of the primers used for the mouse GAPDH gene are 5'-TTGCTGTTGAAGTCGCAGGAG-3' and 5'-TGTGTCCGTCGTGGATCTGA-3' (Sigma, Oakville, Ontario, Canada). Cyclophilin, a housekeeping gene, was used as an internal control to normalize the GAPDH gene expression. Mouse cyclophilin mRNA amplified using the following primers: 5'-AGGGTTTCTCCACTTCGATCTTGC-3' and 5'-AGATGGCACAGGAGGAAAGAGCAT-3' (Sigma, Oakville, Ontario, CA).

3.3 Results

3.3.1 Physicochemical Characterization of siRNA Complexes

The binding of siRNA with C6M3 was investigated using agarose gel electrophoresis. A 21-mer siRNA that target the eGFP gene was used in this experiment. C6M3-siRNA complexes prepared using a series of molar ratios were investigated. As shown in Figure 3.1, lane 1, siRNA alone easily migrated through the gel due to its small size and negative charge. Due to the larger size and positive charge of the cationic C6M3-siRNA complexes, their migration through the gel was impeded. At a molar ratio of 10/1, the siRNA molecules were all bound to C6M3 because no free siRNA was detected in the agarose gel.

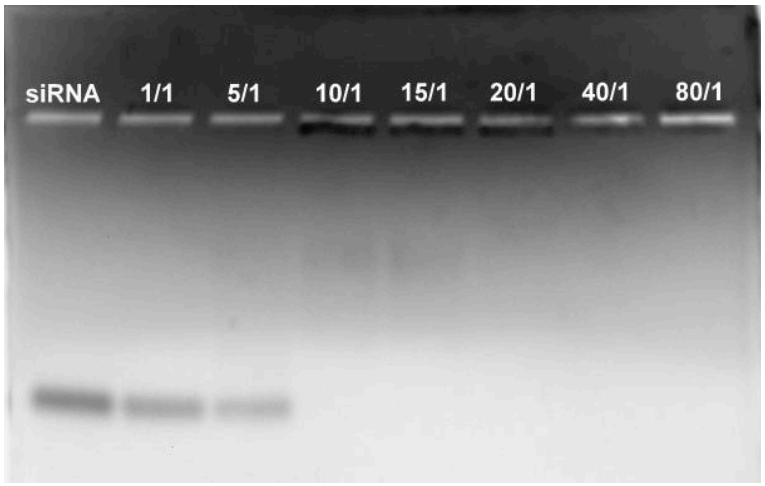

Figure 3.1. Binding ability of siRNA to C6M3 studied by agarose gel-shift assay. The formed C6M3-siRNA complexes, stained with ehidium bromide, were investigated by electrophoresis on agarose gel (1.2% wt/vol). siRNAs, targeting eGFP genes, were complexed with C6M3 at a series of molar ratios from 1/1 to 80/1. Lane 1 was siRNA control, and lanes 2-8 indicated correlated molar ratios. The amount of siRNA was 300 ng/well.

The interactions between C6M3 and siRNA were further studied by ITC while the siRNA (in RNase-free water) was titrated with C6M3 at 25^{o}C. As shown in Figure 2A, the heat exchange during the titration of siRNA by C6M3 was detected by the machine and output as raw data. By fitting the raw ITC data to a single-site model (Figure 3.2B), the thermodynamic parameters of the interaction were obtained and listed in Table 3.1.

Table 3.1. Thermodynamic parameters when titrating siRNA with C6M3 in water.

Ka (1/M)	ΔH (kJ/mol)	n	TΔS (kJ/mol)	ΔG (kJ/mol)
$8.59 \cdot 10^{8}$	-16.12	6.97	34.87	-50.99

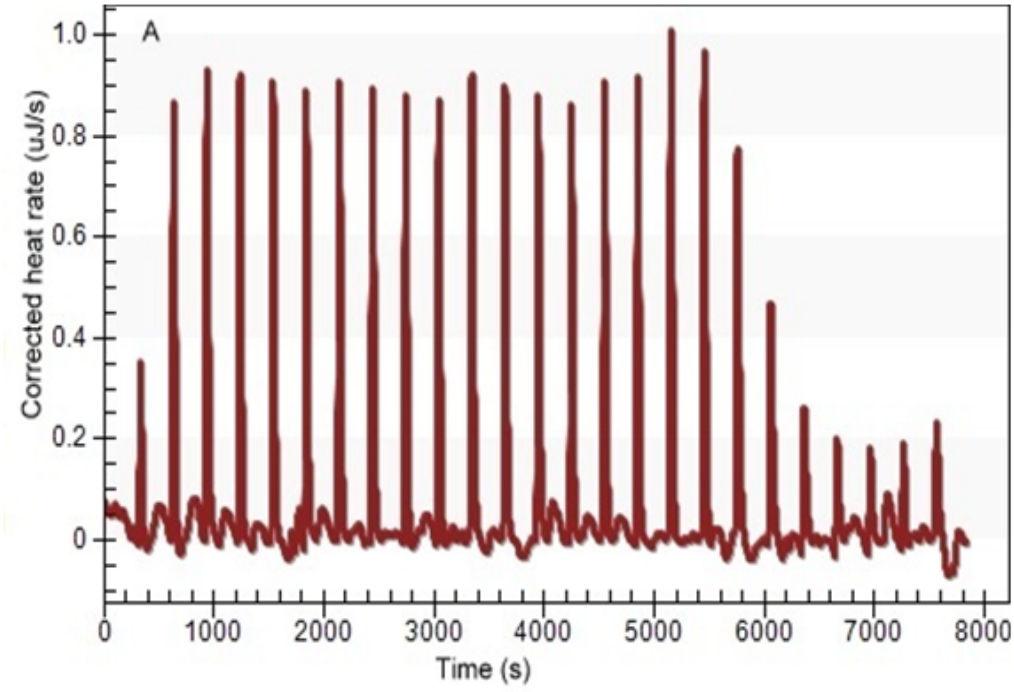
A
Corrected heat rate (uJ/s)
1.0
0.8
0.6
0.4
0.2
0
0
1000
2000
3000
4000
5000
6000
7000
8000
Time (s)

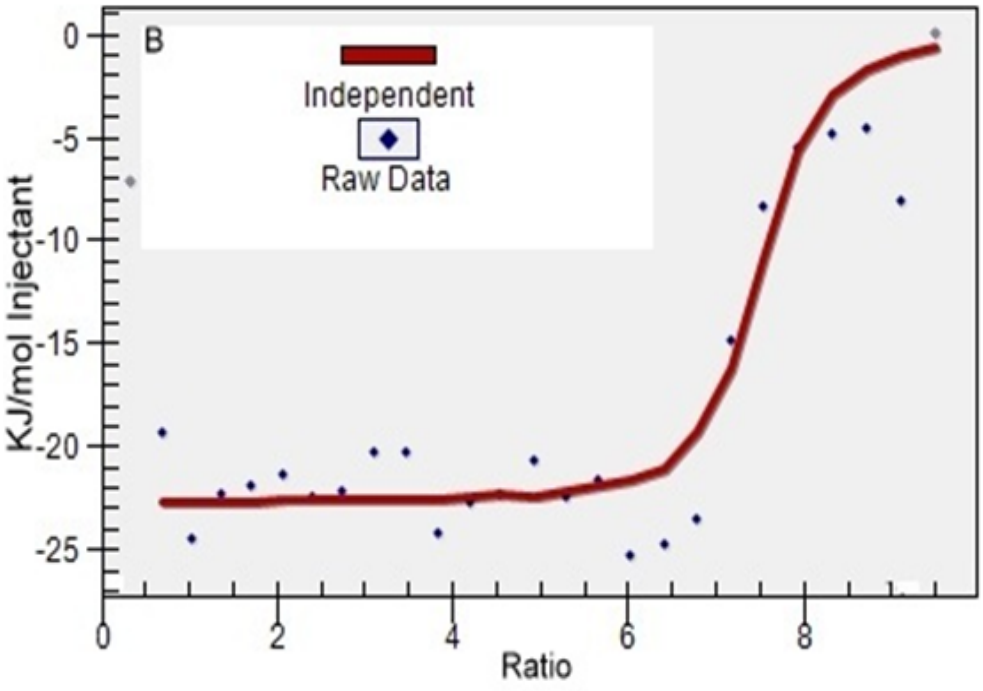
B
Independent
Raw Data
KJ/mol Injectant
0
-5
-10
-15
-20
-25
0
2
4
6
8
Ratio

Figure 3.2. Calorimetric titration of siRNA with C6M3 at room temperature in RNasefree water. A) Corrected thermogram of calorimetric titration of siRNA with C6M3, B) Binding analysis of siRNA with C6M3 by fitting the raw data with an independent model. C6M3 concentration was 250 µM, siRNA concentration was 10 µM.

The obtained molar stoichiometry of 6.96 was very close to the theoretical value of 7, considering that the C6M3 peptide contains 6 positively charged arginine residues and there are 21 pairs of negatively charged nucleotides in the siRNA molecule. With an enthalpy of -16.12 kJ/mol, a ΔS of 117.0 J/(mol·K), and an entropy of -34.87 kJ/mol, the binding was predominantly entropy-driven. Moreover, the Gibbs free energy calculated using the equation $\Delta G=\Delta H-T\Delta S$ was -50.99 kJ/mol, indicating that the C6M3 peptide and siRNA formed complexes spontaneously [102,103].

Table 3.2 shows the detailed results of the size and charge characterization of C6M3-siRNA formulations evaluated in this study. As shown in Table 3.2, the particle size decreased over the increase of molar ratios. The possible reason is that at higher molar ratios, the nanoparticles were more condensed [104]. The size of C6M3-siRNA complexes remained in the range of 70–100 nm, which indicated that the complexes most possibly entered cells through endocytosis [105]. At a molar ratio of 10/1, the C6M3-siRNA complexes have an approximately neutral zeta potential. Increasing the molar ratios, C6M3-siRNA complexes exhibited a more positive surface charge due to the addition of more cationic peptides. In order to increase the affinity of C6M3-siRNA complexes with negatively charged cell membranes, we usually use molar ratios higher than 10/1 for the cell transfection experiments.

Table 3.2. The hydrodynamic diameter and zeta potential of the C6M3-siRNA complexes at different molar ratios were measured by dynamic light scattering (DLS).

Sample	Size ± SD (nm)	Zeta potential ± SD (mV)
C6M3-siRNA 10/1	97 ± 3	0.4 ± 6.17
C6M3-siRNA 20/1	80 ± 1	23 ± 7.91
C6M3-siRNA 40/1	72 ± 1	30.5 ± 6.50

The siRNA concentration was fixed as 100 nM. At different molar ratios, the amount of C6M3 was adjusted. Results are expressed as mean ± standard deviation (n=3).

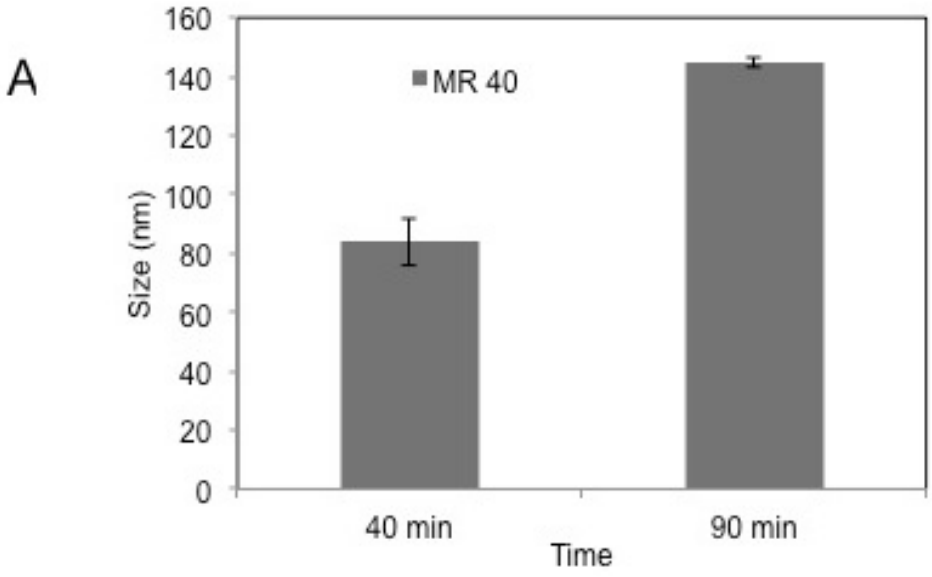

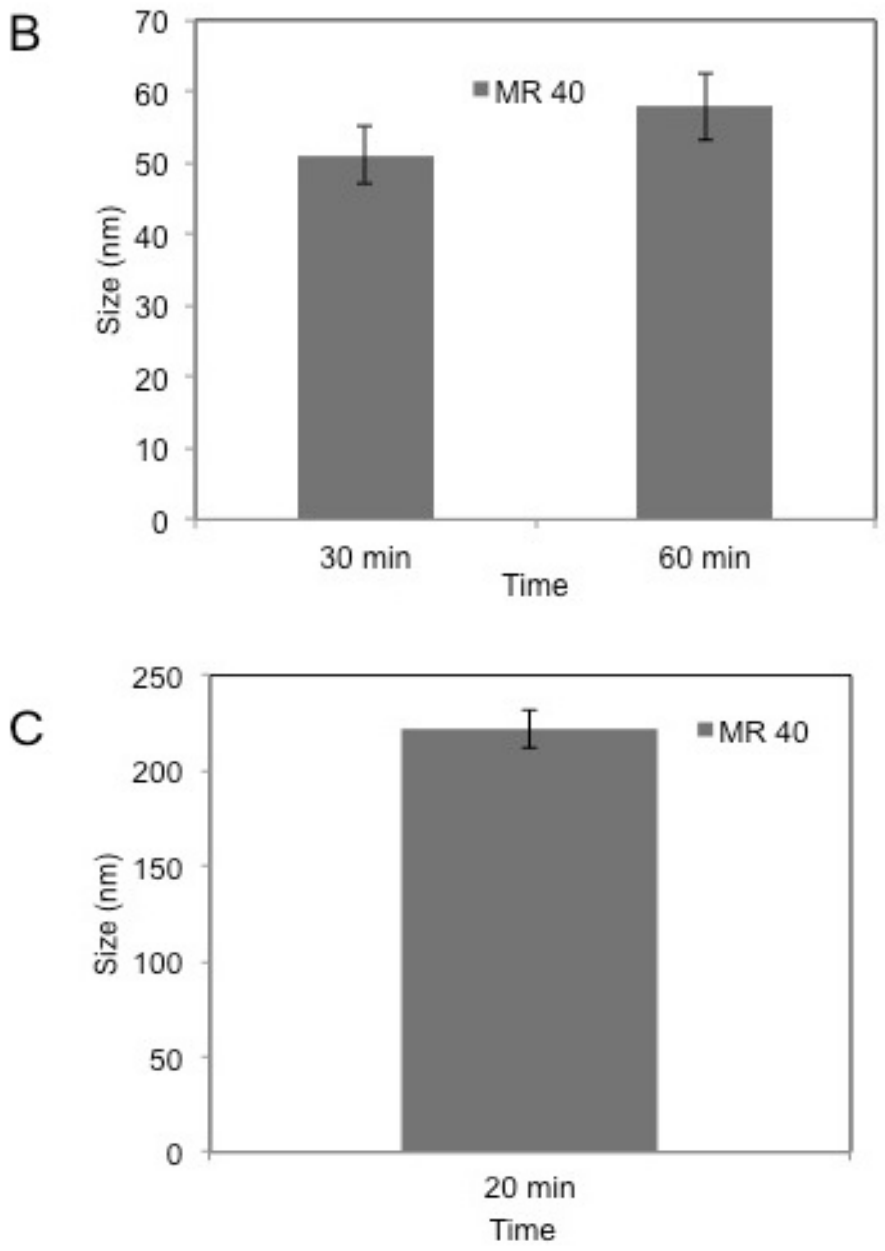

Figure 3.3. (A) Size of Peptide-siRNA complexes at molar ratio 40/1 in RNase-free water at 25°C, after incubation for 40 min and 90 min; (B) size of C6M3-siRNA complexes at molar ratio 40/1 at 37 °C, after incubation for 30 min and 60 min; (C) size of C6M3-siRNA complexes at molar ratio 40/1 in Opti-MEM at 25°C, after incubation for 20 min. siRNA concentration was at 100 nM. MR = molar ratio (peptide/siRNA).

Figure 3.3A shows that in RNase-free water, after incubation for 40 min at 25^{o}C, the particle size of C6M3-siRNA complexes (molar ratio 40/1) slightly increased. When the incubation time was increased to 90 min, the particle size increased to 140 nm, possibly due to the aggregation of the particles. This data indicated the particle size remained almost the same up to 40 min and significantly increased after incubation for 90 min. Figure 3.3B shows that after the peptide C6M3 and siRNA formed complexes at 25^{o}C, the particle size changed after incubation at 37^{o}C for 30 min and 60 min respectively. At 25^{o}C, C6M3-siRNA complexes (molar ratio 40/1) in RNase-free water displayed size distribution around 70 nm; at 37^{o}C, the particle size decreased to 50 nm (30 min). Considering the C6M3-siRNA complexes formation process is entropy driven (ITC data), increasing the temperature leads to the increase of hydrophobic forces, which may increase the compactness of the particles. Moreover, at 37^{o}C , increaseing the incubation time to 60 min, the particle size remained almost the same as that after incubation for 30 min. At 25^{o}C, C6M3-siRNA complexes (molar ratio 40/1) prepared in Opti-MEM exhibited size distribution around 220 nm (Figure 3.3C), which was much higher than that prepared in RNase-free water. This difference is possibly caused by the ionic effect in the Opti-MEM.

Figure 3.4A shows that C6M3 formed complexes with siRNA displaying a spherical shape. Moreover, the size distribution of C6M3-siRNA complexes was consistent with the DLS results. The impact of siRNA on the secondary structure of C6M3 was evaluated using CD spectroscopy. As shown in Figure 3.4B, C6M3 in water exhibited a maximum spectrum of approximately 190 nm and a minimum of approximately 208 nm, which together indicated a helical conformation. When a small amount of siRNA (molar ratio of 20/1) was added, a shift in the spectrum minimum from 207 nm to 210 nm and a second minimum spectrum of approximately 222 nm were observed. Adding more siRNAs to attain a molar ratio of 10/1 increased the absolute values in spectrum minima at 208 and 222 nm, and the maximum around 190 nm. These results indicated an increase in the α helical secondary structure of the peptide occurred upon the addition of siRNA. The more siRNA was added, the more helical content of C6M3 secondary structure adopted. The conformational changes of the peptide after forming complexes with siRNA confirm that once siRNA neutralized some of the

positive charges of the peptide, the repulsion between these charges decreased. Therefore, it became much easier for the peptide to form typical α helical secondary structure that was reported to facilitate the cellular uptake of peptide-siRNA complexes [106].

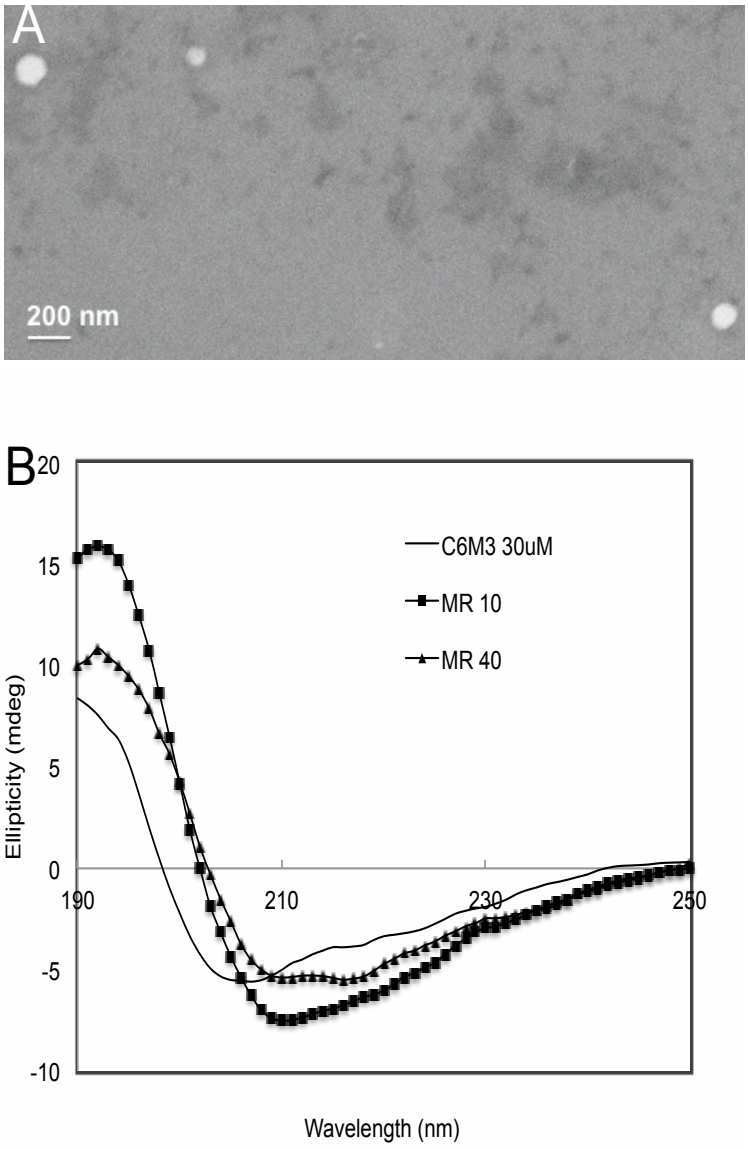

Figure 3.4. (A) Morphology of C6M3-siRNA complexes at a molar ratio of 20/1, where siRNA concentration was 100 nM. (B) CD spectra of C6M3 alone and C6M3-siRNA at different molar

ratios. MR = molar ratio (peptide/siRNA). C6M3 concentration was fixed as 30 μM and C6M3-siRNA complexes were formulated at molar ratios of 10/1 and 40/1.

3.3.2 Cytotoxicity of C6M3-siRNA Complexes

As shown in Figure 3.5, the viability of cells treated with C6M3-siRNA complexes was more than 90%. However, cells treated with Lipofectamine 2000 showed significant toxicity, with cell viability of 57%. These results clearly show that peptide C6M3 induced much lower cytotoxicity than Lipofectamine 2000. Moreover, peptide alone at corresponding concentrations of different molar ratios achieved >90% cell viability.

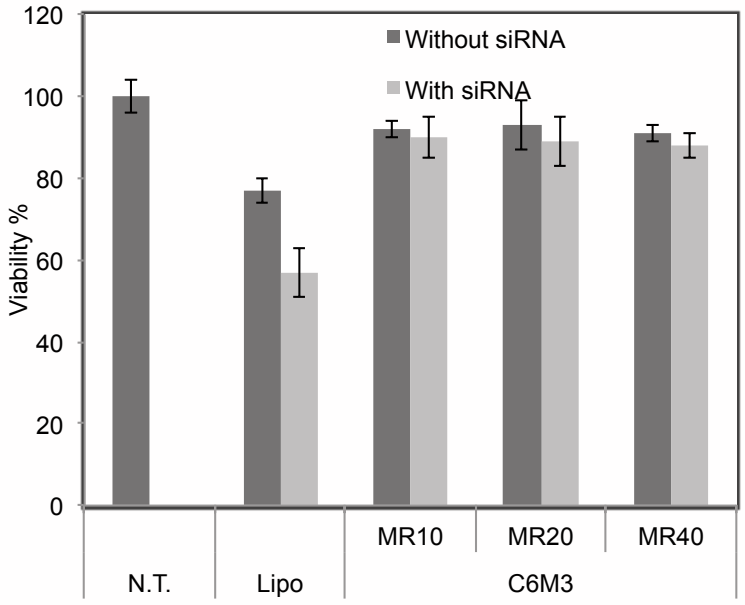

Figure 3.5. Viability of CHO-K1 cells after 48 h treatment. N.T.= Non treated, MR=peptide/siRNA molar ratio, Lipo=Lipofectamine 2000. siNRA concentration was at 100 nM. (n=3)

3.3.3 Cellular Uptake of siRNA Complexes

CHO-K1 cells were treated with the C6M3-Cy3-labeled siRNA complexes to study the intracellular localization and cellular uptake of siRNA. When provided in complexes with a peptide/siRNA molar ratio of 20/1 (Figure 3.6), the siRNA was localized to regions in close proximity to the nuclear membrane. The siRNAs were

distributed in a non-homogeneous pattern at the periphery of the nucleus, indicating the possibility of endocytotic delivery [107]. The efficiency of C6M3 to deliver siRNA into CHO-K1 cells was evaluated using fluorescence-activated cell sorting (FACS). As shown in Figure 3.7, the treatment of CHO-K1 cells with Cy3-labeled GAPDH siRNA alone achieved almost no uptake, implying that siRNA without an efficient carrier was not able to enter the intracellular environment. However, the efficiency of cellular uptake of the siRNA significantly increased with the increase in the C6M3 peptide/siRNA molar ratio from 10/1 to 40/1. In addition, at molar ratios of 40/1, C6M3-Cy3-labeled siRNA complexes entered more cells than Lipofectamine 2000-siRNA complexes, suggesting the pronounced delivery efficiency of C6M3.

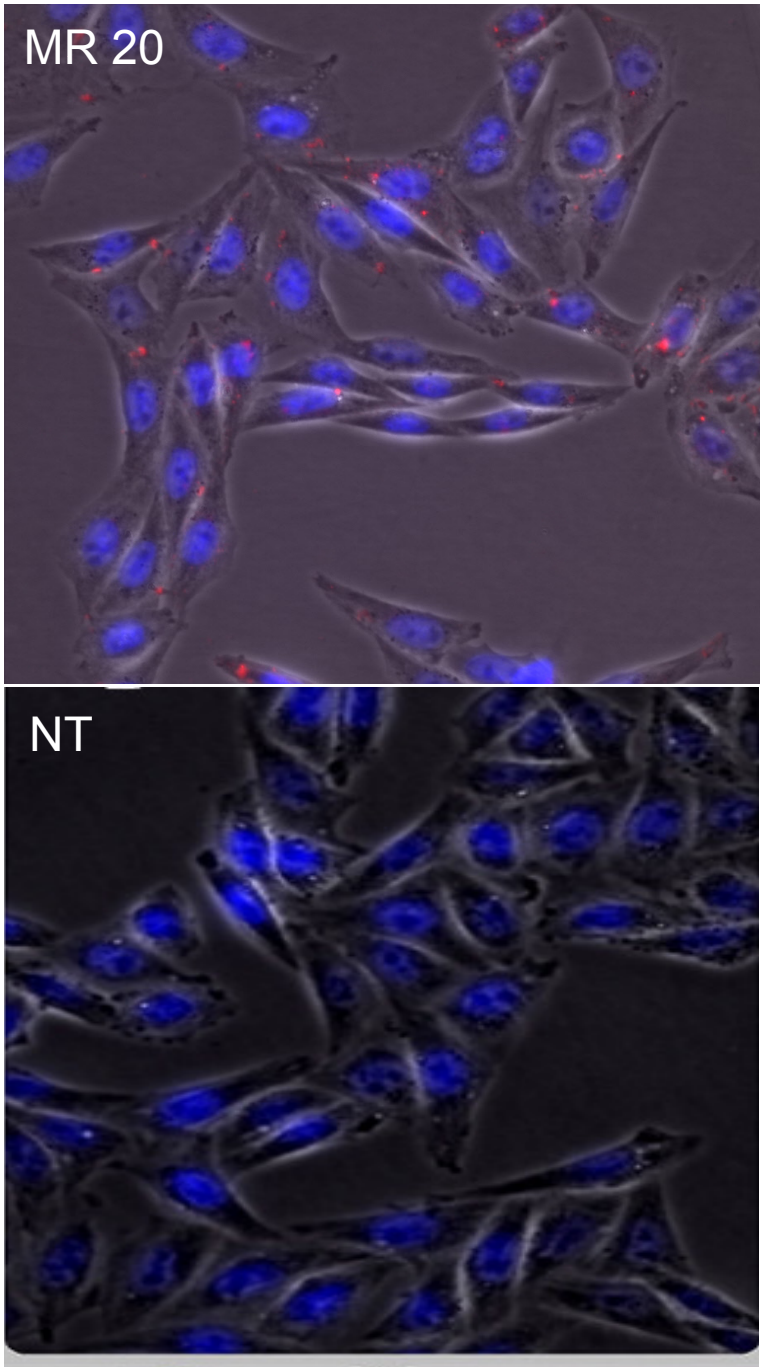

Figure 3.6. The fluorescence microscopy image of C6M3-siRNA complexes at molar ratio 20/1 (magnification: 40x). The red fluorescence indicated Cy3-labeled siRNA, blue fluorescence represented DAPI stained nuclei. The lower panel was non-treated (NT) cells, used as a control. siNRA concentration was at 100 nM.

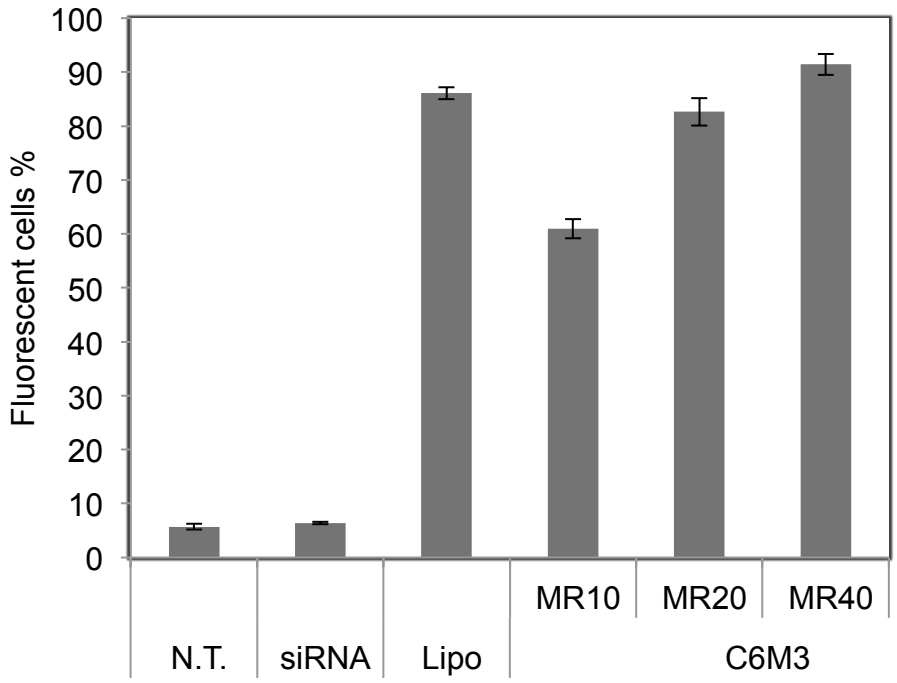

Figure 3.7. Cellular uptake of Cy3-labeled siRNA. Non-treated (N.T.) sample was negative control; Lipo = Lipofectamine 2000, was positive control (1 ul of Lipo/well). MR = molar ratio (peptide/siRNA). siRNA concentration was at 100 nM.

3.3.4 *In Vitro* Transfection

The efficiency of GAPDH gene silencing by C6M3-siRNA complexes at the mRNA level was investigated using qRT-PCR. Lipofectamine 2000 was used as the positive control. As shown in Figure 3.8, the Lipofectamine 2000-siRNA complexes induced the silencing of GAPDH gene by 84%, and the C6M3-siRNA complexes at 40/1 achieved 69% GAPDH gene silencing efficiency. The significant silencing efficiency of GAPDH gene induced by C6M3-siRNA complexes implied that the C6M3 peptide could effectively deliver bioactive siRNA into the cytosol and induce specific gene silencing.

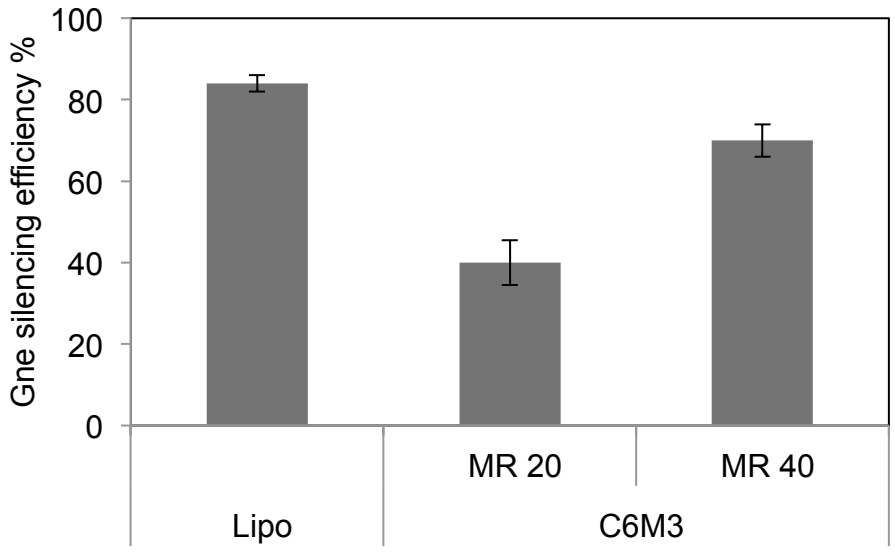

Figure 3.8. qRT-PCR analysis of GAPDH gene in CHO-K1 cells. GAPDH siRNA concentration was 100 nM. NT= non-treated sample, Lipo=Lipofectamine 2000, MR= peptide/siRNA molar ratio.

3.4 Discussion

Here, we evaluated the ability of C6M3 to form complexes with siRNA and deliver siRNA to the cytosol with concomitant silencing of GAPDH expression. Based on the data of ITC and zeta potential, the complex formation is not only involving electrostatic force but also hydrophobic interaction. To investigate whether this complex formation could promote internalization of the peptide-siRNA complexes, FACS, a quantitative method using fluorescently labeled siRNA, was performed. Interestingly, with the increase of molar ratios from 10/1 to 40/1, the uptake efficiency of siRNA increased. The possible reasons are that at higher molar ratios, the peptide-siRNA complexes display higher positive charge resulting in stronger affinity with the negatively charged cell membrane and higher contents of tryptophan enhancing the peptide-membrane interaction.

The modification of C6 has resulted in the following changes. With the same siRNA concentration, siRNA molecules were entirely associated with C6M3 at a molar ratio of 10/1,

while a very small amount of free siRNA was observed when interacting with C6 at a molar ratio of 10/1. This result is further confirmed by the zeta potential data. At a molar ratio of 10/1, C6M3-siRNA complexes exhibited a slight positive surface charge (0.4 mV), while C6-siRNA complexes obtained a negative surface charge (-13.1 mV). Moreover, C6M3-siRNA complexes showed smaller particle sizes (70-100 nm) than C6-siRNA complexes (170-260 nm). The ITC data showed that both C6 and C6M3 could spontaneously form complexes with siRNA. However, a higher value of Gibbs free energy was observed when titrating siRNA with C6M3 (-50 kJ/mol) than with C6 (-40 kJ/mol), suggesting the interaction of siRNA and C6M3 is highly favorable. In water, C6M3 adopted helical secondary structure, while C6 adopted random coil structure. This conformational change may facilitate C6M3 forming complexes with siRNA more efficiently with relatively small particle sizes due to the defined helical secondary structure.

C6M3-siRNA complexes exhibited particle size ~100 nm in water and ~200 nm in Opti-MEM. Previous studies show that particles with the size range from 50 nm to 200 nm usually enter cells through caveolae and clathrin mediated endocytotic pathway [74]. Fluorescence microscopy images of C6M3-Cy3-labeled siRNA complexes (Figure 3.6) also indicated the complexes entered cells possibly through endocytotic pathway [95]. Previous studies showed that histidine residues were incorporated in CPPs to enhance the endosomal escape of siRNAs [108,109]. Due to the pH drop in endosome, the imidazole ring of histidine was protonated. The protonation induced an extensive inflow of water and ions into the endosomal environment, thereby resulting in disruption of the endosomal membrane and release of the entrapped components [87]. Taken together, the incorporation of tryptophan and histidine in C^M3 sequence led to over two-fold increase of GAPDH silencing efficiency , compared to that of C6-siRNA complexes (25%), confirmed by the aRT-PCR analysis. Additionally, Effective *in vivo* RNAi was achieved in a human non-small lung tumor xenograft model through intratumor injection of the C6M3-Bcl-2 siRNA complexes (molar ratio: 60/1). This treatment induced marked tumor suppression, with an inhibition rate of 55%, through suppression of antiapoptotic Bcl-2 protein in mice. [110]

3.5 Conclusions

C6M3, an 18-mer-amphipathic peptide, formed complexes with siRNA exhibiting particle sizes from 50 nm to 220 nm. C6M3 adopted helical secondary structure in water and became more so upon binding to siRNA. Zeta potential and agarose gel experiments proved that siRNA molecules were completely associated with C6M3 at a molar ratio of 10/1. ITC data revealed that the stoichiometry between C6M3 and siRNA is 7/1, which is consistent with the theoretical value considering each peptide consists of 6 positive charge residues (R) and siRNA contains 21 negative charge base pairs. However, FACS results revealed that higher molar ratios were required to achieve better siRNA uptake efficiency. GAPDH gene silencing experiment and cell viability data showed that C6M3-siRNA complexes induced 69% silencing of GAPDH gene with minimal cytotoxicity (<10%). These data demonstrate that C6M3 is a promising carrier for siRNA delivery and the modification strategy is useful.

Chapter 4[†]

Design and Characterization of A New Peptide GL1 for Short Interfering RNA Delivery

Abstract

RNA interference holds tremendous potential as one of the most powerful therapeutic strategies. However, the properties of short interfering RNA (siRNA), such as hydrophilicity, negative charge, and instability in serum have limited its applications; therefore, significant efforts have been undertaken to improve its cellular uptake. Cell penetrating peptides have been utilized to deliver various biologically active molecules, such as proteins, liposomes, nanoparticles, peptide nucleic acids, and recently small interfering RNAs. Here, we introduce a new cell penetrating peptide GL1(Ac-GLWRAWLWKAFLASNWRRLLRLLR-NH_2) to improve the intracellular uptake of siRNA. This peptide consists of four tryptophan residues that facilitated its binding with the cell membrane, five arginine residues and one lysine residue which are positively charged at physiological pH, which induced the formation of peptide-siRNA complexes and enhanced the affinity of the peptide and cell membrane. Moreover, GL1 adopted helical secondary structure due to the altered distribution of polar and nonpolar residues in the sequence. In this study, we investigated the effect of peptide/siRNA molar ratio on the particle size, surface charge, secondary structure, and uptake efficiency. The results showed that GL1 formed stable complexes with siRNA mainly through electrostatic interaction and hydrophobic interaction, and the complexes displayed a spherical shape with the size of ~100 nm and positive surface charge. Utilizing the techniques of fluorescence microscopy and flow cytometry, the intracellular localization of

[†] This chapter is based on a paper. B. Chen, W. Xu, R. Pan, P. Chen. Design and Characterization of A New Peptide Vector for Short Interfering RNA Delivery. Journal o Nanobiotechnology, 2015, accepted.

Cy3-labeled GAPDH siRNA was visualized and the cellular uptake was quantified. It is worth noting that in the serum free environment, compared to Lipofectamine 2000, GL1 achieved higher cellular uptake of siRNA (~95%); in the presence of serum, GL1 retained the same level of siRNA cellular uptake (~84%) as Lipofectamine 2000. In addition, the viability of cells treated by GL1 in all studied molar ratios was >85%, which was significantly higher than that treated by Lipofectamine 2000 (~70%). Taken together, the peptide GL1 demonstrated promise as a siRNA delivery system.

4.1 Introduction

The discovery of RNA interference (RNAi) has changed the field of gene therapy. RNAi is a post-transcriptional gene silencing process that can specifically and potently knock down the expression of target genes both in vitro and in vivo [31,111]. RNAi can be induced by short interfering RNA (siRNA). siRNAs are double stranded RNA fragments with 21 to 23 nucleotides that are capable of inducing the cleavage of mRNAs with the complementary sequence [31,111,112]. It is currently accepted that RNAi is one of the most important strategies for sequence-specific gene silencing in basic research and a potentially powerful therapeutic treatment for various human diseases [113],[114]. However, siRNA induced RNAi at cellular level is limited by its poor cellular uptake associated with low permeability of the cell membrane to RNA [115]. Thus, an effective and safe transport system to condense and deliver synthesized siRNA into cells is mandatory. During the last two decades, a new family of peptides known as cell-penetrating peptides (CPPs) were identified and thoroughly studied. CPPs present the ability to cross cellular membranes by a remarkably low toxic process and to promote the cellular internalization of biomolecules such as peptides, proteins, nucleic acids, peptide nucleic acids (PNA), liposomes, and nanoparticles [116–119]. However, the efficacy of siRNA delivery mediated by CPPs remains unsatisfactory, mainly due to the insufficient delivery efficiency, cytotoxicity, and/or sensitivity to the medium [115].

In order to increase the potency of such vectors, we designed a new peptide GL1. The following criteria were considered for the peptide design and its sequence contains: (1) hydrophobic residues, such as tryptophan, to facilitate membrane binding owing to its strong preference for the lipid membrane interfacial region [120]; (2) cationic residues, such as arginine and lysine, to assist the formation of peptide-siRNA complexes and peptide-membrane interactions through electrostatic interaction and hydrogen bonding [120]; (3) altered distribution of the polar and nonpolar residues, to achieve better interaction with the cell membrane due to the formation of helical secondary structure [121]. The prevailing hypothesis is that the cationic peptide GL1 electrostatically complexes with the anionic siRNA to produce a neutral or positively charged complex that has sufficient stability to allow intracellular delivery of siRNA. In this study, we investigated the physicochemical characteristics of GL1 when interacting with siRNA and evaluated the effect of its physicochemical characteristics on siRNA delivery efficiency and cytotoxicity. Chinese hamster ovary (CHO-K1) cells are a cell line derived from the ovary of the Chinese hamster and often used in studies of genetics, toxicity screening, and nutrition and gene expression because of its rapid growth rate. Thus, CHO-K1 was used as a model system to test the biological responses for siRNA delivery in this study.

4.2 Materials & Methods

4.2.1 Materials

The GL1 peptide (Ac-GLWRAWLWKAFLASNWRRLLRLLR-NH_2) with a molecular weight of 3123.8 g/mol, was synthesized by CanPeptide Inc. (Quebec, CA) with 95% purity. Cy3-labeled GAPDH siRNA was purchased from Ambion (SilencerTM GAPDH siRNA kit). The siRNA targeting sequence for eGFP (GCGACGUAAACGGCCACAAGU) was purchased from Dharmacon. The sense sequence is GACGUAAACGGCCACAAGUUC and the antisense sequence is ACUUGUGGCCGUUUACGUCGC. The negative control siRNA used here was purchased from Ambion. The MTT (3-(4,5-dimethylthiazol-2-yl)-2,5-

diphenyltetrazolium bromide, a yellow tetrazole) assay kit was purchased from Sigma-Aldrich (Oakville, CA).

4.2.2 Methods

4.2.2.1 Cell Line

Chinese hamster ovary (CHO-K1) cells were purchased from American Type Culture Collection (ATCC CCL-61). The cells were cultured in F-12K medium (Thermo Scientific, Ottawa, Canada) with 10% fetal bovine serum (FBS) (Sigma-Aldrich, Oakville, Canada). The cells were incubated at 37ºC in a humidified atmosphere with 5% CO_2.

4.2.2.2 Preparation of GL1 and GL1-siRNA complexes

The preparation of GL1 and GL1-siRNA complexes followed the same procedures as presented in chapter 3.

4.2.2.3 Gel Electrophoresis

This experiment followed the same procedures as presented in chapter 3.

4.2.2.4 Isothermal Titration Calorimetry (ITC)

The isothermal titration calorimetry experiments were conducted using a Nano-ITC calorimeter (TA Instruments). A 500 μM GL1 peptide solution and a 10 μM siRNA solution were both prepared in RNase-free water. This experiment followed the same procedures as presented in chapter 3.

4.2.2.5 Size and Zeta Potential Measurements

Particle size measurements were done with a Zetasizer Nano ZS (Malvern, United Kingdom) with transparent ZEN0040 disposable microcuvette cells (40 μl) at 25°C. The GL1-siRNA samples were prepared as mentioned above with a siRNA concentration of 100nM. The zeta potentials were measured in a Clear DTS1070 zeta dip cell with the same machine. For zeta potential measurement in serum conditions, GL1-siRNA complexes were freshly prepared and diluted 1:10 with F12K+10% FBS. The complexes were incubated in a serum-supplemented medium for 10 min before the measurement.

4.2.2.6 Scanning Electron Microscopy (SEM)

This experiment followed the same procedures as presented in chapter 3.

4.2.2.7 Circular Dichroism (CD) Spectroscopy

This experiment followed the same procedures as presented in chapter 3.

4.2.2.8 Fluorescence Microscopy and Fluorescence-Activated Cell Sorting (FACS)

This experiment followed the same procedures as presented in chapter 3. Images were taken with an inverted fluorescence microscope (Zeiss AxioObserver Z1, CA) and analyzed using AxioVision software.

The uptake of Cy3-labeled siRNA into the CHO-K1 cells was quantified with a BD FACSVantage SE Cell Sorter flow cytometry (BD Biosciences, United States). This experiment followed the same procedures as presented in chapter 3.

4.2.2.9 *In vitro* gene silencing efficiency

CHO-K1 cells were seeded at 3,5000 cells/well in 24-well plates and incubated for 24 h. Next, the cells were incubated with various complex formulations in Opti-MEM at 37^{o}C for 4 h. Then, the cells were incubated for an additional 48 h in complete culture medium with siRNA concentration of 50 nM. To determine the serum effect on gene silencing efficiency, the cells were directly incubated with various complex formulations in complete culture medium for 52 h and then prepared for analysis.

For qRT-PCR analysis, the total RNA was extracted from the treated cells using the SV Total RNA Isolation System (Promega, CA, USA). A Nanodrop (Nanodrop spectrophotometer ND-1000, Thermo Scientific, Ottawa, CA) was used to determine the RNA concentrations. The RNA samples were reverse-transcribed into cDNA using a Bio-Rad iScript cDNA synthesis kit according to the manufacturer's protocol. After the cDNA was synthesized, PCR was performed with Brilliant II fast SYBR Green QPCR Master Mix (Agilent Technologies, Wilmington, DE, USA) using an Mx3005P^{TM} real time PCR System (Agilent Technologies). The sequences of the primers used for the mouse GAPDH gene are 5'-TTGCTGTTGAAGTCGCAGGAG-3' and 5'-TGTGTCCGTCGTGGATCTGA-3'

(Sigma, Oakville, Ontario, Canada). Cyclophilin, a house-keeping gene, was used as an internal control to normalize the GAPDH gene expression. Mouse cyclophilin mRNA amplified using the following primers: 5'-AGGGTTTCTCCACTTCGATCTTGC-3' and 5'-AGATGGCACAGGAGGAAAGAGCAT-3' (Sigma, Oakville, Ontario, CA).

4.2.2.10 Cytotoxicity Assay

The cytotoxicity of peptide-siRNA complexes was determined by the MTT assay. In brief, cells were seeded at 5,000 cells/well in clear, flat-bottomed, 96-well plates (Costar) 24 h before treatment. After being washed, 100 μl of Opti-MEM that contained peptide-siRNA complexes at different molar ratios was added to the wells and incubated for 4 h. Thereafter, 50 μl of 30% serum containing medium was added, and the cytoxicity of the relevant reagents was determined by the MTT assay after 48 h. The absorbance at 570 nm was read on a plate reader (FLUOstar OPTIMA, BMG, Germany). The background absorbance of the multiwell plates at 690 nm was determined and subtracted from the 570 nm measurement. The results obtained from triplicate wells were averaged and normalized to the value obtained from the non-treated cells.

4.3 Statistical Analysis

Results were expressed as mean values ± SD. Data were analyzed by two tailed T test and only p-values < 0.05 were considered statistically significant.

4.4 Results & Discussion

4.4.1 Effect of Peptide to siRNA Molar Ratio on Complex Formation

The ability of GL1 to interact with siRNA was investigated by gel electrophoresis. Binding between peptide and siRNA prevented RNA from being stained by EtBr. As shown in Figure 4.1, as molar ratio increased, the intensity of siRNA decreased sharply due to the formation of GL1-siRNA complexes. At molar ratio 10/1, the intensity of siRNA was significantly low. At a slightly higher molar ratio 15/1, no free siNRA was detected on the agarose gel. This

result indicated that the minimal molar ratio for siRNA delivery was around 10/1. This direct binding between cationic peptide and anionic siRNA would be initiated via electrostatic interactions. The formation of GL1-siRNA complexes and the thermodynamic parameters associated with the binding between peptide and siRNA was further investigated using isothermal titration calorimetry by titrating the siRNA with GL1. The heat exchange during the titration of siRNA by GL1 (in RNase-free water) was detected by the machine and output as raw data. By fitting the raw data (upper panel of Figure 4.2) to a single-site model (lower panel of Figure 4.2), the thermodynamic parameters during the interaction were obtained and listed in Table 4.1.

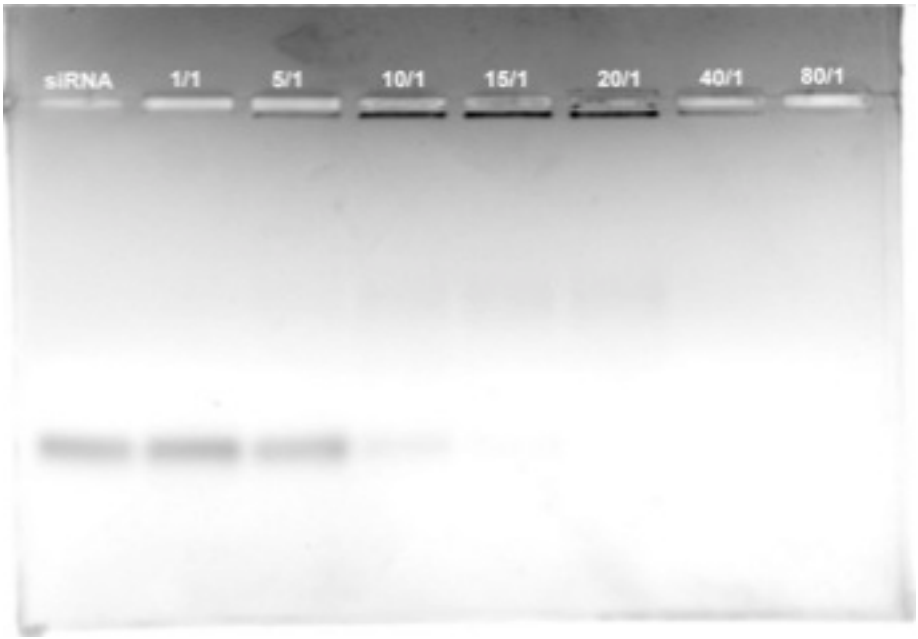

Figure 4.1. Binding ability of siRNA to GL1 studied by agarose gel-shift assay The formed GL1-siRNA complexes, stained with ehidium bromide, were investigated by electrophoresis on agarose gel (1.2% wt/vol). siRNAs, targeting eGFP genes, were complexed with GL1 at a series of molar ratios from 1/1 to 80/1. Lane 1 was siRNA control, and lanes 2-8 indicated correlated molar ratios. The amount of siRNA was 300 ng.

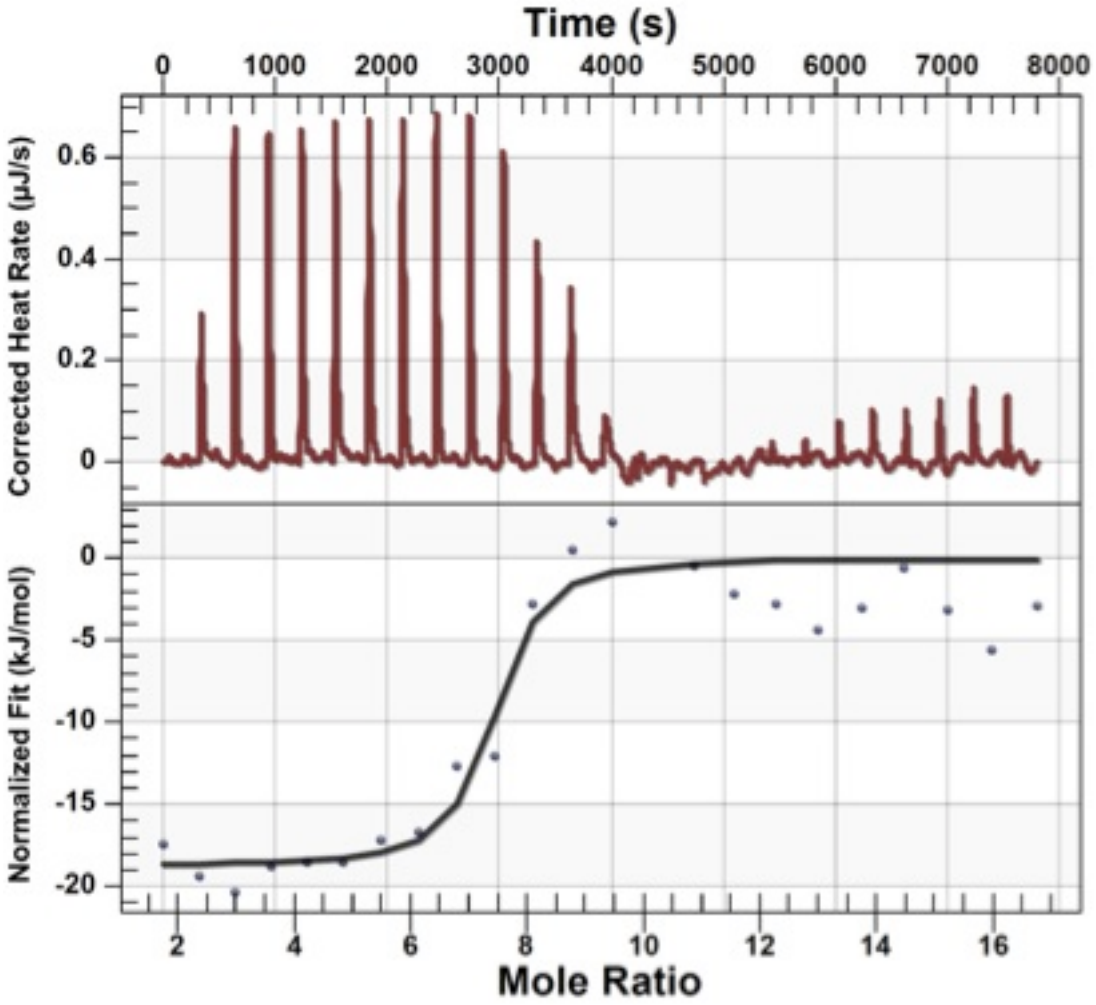

Figure 4.2. Calorimetric titration of siRNA with GL1 at 25 ^{o}C in RNasefree water at pH 6. (a) Corrected thermogram of calorimetric titration of siRNA with GL1, (b) Binding analysis of siRNA with GL1 by fitting the raw data with an independent model. GL1 concentration was 500 µM and siRNA concentration was 10 µM.

Table 4.1. Thermodynamic parameters when titrating siRNA with GL1 in water.

Ka (1/M)	ΔH (kJ/mol)	n	K_d (M)	ΔS (J/(mol·K))
$4.47 \cdot 10^{8}$	-18.71	7.16	$2.24 \cdot 10^{-7}$	64.56

GL1 represents high affinity for siRNA with the dissociation constant of 2.24E-7 M. The obtained molar stoichiometry was 7.16, which implied that 7.16 moles GL1 could condense 1 mole siRNA. Theoretically, 7 moles GL1 could condense 1 mole siRNA, since the GL1 peptide contains 6 positively charged residues (Arginine and Lysine) and the siRNA molecule consists of 21 pairs of negatively charged nucleotides. The experimental data was consistent with the theoretical value. In the ITC experiment, due to the stirring throughout the titration process, peptide and siRNA could interact to its full extent. However, in the gel experiment, the peptide and siRNA solution was mixed first and then incubated for 20 min without further mixing. The difference in the experimental settings leads to the slight difference in the molar stoichiometry. With an enthalpy of -18.71 kJ/mol, ΔS of 64.56 J/(mol·K), and entropy of -19.24 kJ/mol, the binding was entropy-driven, but enthalpy was also a major factor. Moreover, through calculation using the equation $\Delta G=\Delta H-T\Delta S$, ΔG was -37.94 kJ/mol indicating that the formation of GL1-siRNA complexes was a thermodynamically favored process [102,103].

4.4.2 Particle Size and Zeta Potential

Considering that particle size and zeta potential are important characteristics of delivery systems associated with the delivery efficiency [122], dynamic light scattering was applied to gain a view of the physicochemical properties of GL1-siRNA complexes. It has been reported that 200 nm is the approximate limit for cellular uptake by macropinocytosis and

nanoparticles larger than 200 nm may hinder its cellular internalization [123,124]. As shown in Figure 4.3a, particle sizes remained in the range of 80-100 nm, which fell in the range suitable for cellular uptake. Interestingly, at molar ratio 40/1, particle size slightly decreased. Previous studies prove that as molar/charge ratio increased, stronger electrostatic repulsion between complexes occurs, leading to smaller nanoparticles [104,125]. The other possible reason is that excess peptides formed smaller nanoparticles, thus decreased the average size. It is generally accepted that nanoparticles with positive surface charge induce uptake via electrostatic interaction with the anionic cell membranes [126]. Figure 4.3b shows that at molar ratio 20/1 and 40/1, nanoparticles displayed positive surface charge and the absolute values increased at higher molar ratio due to the addition of more cationic peptides. This positive surface charge allows interaction of GL1-siRNA complexes with the polyanionic glycosaminoglycans on the cell surface [127]. However, in serum-containing media, GL1-siRNA complexes exhibited a negative surface charge, indicating that serum proteins interacted with the outer layer of the complex and induced a negative surface charge. This result suggests that in serum conditions the uptake of GL1-siRNA complexes may be mediated by scavenger receptors, which were involved in the cellular uptake of negatively charged macromolecules [128].

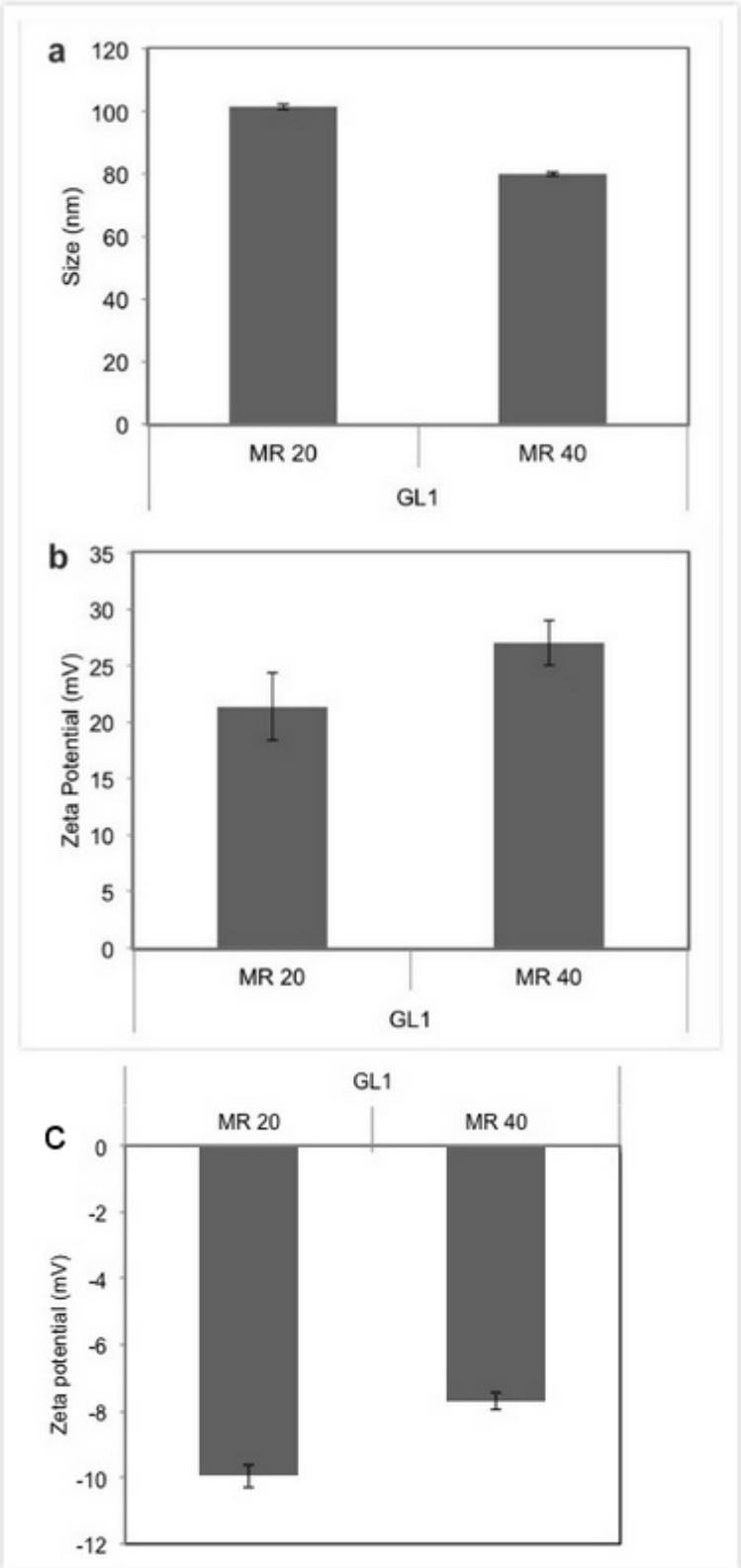
a
120
100
80
60
40
20
0
Size (nm)
MR 20
MR 40
GL1
b
35
30
25
20
15
10
5
0
Zeta Potential (mV)
MR 20
MR 40
GL1
c
GL1
MR 20
MR 40
0
-2
-4
-6
-8
-10
-12
Zeta potential (mV)

Figure 4.3. (a) The hydrodynamic diameter and (b) zeta potential of the GL1-siRNA complexes prepared in RNase free water at different molar ratios were measured by dynamic light scattering (DLS); (c) zeta potential of the GL1-siRNA complexes in serum-supplemented F12K media. The siRNA concentration was fixed at 100 nM. At different molar ratios, the amount of GL1 was adjusted. Results are expressed as mean ± standard deviation (n=3).

4.4.3 Morphology and Secondary Structure

Moreover, Figure 4.4a shows the morphology of the GL1-siRNA complexes formed at molar ratio 40/1 observed under SEM. The SEM image shows that GL1 and siRNA form spherical nanoparticles with the size less than 100 nm. As shown in Figure 4.4b, The CD-spectrum of GL1 is characterized by a maximum at 190 nm, a minimum at 207 nm, and a slight shoulder at 220 nm which implies that GL1 adopts α-helical structure. Upon adding siRNA to retain the peptide/siNRA molar ratio 10/1, GL1 CD-spectrum displayed a minimum at 210 nm, a maximum at 190 nm, a slight shoulder at 220 nm, and the absolute values of the minimum and maximum increased, which reveals that GL1 adopts a higher content of α-helical structure. Adding more siRNA to retain the peptide/siRNA molar ratio at 5/1, GL1 represented a similar CD-spectrum and the absolute values of the minimum and maximum further increased. Similar phenomena have been reported for other CPPs [129] and this conformational change is due to the presence of anionic component, siRNA, which can screen the positive charge of arginine residues in one face of the helical structure, thus, forming a stable helical structure. This stable helical structure facilitates better interaction with cell membranes and enhances cellular internalization [106].

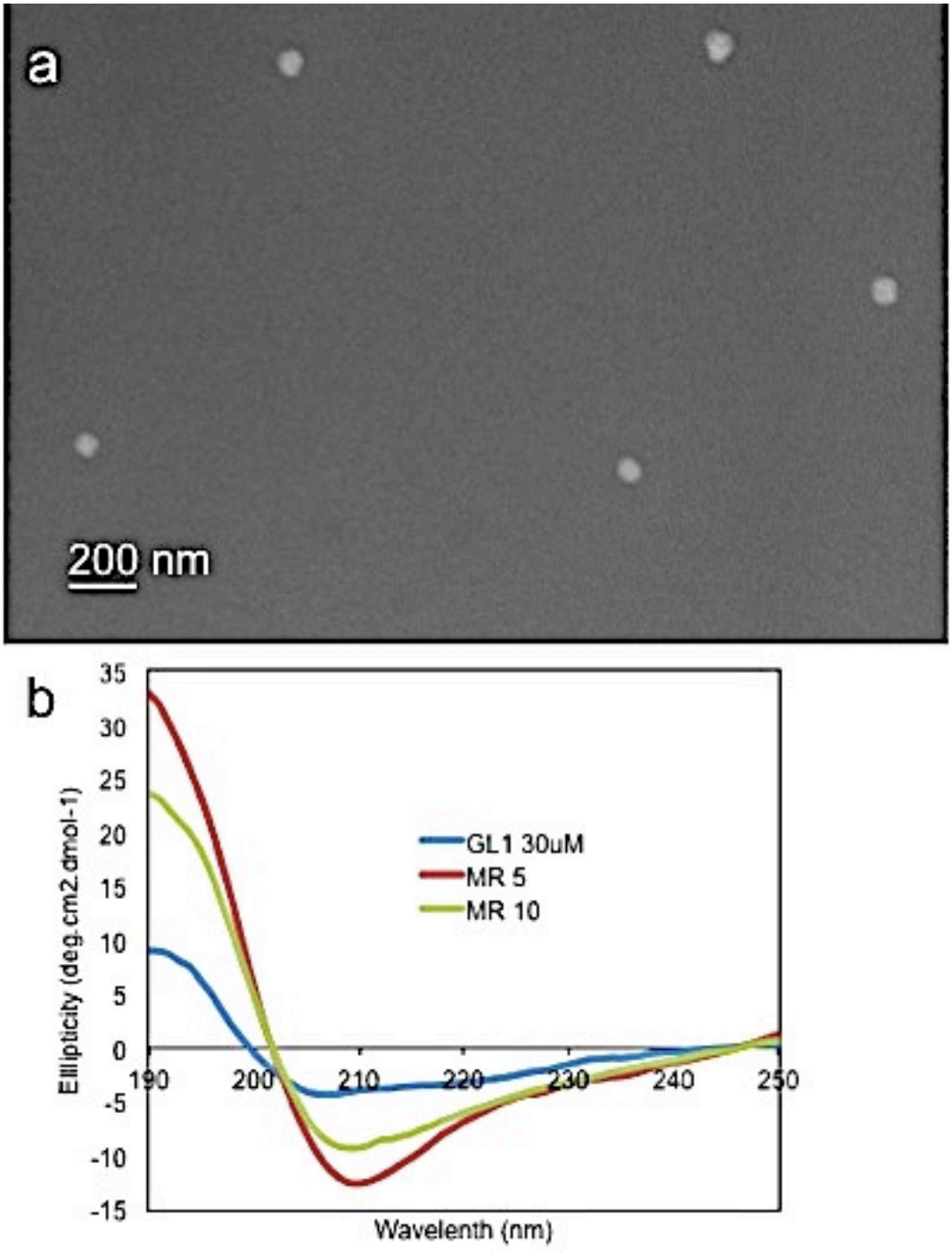

Figure 4.4. (a) SEM image of GL1-siRNA complexes at molar ratio 40/1, siRNA concentration was 100 nM. (b) CD spectra of GL1 alone and GL1-siRNA at different molar ratios. GL1

concentration was fixed at 30 μM and GL1-siRNA complexes were formulated at molar ratios of 5/1 and 10/1.

4.4.4 Cellular Uptake and Localization of siRNA Complexes

The cellular localization of siRNA was shown in Figure 4.5a. The siRNAs were localized in cytosol and to regions in close proximity to the nuclear membrane and were distributed in a non-homogeneous pattern at the periphery of the nucleus. Previous studies demonstrated that localization of siRNA [130], Dicer [131], and RNAi activity [132] was restricted to the cytoplasm and siRNA entry into living cells was localized to perinuclear regions [53]. Our data indicating that siRNA localization was perinuclear (Figure 4.5a, upper panel) was in consonance with the previous studies.

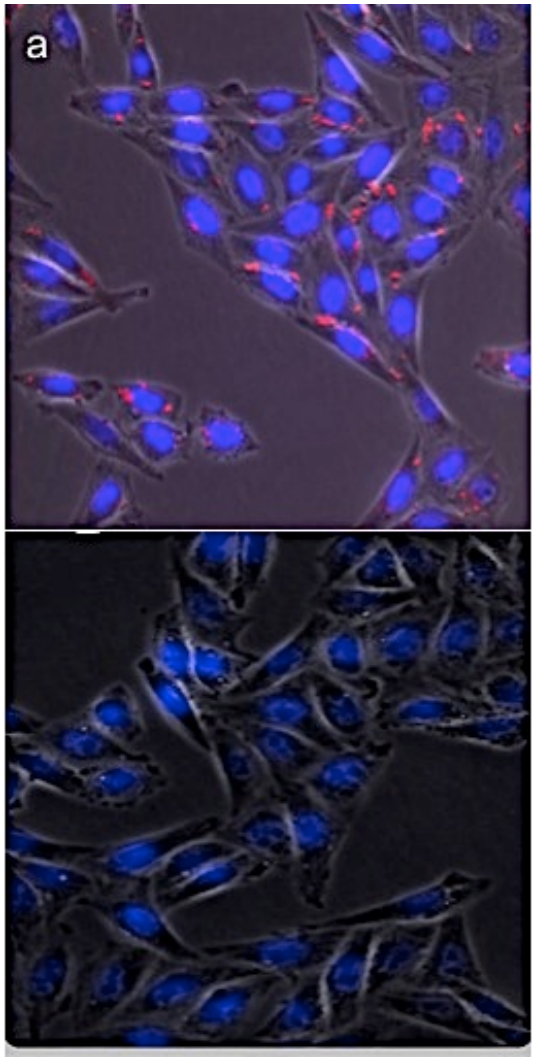
a

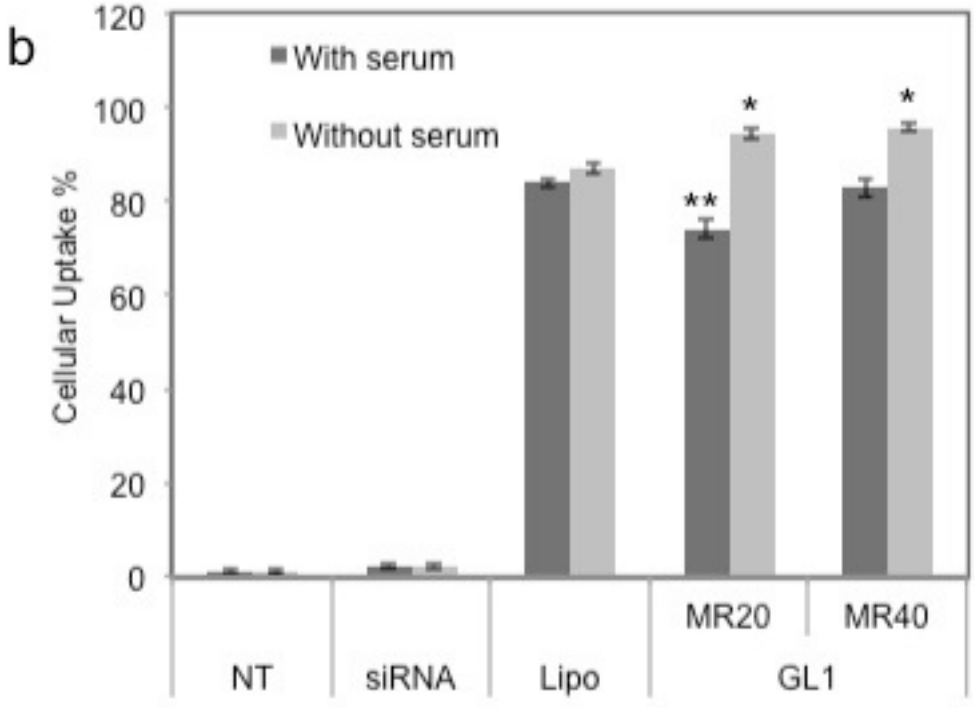
b
120
100
80
60
40
20
0
Cellular Uptake %
With serum
Without serum
**
*
*
MR20
MR40
NT
siRNA
Lipo
GL1

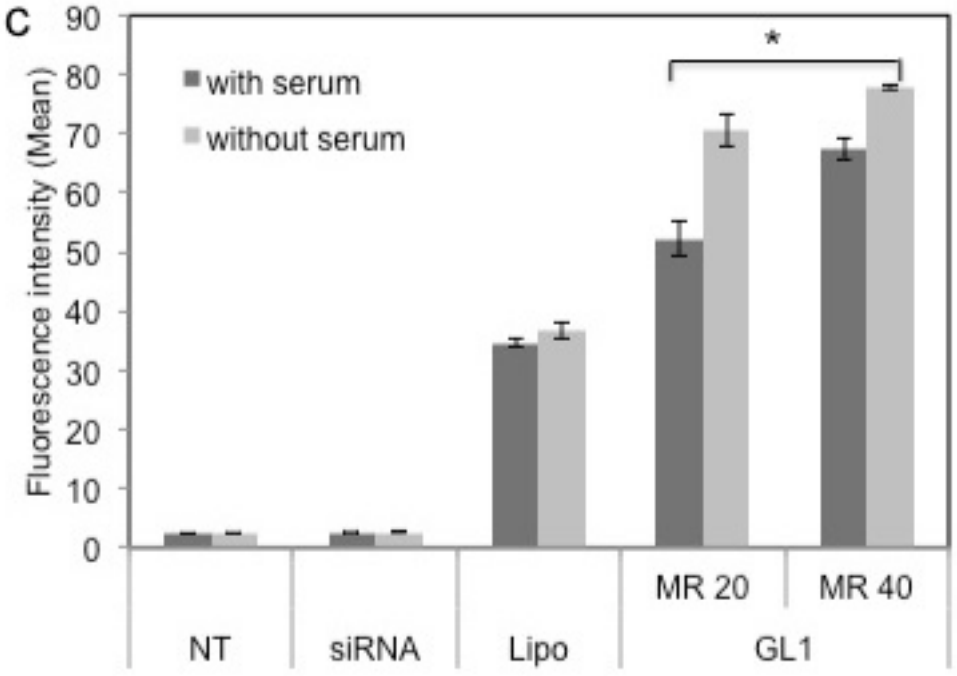
c
90
80
70
60
50
40
30
20
10
0
Fluorescence intensity (Mean)
with serum
without serum
*
MR 20
MR 40
NT
siRNA
Lipo
GL1

Figure 4.5. (a) Fluorescence microscope image of GL1-siRNA complexes at molar ratio 40/1 (magnification: 40x). The red fluorescence indicated Cy3 labeled siRNA, blue fluorescence represented DAPI stained nuclei. The lower panel was non-treated cells, used as a control. (b) FACS results of cellular uptake of siRNA. * P value<0.05, in a serum free environment, the uptake of siRNA at molar ratios of 20/1 and 40/1 is significantly different from that after Lipo treatment. ** P value<0.05, in a serum environment, the uptake of siRNA at a molar ratio of 20/1 is significant from that at a molar ratio of 40/1 and after Lipo treatment. (c) Relative fluorescent intensities at different treatment conditions. * P value <0.05, the fluorescence intensity at molar ratios of 20/1 and 40/1 with or without serum is significantly different from that after the other treatments. Non-treated sample was negative control; Lipo-siRNA complexes were positive control. Cy3 labeled GAPDH siRNA was used here. siRNA concentration was 100 nM in both experiments. (N.T.= Non-treated, MR=peptide/siRNA molar ratio, Lipo=Lipofectamine 2000). Results are expressed as mean ± standard deviation (n=3).

siRNA cellular uptake was quantified by FACS. As shown in Figure 4.5b, c, either with or without the presence of serum, siRNA alone represented almost no uptake in CHO-K1 cells, which also confirmed the limitation of siRNA alone in cellular uptake. Without the presence of serum, peptide GL1 achieved 95% uptake of siRNA at molar ratio 20/1 and 40/1, which is higher than Lipofectamine 2000 (Lipo, 87%), one of the most efficient and commercially available transfection reagents. Due to the serum effect, the uptake of siRNA decreased to 75% (molar ratio 20/1) and 84% (molar ratio 40/1). However, at molar ratio 40/1, GL1 still achieved the same level of uptake as Lipo with the presence of serum. However, with or without serum, GL1-siRNA treated cells exhibited higher fluorescence intensity than Lipo and fluorescence intensity increased with the peptide/siRNA molar ratio. This result indicated that peptide GL1 could effectively protect siRNA and efficiently deliver siRNA to cells even in the presence of serum.

4.4.5 Gene Silencing Efficiency *In Vitro*

With or without serum, the GAPDH gene silencing efficiency induced by GL1-siRNA complexes (MR 40/1) at the mRNA level was investigated using qRT-PCR. Lipofectamine

2000 was used as a positive control. As shown in Figure 4.6, GL1-siRNA complexes at a molar ratio of 40/1 achieved 58% and 47% gene silencing efficiency with and without serum respectively. This result indicated that GL1 could efficiently deliver siRNA to cells and induced the specific gene silencing. With serum, gene silencing efficiency of GL1-siRNA complexes decreased compared to that without serum, respectively. This trend was consistent with the cellular uptake result. The Lipofectamine 2000-siRNA complexes induced 80% and 74% GAPDH gene silencing with and without serum. The possible reason that GL1-siRNA complexes did not achieve similar gene silencing efficiency was that the complexes were retained inside endosomes following endocytosis [133].

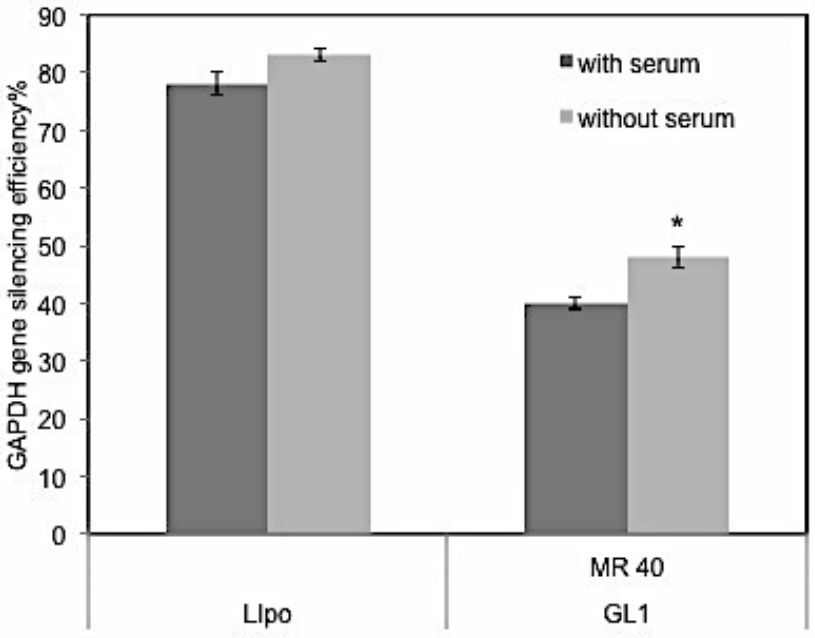

Figure 4.6. Gene silencing efficiency *in vitro*. Silencing of GAPDH gene in CHO-K1 cells was evaluated by quantitative real time polymerase chain reaction (qRT-PCR). GAPDH siRNA concentration was 50 nM. Lipo was the positive control, and scrambled siRNA was used as the negative control. Results are expressed as mean ± standard deviation (n = 3). * P value<0.05, the gene silencing efficiency at a molar ratio of 40/1 in a serum free environment is significantly different from the other treatments.

4.4.6 Cellular Toxicity

For a CPP to be a functional vector, it must achieve high uptake efficiency and exhibit low levels of cytotoxicity. It is well documented that the molar ratio of the positive vector to negative nucleic acid cargo affects toxicity and higher molar ratios may cause higher toxicity [134]. As shown in Figure 4.7, siRNA alone was not toxic. At molar ratio 10/1, GL1-siRNA complexes and GL1 alone did not cause toxicity. At molar ratio ≥ 20/1, viability of cells treated either with GL1-siRNA complexes or GL1 alone had a slight drop owing to relatively higher surface charge, but it was still above 85%. Moreover, Lipo alone and Lipo-siRNA complexes achieved lower cell viability ~70%. Thus, peptide GL1 showed attractive characteristics with regards to the criteria of cytotoxicity.

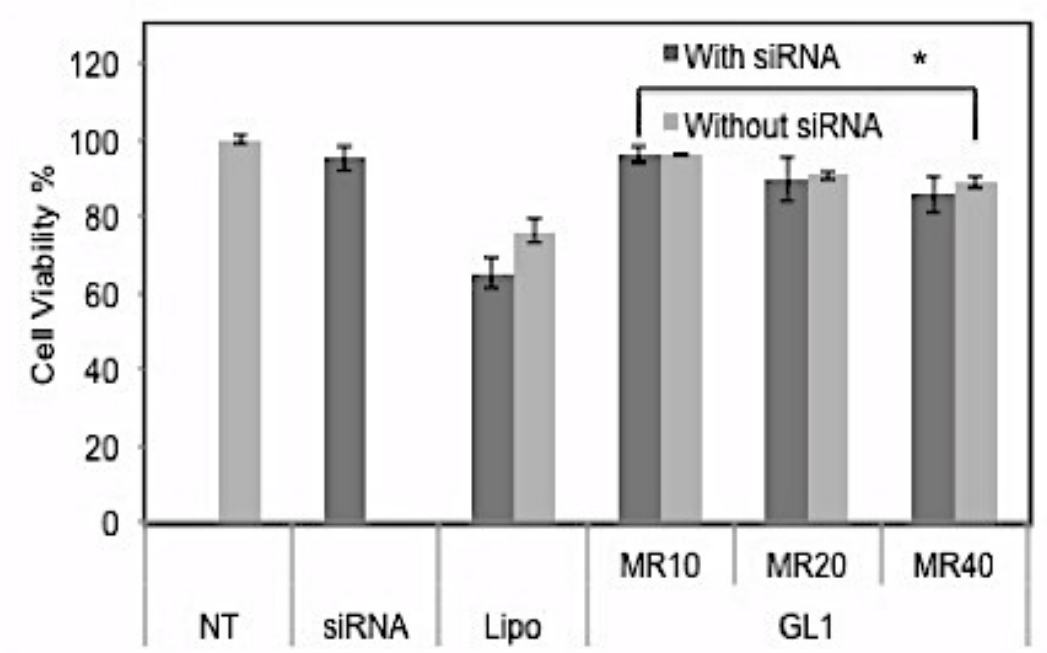

Figure 4.7. Cell viability results of CHO-K1 cells treated with naked Lipofectamine 2000 or GL1, and the complexes with siRNA (50 nM) at different molar ratios. (N.T.= Non-treated, MR=peptide/siRNA molar ratio, Lipo=Lipofectamine 2000). Results are expressed as mean ± standard deviation (n=3). * P value < 0.05, the cell viability after GL1 treatment is statistically significant than that after Lipo treatment.

Here, an amphipathic, cationic peptide GL1 was designed and investigated. Structurally, GL1 has dispersed cationic amino acids along the sequence, which differs from the arginine rich peptide R9, R9-hLF, and Tat [135]. The peptide MPG and MPG-like peptides consist of a hydrophobic domain and a hydrophilic domain which contributes to their amphipathic property [136,137]; while PF6 and PF14 incorporated a stearyl moiety in their sequences to improve amphiphilicity. However, peptide GL1 has hydrophilic and hydrophobic amino acids dispersed along the sequence, which leads to its amphipathity and helical secondary structure. Another significant difference of GL1 from the peptides mentioned above is that GL1 utilizes four tryptophan amino acids distributed along the sequence to enhance cellular uptake of GL1-siRNA complexes via strong peptide-membrane interaction. Gel electrophoresis results show that GL1 can form complexes with siRNA and encapsulate all the free siRNA at molar ratio 15/1. However, hLF, R9, R9-hLF, Tat, TP10, PF6, and PF14 require much higher molar ratio, near 50/1 to encapsulate all the free siRNA [135]. The ITC data further proved that GL1 had a strong affinity with siRNA (K_d = 2.24E-7 M) and the interaction of GL1 with siRNA was thermodynamically favored (ΔG = -37.94 kJ/mol). Additionally, a similar value of Gibbs free energy was reported in our previous study of an amino acid pairing peptide C6 [95]. CADY, a 20-residue secondary amphipathic peptide also encapsulated all the siRNA at molar ratio 15/1 and adopted helical secondary structure. Compared to GL1, CADY displayed even stronger binding affinity with siRNA (K_d: 0.152E-7 M) [138]. Interestingly, CADY enters cells not through the endosomal pathway but GL1 does, which may lead to the difference in the efficiency of intracellular release of siRNA.

The size of GL1-siRNA complexes slightly decreased from 100 nm to 80 nm when increasing the molar ratio from 20/1 to 40/1 possibly due to stronger electrostatic repulsion at higher molar ratio. Moreover, GL1-siRNA complexes displayed positive surface charge at a molar ratio of 20/1 (~ 21 mV). At a molar ratio of 40/1, due to the addition of more cationic peptide, GL1-siRNA complexes' surface charge increased to 27 mV. Interestingly, GL1 adopted a higher content of helical structure upon interaction with siRNA, possibly due to the decrease of the charge repulsion between cationic amino acids after partial positive charge was neutralized by anionic siRNA. The positive surface charge and secondary structure

change suggest that GL1 and siRNA form stable complexes mainly through the intermolecular binding and electrostatic interaction, which was consistent with some reported CPPs [139]. These favourable physicochemical characteristics lead to the significant cellular uptake of Cy3-labeled siRNA (95%), which is higher than Lipo (87%) in a serum free environment. In the presence of serum, GL1-siRNA complexes exhibited negative charge. This is possibly because excess anionic serum protein neutralizes the positive surface charge of GL1-siRNA complexes and displays negative charge. Due to the serum effect, cellular uptake of GL1-siRNA complexes dropped to 85%, which is still comparable to Lipo. Moreover, GL1-siRNA complexes induced 49% or 40% GAPDH gene silencing with serum or without serum respectively, with minimal cytotoxicity. Taken together, our experimental data strongly supported our hypothesis that the cationic peptide GL1 electrostatically complexes with the anionic siRNA to produce a positively charged complex that has sufficient stability to allow efficient intracellular delivery of siRNA and induce specific gene silencing efficiency. Note that GL1 delivered higher amount of siRNA to cells than Lipo but induced lower gene silencing efficiency than Lipo, possibly due to insufficient endosomal release of siRNA. Further modifications of GL1 to enhance endosomal release are required.

4.5 Conclusions

In this study, we have investigated the physicochemical characteristics of the peptide GL1, and evaluated its siRNA delivery efficiency and cellular toxicity on the CHO-K1 cell line. The major conclusions include the following: GL1 could form complexes with siRNA cargo at molar ratio ~10/1 mainly via electrostatic interaction and hydrophobic interaction; GL1 could spontaneously condense siRNA to form spherical particles with sizes on the nanoscale (80-100 nm); GL1 adopted α-helical secondary structure and became more so upon interaction with siRNA molecules to form stable complexes; at molar ratio 40/1, GL1 achieved higher cellular uptake of Cy3-labeled siRNA (95%) than Lipofectamine 2000 in serum free environment and retained the same level of uptake as Lipofectamine 2000 (84%) with the presence of serum; in all the studied molar ratios, GL1 achieved higher cellular

viability (>85%) compared to Lipofectamine 2000 (~70%). Therefore, GL1 demonstrated the potential for future applications as a vector for siRNA delivery.

Chapter 5‡

Peptide GL1 mediated siRNA Delivery in Multicellular Tumor Spheroids and its Therapeutic Effects *In Vivo*

Abstract

siRNAs have shown promise in silencing targeting gene expression in vitro, but this technique has not translated to the clinic for gene therapy. This is partly due to the difference in cell behavior in monolayer culture and in the three-dimensional culture, e.g., tumors, where the penetration and distribution of siRNAs are limited. The multicellular tumor spheroids (MCTS), an in vitro model representing a solid tumor, have been utilized as an improved model for evaluating siRNA carriers. We have previously reported that the peptide GL1 achieves significant siRNA delivery efficiency in monolayer culture. Therefore, we aimed to confirm whether GL1 could achieve similar efficacy as a siRNA delivery system in MCTS and in vivo. Here, we established the MCTS of Chinese hamster ovary cells and evaluated the penetration, efficacy and cytotoxicity of siRNAs delivered by the peptide GL1. The results showed that GL1 could efficiently deliver siRNAs to the MCTS and induced 50% GAPDH gene silencing efficiency with minimal cytotoxicity (<10%). The intratumoral injection of the GL1-Bcl-2 siRNA complexes in a mouse xenograft model induced a pronounced tumor growth inhibition rate (52.6%) through suppression of the antiapoptotic Bcl-2 protein. These data demonstrated the potential of GL1 as a siRNA carrier both in vitro and in vivo.

‡ This chapter is based on a manuscript. B. Chen, Y. Wu, W. Xu, Y. Yuan, P. Chen. GL1 Peptide mediated siRNA Delivery in Multicellular Tumor Spheroids and Therapeutic Effects *In Vivo*. Prepared submission to the Journal of Nanomedicine.

5.1 Introduction

RNA interference (RNAi) has been accepted as a general endogenous mechanism in many organisms to efficiently silence the expression of specific genes through the introduction of synthetic small interfering RNA (siRNA), whose sequence is complementary to the endogenous mRNA. [140] Theoretically, RNAi can be used to silence nearly any gene in the body through the appropriate design of siRNA, which broadens its therapeutic potential as compared to typical small-molecule drugs [111]. However, the nature of naked siRNA, such as large molecular weight, negative charge, and being prone to nuclease degradation have hindered the efficacy of siRNA therapeutics [141,142]. Thus, the development of safe and effective delivery systems to deliver siRNAs to the target tissues is critical.

Two common strategies for targeted delivery are: 1) active targeting, involving attachment of targeting moieties to the surface of carriers, such as antibodies [143]; and 2) passive targeting, based on the enhanced permeability and retention (EPR) effect (such as tumors, which have leaky blood vessels). The EPR effect involves two major components, first altered bio-distribution, where the nano-sized particles show differential accumulation in the tumor tissues reaching higher concentration than that in the plasma or other organs. The other aspect of the EPR effect is increased plasma half-life. Nano-sized particles exceed the limit of renal excretion threshold and escape renal clearance due to their relatively large sizes.

The investigation of carriers for siRNA delivery begins with in vitro testing. Such testing of delivery methods against target cells is generally performed in monolayer culture, multi-well plate-based cell culture formats [144]. However, due to the lack of appropriate physiological barriers presented in monolayer culture, the results gained from monolayer culture platforms often differ from the in vivo. Therefore, an in vitro model that is more physiological than monolayer culture is required for better prediction of siRNA delivery efficacy.

Platforms such as scaffolds, microfluidics, and hydrogels can produce 3D cell culture models for testing of gene/drug delivery and toxicity [145]. Spheroids are micro-scale, spherical cell clusters formed by self-assembly and also one of the most common and

versatile methods of culturing cells in 3D. The following features of spheroids make them a more physiological platform for siRNA delivery testing: 1) spheroids mimic the multicellular arrangement and extracellular matrix deposition that are found in vivo but absent in monolayer culture; 2) spheroids display sizeable cell-cell interactions such as tight junctions that are comparable to those in in vivo tissues; 3) as in vivo tissues, spheroids show the diffusional limits to mass transport of nanoparticles, nutrients and other factors; 4) due to nutrient and oxygen transport limitations, spheroids with radii of 200 μm and larger can develop zones of proliferating cells on the outer layers of the spheroids and quiescent cells on the inside, while significantly larger spheroids can also develop central necrosis present in many cancers. [146] Taken together, spheroids provide an improved model for testing siRNA delivery compared to conventional cell culture but the challenge is how to form and maintain spheroids of uniform size. A variety of methods for spheroid generation were reviewed in detail previously [146]. A very recently developed method to form spheroids utilizing the hanging drop method has attracted researchers' attention because of its simplicity, reproducibility, stability, and high throughput [147–149].

Previously, we have shown that our peptide GL1 demonstrated a strong potential as a siRNA delivery system in Chinese hamster ovary (CHO-K1) cells in monolayer culture. In order to further confirm its potential, we developed the CHO-K1 spheroids using the hanging drop method and evaluated the GAPDH gene silencing efficiency and cytotoxicity induced by GL1-siRNA complexes in the spheroid model. Moreover, the therapeutic efficacy of Bcl-2 siRNA delivered by GL1 peptide was evaluated in an animal xenograft model. The results elucidated the promise of GL1 as a safe and efficient siRNA delivery system both in vitro and in vivo.

5.2 Materials & Methods

5.2.1 Materials

The GL1 peptide (Ac-GLWRAWLWKAFLASNWRRLLRLLR-NH_2) with a molecular weight of 3123.8 g/mol, was synthesized by CanPeptide Inc. (Quebec, CA) with 95% purity.

Cy3-labeled GAPDH siRNA and GAPDH siRNA were purchased from Ambion (SilencerTM GAPDH siRNA kit). The negative control siRNA used here was purchased from Ambion. The WST-1 cell proliferation assay kit was purchased from Cayman Chemical.

5.2.2 Methods

5.2.2.1 Cell Culture

The culture of Chinese hamster ovary (CHO-K1) cells in this chapter followed the same procedures as presented in chapter 3.

5.2.2.2 Preparation of GL1 and GL1-siRNA complexes

The preparation of Gl1-siRNA complexes followed the same procedures as presented in chapter 3.

5.2.2.3 Generation of Tumor Spheroids from CHO-K1

When the confluence of CHO-K1 cells was greater than 85%, the cells were detached with trypsin/EDTA and counted using a haemocytometer. Dead cells were excluded from counting using 75% (v/v) trypan blue stain exclusion. Cells were seeded in F12-K medium supplemented with 10% (v/v) FBS at desired cell density (total volume 45 μl/well), in a 96-well hanging drop plate (3D Biomatrix). Cells were incubated at 37ºC in a humidified atmosphere with 5% CO_2.

5.2.2.4 Light Microscopy

Morphology of CHO-K1 spheroids was observed by light microscopy. The diameter of the spheroids at different seeding densities was measured under a light microscope on day 2, 4, 6, and 9. The measurement was done using 8 spheroids at each cell density from each time point.

5.2.2.5 Scanning Electron Microscopy (SEM)

CHO-K1 cells were seeded at 10,000cells/well in a 96-well hanging drop plate (3D Biomatrix) and incubated at 37ºC in a humidified atmosphere with 5% CO_2. After incubation of 72 h, cells formed a spheroid in each well. The spheroids were transferred to a round-bottom clear standard 96-well plate. The culture medium was then discarded and PBS was added to wash the spheroids twice. After discarding the PBS, 80 µl of 4% Glutaraldehyde (v/v, dissolving in PBS) was added to each well and the sample was incubated at 4ºC overnight. The next day, the solution was discarded and 80 µl PBS was added to wash the sample twice. The spheroids were then placed on a silicon wafer and dehydrated through a series of Ethanol solution at concentrations of 50%, 75%, 90%, and 95%. Lastly, the spheroids were allowed to air dry at room temperature. Before imaging, samples were coated with 10 nm-thick gold to achieve better conductivity. Finally, the samples were imaged under a LEO FESEM 1530 field-emission SEM at 5 kV.

5.2.2.6 Confocal Laser Scanning Microscopy

CHO-K1 cells were seeded at 50cells/well in a 96-well hanging drop plate (3D Biomatrix) and incubated at 37ºC in a humidified atmosphere with 5% CO_2. After incubation of six days, cells formed a spheroid in each well. After taking out 5 µl of culture medium from each well, 10 µl of Opti-MEM that contained GL1-Cy3 labeled- siRNA complexes at molar ratio 60/1 was added to the wells and incubated for 24h and 48h respectively. Thereafter the spheroids were transferred to a chamber. The culture medium was discarded and the spheroids were washed twice with PBS. Then the spheroids were fixed with 4% Paraformaldehyde (PFA) and incubated for 30 min at 37ºC. The PFA was removed and the spheroids were washed with PBS twice; DAPI was added at the end to stain the nuclei of cells. Then images were taken with Olympus Upright BX51 confocal microscope.

LIVE/DEAD Viability/Cytotoxicity Kit (calcein AM and ethidium homodimer (EthD-1), Invitrogen) was used to visualize the structure of CHO-K1 cellular spheroids. Calcein AM is a cell permeant dye used to stain live cells. In live cells, the nonfluorescent calcein AM is converted to a green-fluorescent calcein after acetoxymethyl ester hydrolysis by intracellular

esterases. EthD-1 was used to identify dead/dying cells as it exclusively enters cells with disrupted cell membrane to bind DNA and emit red fluorescence. CHO-K1 cells were seeded at 10000cells/well in a 96-well hanging drop plate (3D Biomatrix) and incubated at 37ºC in a humidified atmosphere with 5% CO_2. After incubation of six days, the LIVE/DEAD Viability/Cytotoxicity Kit was applied per manufacturer's instruction. Thereafter, cell spheroids were fixed following the procedure mentioned above. Images were taken with Olympus Upright BX51 confocal microscope.

5.2.2.7 Cytotoxicity

The cytotoxicity of peptide-siRNA complexes was determined by the WST-1 assay. In brief, cells were seeded at 10,000 cells/well in 96-well hanging drop plates (3D Biomatrix) 72 h before treatment. After taking out 5 μl of culture medium from each well, 10 μl of Opti-MEM that contained samples was added to the wells and incubated for 72 h. Thereafter cell spheroids were transferred to a clear, round bottom standard 96-well plate (Costar) and the cytotoxicity of each treatment was determined by the WST-1 assay. The assay is based on the enzymatic cleavage of the tertrazolium salt WST-1 to formazan by cellular mitochondrial dehydrogenases in viable cells. The absorbance at 450 nm was detected with a plate reader (FLUOstar OPTIMA, BMG, Germany). Each treatment included 6 replicates and the results were averaged and normalized to the non-treated group.

5.2.2.8 *In Vitro* Gene Silencing Efficiency

The GAPDH gene silencing efficiency of peptide-siRNA complexes was determined by qRT-PCR. Briefly, cells were seeded at 10,000 cells/well in 96-well hanging drop plates (3D Biomatrix) 72 h before treatment. After taking out 5 μl of culture medium from each well, 10 μl of Opti-MEM that contained samples was added to the wells and incubated for 72 h. Each treatment had five replicates. Thereafter cell spheroids with the same treatment were transferred to an 1.5 ml Eppendorf tube and centrifuged at 200 rcf for 5 min. The supernatant was removed and the pellet was washed with PBS twice. Then Trizol reagents were added for RNA extraction, followed by cDNA synthesis and PCR.

5.2.2.9 Human Non-small Lung Cancer Xenograft Tumor Model and Tumor Suppression Study[§]

Six-week-old male BALB/c nude mice were obtained from B&K Universal Group Limited (Shanghai, China). The mice were maintained under a 12-h light/dark cycle at 25°C with a humidity of 60±10%. The non-small-cell lung carcinoma-derived A549 cells were obtained from American Type Culture Collection (ATCC) and cultured in Dulbecco's Modified Eagle's Media-high glucose (DMEM) (Invitrogen) supplemented with 10% heat-inactivated fetal bovine serum (FBS) and 1% antibiotics (streptomycin + penicillin). The nude mouse animal model was established by subcutaneous inoculation of 5×10^6 A549 cells in the right axilla.

When the tumor volume reached 100-200 mm^3, the mice were randomly divided into five groups: model group, saline group, GL1 group, Bcl-2 siRNA group, GL1-Bcl-2 siRNA group and each group had 8 mice. The drugs were applied through intratumoral injection and low-dose multi-point injections. The treatments, a dose of 4 μg of siRNA per mouse, were given every 3 days for a total of nine treatments. The mice in the saline group were injected with 20 μl of saline and those in the GL1 group were given the same concentration of GL1 as the mice in the GL1-siRNA group. The body weights of the mice and the tumor diameters were measured daily. The estimated tumor volume was calculated using the formula: tumor volume = $0.5 \times (\text{width})^2 \times \text{length}$. The mice were sacrificed on the 27^{th} day of treatment. The procedures and care administered to the animals have obtained the approval of the institutional ethics committee, under a permit of animal use (Approval ID: (2012) 005) in No.3 People's Hospital affiliated with Shanghai Jiao Tong University School of Medicine, in compliance with the Experimental Animal Regulation by the National Science and Technology Commission, China. Tumors were weighed after they were dissected from the mice.

[§] This experiments were designed by us and conducted in NO.3 People's Hospital affiliated to Shanghai Jao Tong University School of Medicine

5.2.2.10 Western Blot**

A total protein extraction kit (Kangchen Biotechnology, Shanghai, China) was utilized to extract protein according to the manufacturer's instructions. The total protein was stored at -20°C until use. The antibodies used included Bcl-2 rabbit polyclonal IgG (Santa Cruz Biotechnology, Dallas, USA), horseradish peroxidase (HRP) conjugated goat anti-rabbit IgG (Kangchen Biotechnology, Shanghai, China) and goat antiglyceraldehyde-3-phosphate dehydrogenase (GAPDH) (Kangchen Biotechnology, Shanghai, China). Protein samples were separated by 12% SDS-PAGE gels and then transferred to nitrocellulose (NC) membranes. After blocking with blocking buffer for 2h, the membranes were incubated with polyclonal rabbit anti-Bcl-2 (1:1000, overnight at 4°C). HRP-goat anti-rabbit IgG (1:2000, 2 h) conjugate was used as a secondary antibody. The bound secondary antibody was detected by enhanced chemiluminescence (Pierce Biotechnology, Rockford, USA). The housekeeping gene, GAPDH, was used as an internal standard.

5.3 Statistical Analysis

Results were expressed as mean values ± SD. Statistical significance was determined by a two-tailed t test. Differences were considered significant if $p < 0.05$.

5.4 Results and Discussion

5.4.1 Morphologic Characterization of CHO-K1 Spheroids

The CHO-K1 spheroids were generated using the hanging-drop method. Cells slowly aggregate in the bottom center of the hanging droplet, and eventually form into a tight spheroid. Figure 5.1a shows the formation of spherical, and compact CHO-K1 spheroids. At a higher cell seeding density with the same time point (day 5), the formed cellular spheroid was more densely packed at the central core region (Figure 5.1c). The diameter of CHO-K1 multicellular spheroids with various seeding densities after incubation of 5 days was measured and the result suggested that at a higher cell seeding density, the spheroids were

** This experiment was designed by us and conducted in NO.3 People's Hospital affiliated to Shanghai Jao Tong University School of Medicine

more condensed leading to a smaller diameter (Figure 5.1b). Under light microscope, the spheroid appeared as a multilayer cell assembly (Figure 5.1c). Under scanning electron microscope, as shown in Figure 5.2a, in the intact spheroid, cells interconnect with one another forming a 3D spherical aggregate and individual cells were not distinguishable; at a higher magnification (Figure 5.2b), these cells held together through extracellular matrix throughout the spheroids. Additionally, the spheroids were resistant to physical transfer and gentle agitation but sensitive to enzyme digestion that could separate the spheroids into individual cells. A similar phenomenon was previously reported [150]. However, in monolayer culture (Figure 5.2c), cells were grown in flat monolayer and fused together through supporting connective structures.

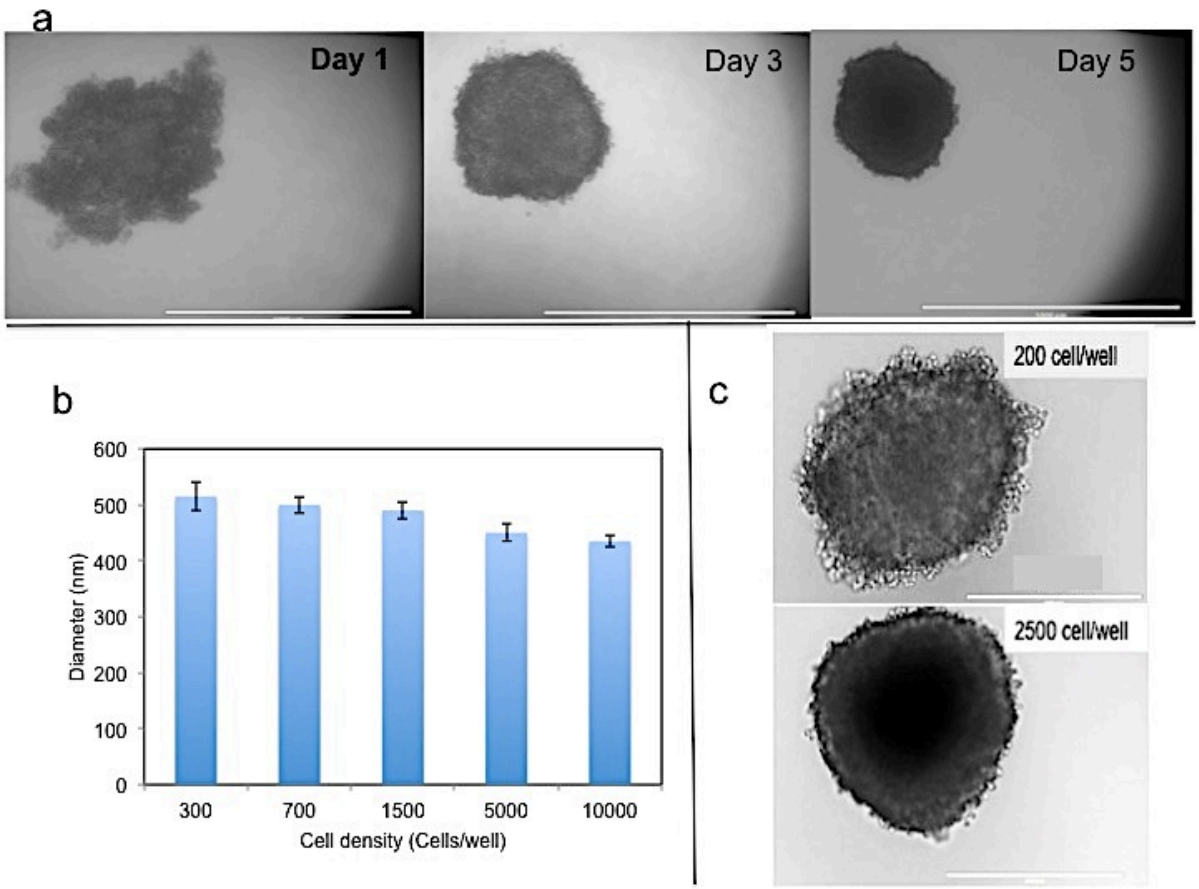

Figure 5.1. Optical characterization of CHO-K1 cellular spheroids. (a) Optical imaging (scale bars: 1000 μm) of CHO-K1 spheroids with seeding density of 1500 cells/well at different time

points. (b) Diameters of CHO-K1 cellular spheroids with seeding densities of 300 cells/well, 700 cells/well, 1500 cells/well, 5000 cells/well, 10000 cells/well at day 5. (c) Optical image of CHO-K1 spheroids with seeding density of 200 cells/well and 2500 cells/well at day 5 (scale bars: 400 µm).

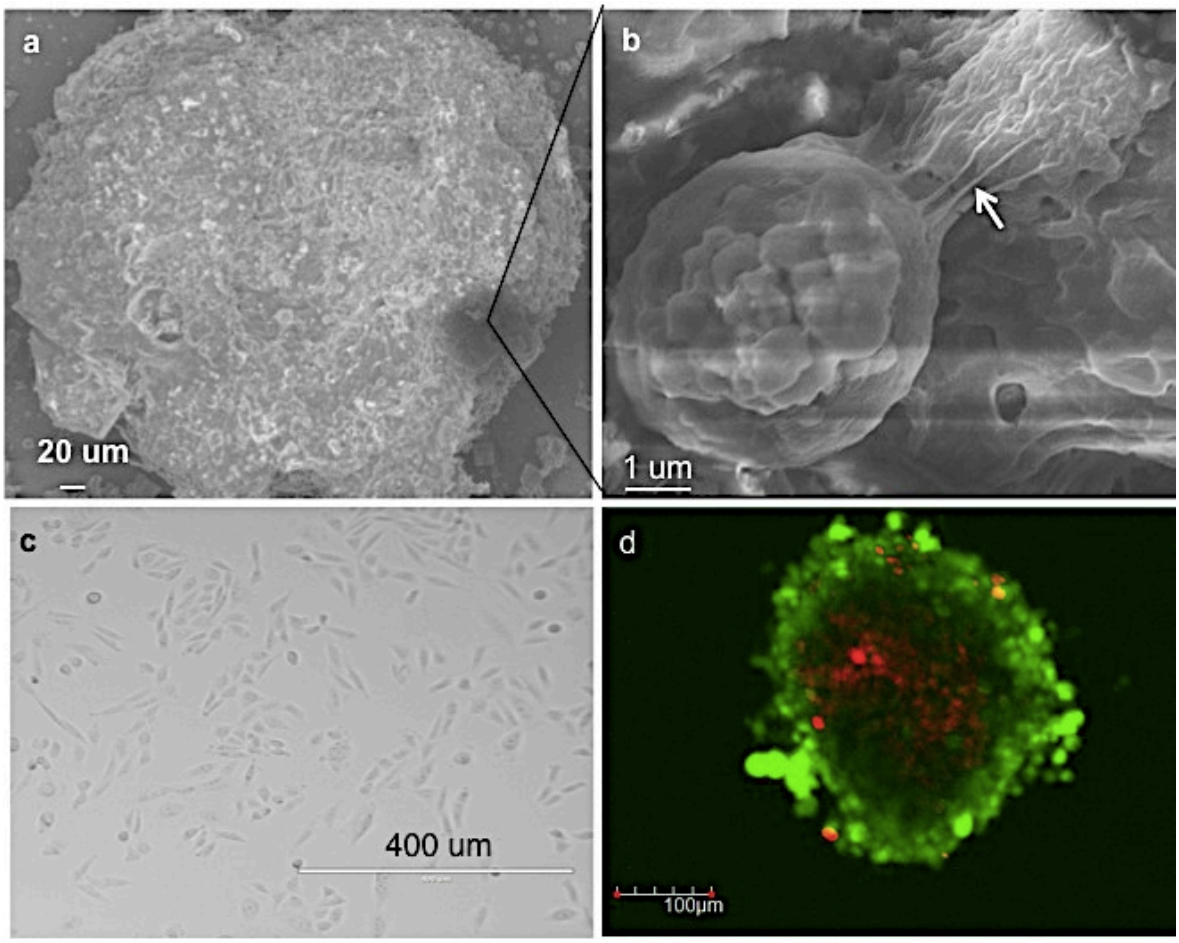

Figure 5.2. Morphology of MCTS of CHO-K1 cells. (a) Under SEM, the structure appeared to be compact and the cells were closely integrated into the solid structure in which individual cells were indistinguishable from each other (scale bar: 20 µm). (b) Single cells within the spheroid culture were connected to adjacent cells though cell-cell junction (arrow). These cell-cell junctions were responsible for the densely packed organization of the cells (scale bar: 1 µm). (c) Under optical microscope, the morphology of cells cultured in monolayer (scale bar: 400 µm). (d) The cell spheroid was stained with Live/dead assay. Under confocal laser microscope, live

cells emitted green fluorescence and dead/dying cells emitted red fluorescence (scale bar: 100 μm).

Next, the internal proliferative status of CHO-K1 spheroids was verified by LIVE/DEAD Viability/Cytotoxicity kit. As shown in Figure 5.2d, the cells within a spheroid were clearly divided into two populations: live cells emitting green fluorescence at the exterior layers and dead/dying cells emitting red fluorescence in the core. These results proved that CHO-K1 spheroids mimicked in vivo solid tumor properties and cell necrosis could happen within the cell spheroids due to the limit of nutrient and oxygen supplies, such as in the center core [151–153].

5.4.2 Penetration of GL1-siRNA Complexes in Tumor Spheroids

To understand the distribution of siRNA within tumor spheroids over time, Cy3-labeled GAPDH siRNA was used for this study, in which Cy3 emitted red fluorescence after excitation. As shown in Figure 3, the GL1-Cy3 labeled siRNA complexes were taken up by the cells at the outer layers of the cell spheroid after 24 h incubation (Figure 5.3a). After 48 h incubation, the complexes were evident in the deeper layers of the cell spheroid and the red fluorescence intensity strongly increased (Figure 5.3b). Cell nuclei were stained with DAPI, a nuclear stain reagent emitting blue fluorescence after excitation, to localize the distribution of GL1-siRNA complexes. However, in monolayer culture of CHO-K1 cells, GL1 could deliver Cy3 labeled siRNA to most of the cells after 4 h treatment. The different cell culture models possibly caused this difference. In cell monolayer, GL1-siRNA complexes were directly in contact with the cells and entered the cells with ease. However, there are more barriers in cell spheroids than in cell monolayer, including three dimensional cell-cell interactions, cell-ECM interaction, ECM, mass diffusion limit, which affected the penetration of peptide-siRNA complexes.

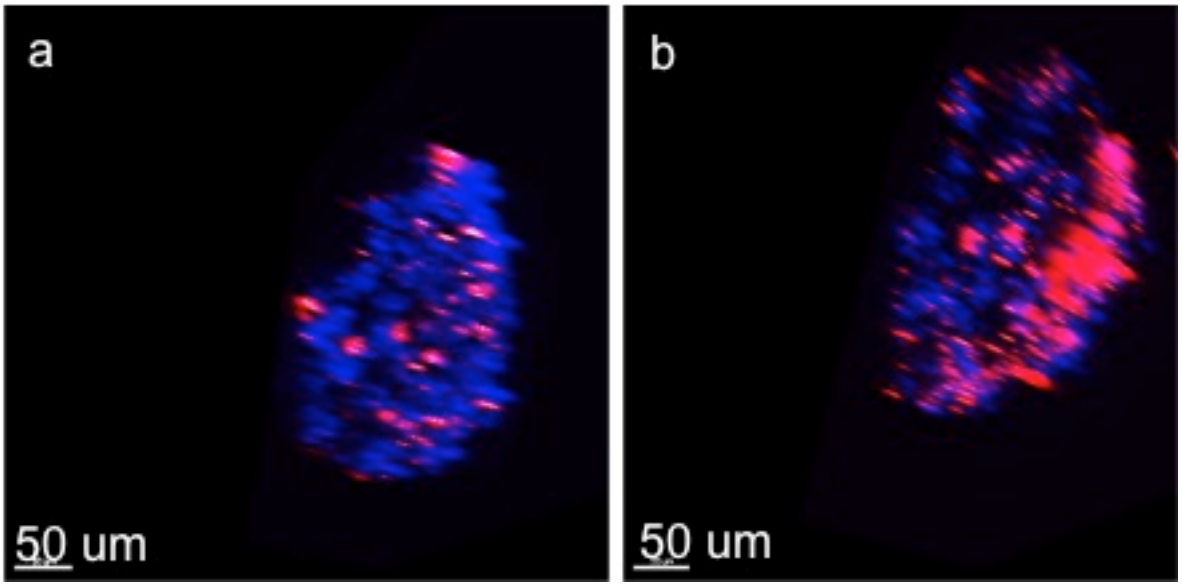

Figure 5.3. Penetration of GL1-Cy3-labeled GAPDH siRNA complexes into CHO-K1 cell spheroids 24 h (a) and 48 h (b) post treatment.

Additionally, cellular penetration also depends on the physicochemical characteristics of the nanoparticles, such as size, surface charge, and shape. Ma H. et al claimed that the positively charged nanoparticles were preferentially retained by the negatively charged ECM and taken up by proliferating cells in the exterior layers, and negatively charged nanoparticles were not hindered by ECM and taken up by viable cells [154]. However, the exact mechanisms for the charge preference are still unclear. They also discovered that with the same charge, smaller nanoparticles penetrated more deeply than larger nanoparticles. [154,155] This indicated that GL1-siRNA complexes with the size of ~80 nm in diameter and positive surface charge could facilitate sufficient siRNA uptake within spheroids and monolayer. However, the cellular internalization of siRNA in spheroids was slowed down due to the limited intercellular space and cell surface area in spheroids when compared with monolayer culture [156]. Thereafter, the cytotoxicity induced by GL1-siRNA complexes was evaluated.

5.4.3 Cytotoxicity

WST-1 assay was used to determine the viability of the spheroids after treatment. As shown in Figure 5.4, siRNA alone did not cause cytotoxicity. Cells treated with Lipofectamine 2000-siRNA complexes exhibited 83% viability. However, cells treated with GL1-siRNA complexes achieved >90% viability, suggesting that GL1 is a relatively safe carrier for siRNA delivery.

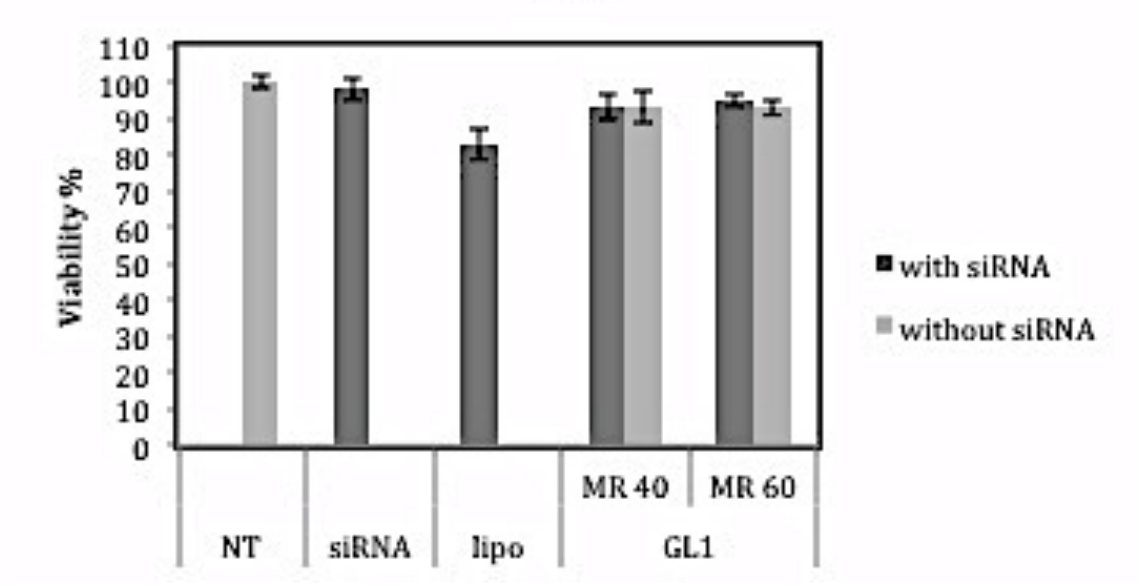

Figure 5.4. Cell viability results of CHO-K1 cells treated with the complexes at different molar ratios or peptide alone at the same concentration as peptide in complex with siRNA at corresponding molar ratio. (N.T.= non-treated cells, MR=peptide/siRNA molar ratio, Lipo=Lipofectamine 2000). Results are expressed as mean ± standard deviation (n=3).

5.4.4 *In Vitro* Transfection Efficiency

In order to evaluate the efficacy of the delivered GAPDH siRNA, RT-PCR measurement of GAPDH mRNA level in the CHO-K1 cell spheroids was performed. A scrambled siRNA was used as a negative control. The GAPDH mRNA level in each sample was normalized to the level measured in cells treated with the negative control. The RT-PCR results exhibited an increase in GAPDH gene silencing efficiency in GL1-siRNA complexes treated cells 72 h

post transfection. Another housekeeping gene cyclophilin was a control and its mRNA level remained relatively stable during the transfection experiments. As shown in Figure 5.5, the gene silencing efficiency induced by GL1-siRNA complexes were molar ratio dependent. At a molar ratio of 20/1 with siRNA concentration of 100 nM, 13% gene knockdown was observed. When increasing the molar ratio to 40/1, the gene knockdown efficiency increased to 40%, which is similar to that of Lipofectamine 2000. At an even higher molar ratio of 60/1, 54% gene knockdown was achieved. The possible reason is that at higher molar ratios, higher amount of peptides can protect siRNA longer and lead to higher siRNA uptake. The relatively large particle size of Lipofectamine 2000-siRNA complexes possibly limited the cellular uptake of siRNA within the multicellular tumor spheroids [157–159], thus leading to a relatively low gene silencing efficiency (38%). However, in CHO-K1 monolayer culture, Lipofectamine 2000-siRNA complexes achieved 80% GAPDH gene knockdown, which was significantly higher than that in 3D culture. This significant difference suggested that the culturing environment could strongly affect the biological outcome of the complexes.

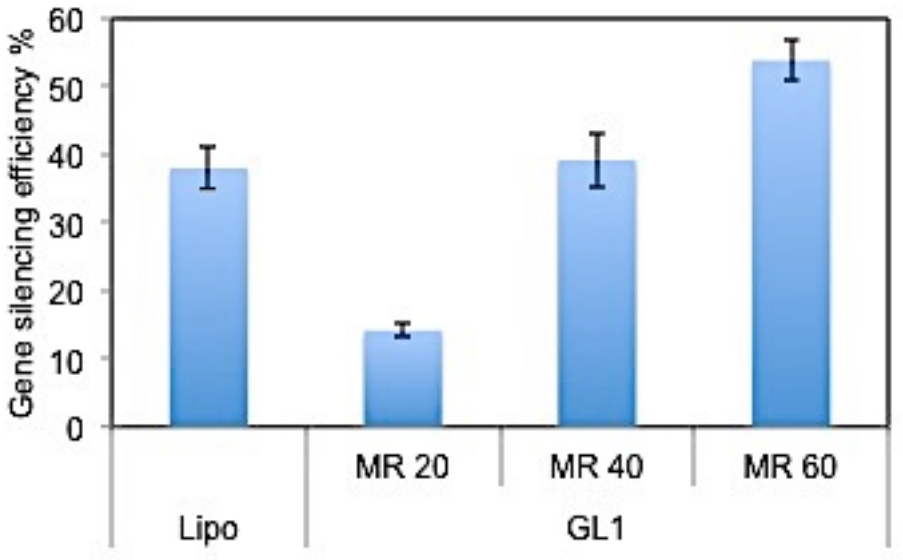

Figure 5.5. Gene silencing efficiency *in vitro*. Silencing of GAPDH gene in CHO-K1 cells was evaluated by quantitative real time polymerase chain reaction (qRT-PCR). GAPDH siRNA concentration was 100 nM. Lipo was the positive control, and scrambled siRNA was used as the negative control. Results are expressed as mean ± standard deviation (n = 3).

5.4.5 *In Vivo* Tumor Growth Suppression

If the average weight of mice in a treatment group (after the tumors were removed) decreased by more than 15% (self-control) during treatment, indicating drug toxicity, the dosage should be reduced and re-tested [160]. Our results show that the body weight of each mouse in each group did not change significantly during the experiment (Figure 5.6a).

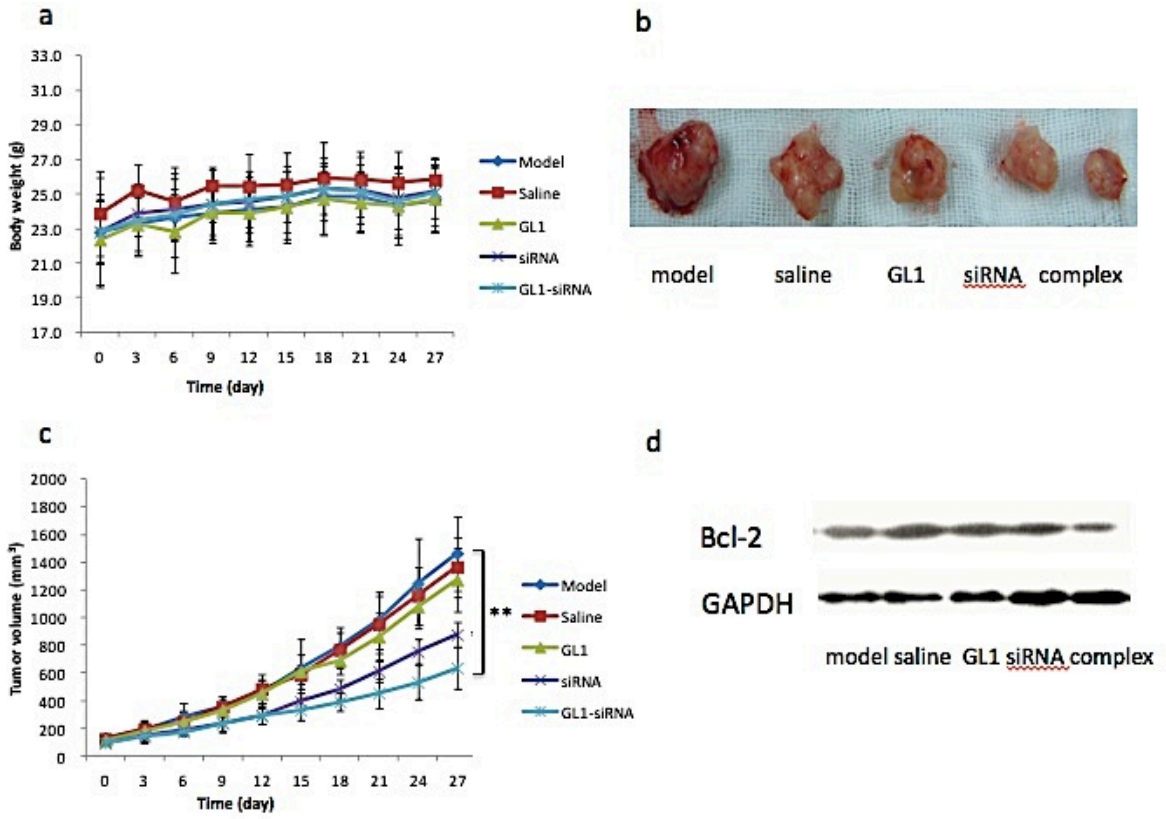

Figure 5.6. Local treatments with GL1/siRNA complexes inhibit tumor growth in a mouse xenograft tumor model. (a) The body weight of each group. Body weights of the mice were measured everyday during the treatment. Data shown is the mean value of eight mice in each group (n=8). (b) Dissected tumor tissues after treatment. Mice were killed by cervical dislocation on the 27th day. Tumors were then separated. Representatives of five treatment groups: model, saline, GL1 peptide, naked Bcl-2 siRNA and GL1/siRNA complex. (c) Antitumor activity of GL1/siRNA complex in a mouse tumor model. The complexes were

administered intratumorally in mice model bearing A549 cancer cells xenografted under the skin. The tumor sizes were measured everyday. Model group: non-treated group with injection of water alone. Data shown is the mean value of eight mice in each group. ** $p<0.05$ versus model group (n=8). (d) Inhibition of Bcl-2.

To monitor the tumor growth, the diameters of tumors were measured daily, and the tumor volume was calculated using the formula provided above. Considering the average value for each group (Figure 5.6c), the volumes of the tumors in the model group, saline group and GL1 group were similar, and the differences were not significant ($p > 0.05$). The volumes of the tumors in the siRNA group and GL1-siRNA group were significantly smaller than those of the other three groups ($p < 0.05$), and the volume of the tumors in the GL1-siRNA group was significantly smaller than that of the siRNA group ($p < 0.05$). At the end of the experiments, tumor tissues were separated and weighed. The tumor weight of GL1-siRNA group (0.6291g) is significantly lower than that of saline treated control (1.3281g) and model group (1.3551g) with a tumor inhibition rate of 52.6%. The representative tumor of each group was shown in Figure 5.6b.

To demonstrate the tumor growth inhibition was induced by Bcl-2 down regulation in tumor cells, the expression of Bcl-2 protein in tumor tissues was detected by Western blot. The results are shown in Figure 5.6d, which demonstrates that the expression of Bcl-2 protein was inhibited in the siRNA group and the GL1-siRNA group and the inhibition was greater in the GL1-siRNA group. Moreover, Bcl-2 protein expression in the saline group and GL1 group was similar to that of the model group. Due to the local intratumoral injection of treatments, there was a decrease in Bcl-2 protein level in the siRNA group. However, the GL1-siRNA group achieved a significantly higher inhibition of Bcl-2 protein expression ($p<0.05$), which represented the advantage of utilizing GL1 as a delivery system.

In the 2D environment, the cell interacts with a basal extracellular “matrix” and with surrounding cells through lateral cell-cell junctions. This is very different from *in vivo* conditions where cells are exposed to the 3D environment. Multicellular spheroids are one of

the most widely used 3D culture systems and resemble many aspects of the physiological conditions within *in vivo* tumor models.

Therefore, we developed multicellular CHO-K1 spheroids to study the peptide GL1 mediated delivery of siRNA. Morphological analysis by light microscopy and SEM demonstrated that the CHO-K1 cells formed tightly packed spheroids (Figure 1a, 2a). Within the spheroid, the cells were spherical shaped, connections between cells were close and compact, and ECMs were observed (Figure 2b). This is close to *in vivo* tumor tissue, but different from monolayer cells (Figure 2c). The cell conditions in the spheroid were determined through confocal laser microscopy after staining the cells with Live/Dead assay. The results indicated that 6-day cultured CHO-K1 spheroids could be divided into two groups (Figure 2d). Outer layer cells of the spheroids made contact with the culture medium were highly proliferative and stained green by calcein AM. Inner layer cells of the spheroids were apoptotic/necrotic cells and stained red by EthD-1. These results suggested that CHO-K1 spheroids mimicked *in vivo* solid tumor properties and cell necrosis could happen within the cell spheroids due to the limit of nutrient and oxygen supplies, such as in the center core.[151–153]

The penetration of peptide-Cy3-labeled siRNA complexes to CHO-K1 spheroids was investigated via the confocal laser microscopy. The results demonstrated that the penetration of the complexes was time dependent (Figure 3). Compared to CHO-K1 cells grown in monolayer, cellular uptake of peptide-siRNA complexes in spheroids was much slower, due to various barriers such as limited intercellular space and ECMs. The GAPDH gene silencing efficiency of peptide-siRNA complexes was molar ratio dependent (Figure 5), whereas higher amounts of peptide could protect siRNA longer and enhance the penetration of the complexes. Additionally, the peptide-siRNA complexes induced >90% cell viability (Figure 4), which is higher than that of Lipofectamine 2000-siRNA complexes.

In order to translate the findings obtained from the in vitro model to the more complex *in vivo* tumor model, we evaluated the antitumor effect of GL1-Bcl-2 siRNA complexes (molar ratio: 60/1) in the animal xenograft model. The intratumoral injection of the complexes

induced a significant tumor growth inhibition rate (52.6%) through the down regulation of Bcl-2 protein expression confirmed through western blot analysis (Figure 6). It is worth noting that all of the mice performed their normal activities throughout the experiment, and no mice died. After dissecting all of the mice, no abnormal viscera, including the heart, liver, spleen, lung, and kidneys was observed, suggesting the complexes are relatively safe to use.

5.5 Conclusions

Our studies suggest that MCTS closely mimic the features of tumors *in vivo*, confirmed through the data of characterizations. Utilizing confocal laser scanning microscopy, we observed that GL1-siRNA complexes could penetrate into the deeper layers of multicellular spheroids over the time. Taking into account that GL1 achieved marked gene silencing efficiency (50%), compared to the commercial transfection reagent, Lipofectamine 2000 (38%), with minimal cytotoxicity in multicellular tumor spheroids (<10%), and that GL1-Bcl-2 siRNA complexes enabled significant anti-tumor effects *in vivo* (52.6%), this indicates that GL1 is a highly promising siRNA delivery vector, both *in vitro* and *in vivo*.

Chapter 6[††]

Effective Small Interfering RNA Delivery In Vitro via A New Stearylated Cationic Peptide STR-HK

Abstract

A crucial bottleneck in RNA interference (RNAi) based gene therapy is the lack of safe and efficient delivery systems. Here, a novel siRNA delivery peptide, STR-HK, was constructed by conjugating a stearyl end to the N-terminus of the peptide sequence "HHHPKPKRKV", where "PKPKRKV" is an altered sequence of the nucleus localization signal (PKKKRKV) and contributes to the cytosol localization of STR-HK-siRNA complexes. Histidine is a linker and plays an important role in disrupting the endosomal membrane via the proton sponge effect. As expected, STR-HK formed complexes with siRNA with a particle size of 80-160 nm in diameter and efficiently delivered Cy3 labeled GAPDH siRNA into PC-3 human prostate cancer cells. The transfection efficiency of STR-HK at molar ratio 60/1 was comparable to that of Lipofectamine 2000, one of the most efficient commercially available transfection reagents. Furthermore, the STR-HK-siRNA complexes exhibited minimal cytotoxicity, which was significantly lower than that of Lipofectamine. Taken together, the strategy of conjugating the stearyl moiety with "HHHPKPKRKV" as a non-viral siRNA delivery system is advantageous.

[††] This chapter is based on a paper. B. Chen, R. Pan, D. Askhatova, P. Chen. Effective Small Interfering RNA Delivery *In Vitro* via A New Stearylated Cationic Peptide. International Journal of Nanomedicine, 2015, 10:1-12.

6.1 Introduction

RNA interference (RNAi) is a specific cellular post-transcriptional gene silencing mechanism, which can be induced by evocation of enzymatic degradation of a corresponding mRNA. Double-stranded small interfering RNA (siRNA) consisting of 21-25 nucleotides plays an important role in this process. siRNA can be synthesized exogenously and delivered to the cytoplasm to be loaded into the RNA-induced silencing complex (RISC). RISC induces the siRNA to unwind in a strand specific manner. The sense strand of siRNA is cleaved and removed, then the remaining antisense strand of the duplex acts as a guide to lead the RISC complex into the complementary sequence of the target mRNA. Upon association of the target mRNA with RISC, AGO protein cleaves the mRNA and interrupts the translation process.[161–163] Being a potent and highly specific therapeutic strategy, siRNAs have been evaluated as potential therapeutic agents for a wide range of gene based diseases. However, the major limitations for the use of siRNA are the instability of naked siRNA in physiological conditions, the nature of negative charge, and hydrophilicity. Currently, various strategies have been applied to improve siRNA's nuclease resistance without interfering with its silencing efficiency [164,165], such as chemical modifications in the nucleobases, the phosphate ester backbone, and conjugation with hydrophobic functional groups [166]. However, this is very time-consuming and costly. Carrier based strategies have been explored as a simple and fast means to protect the siRNA and maximize its therapeutic effects.

A number of delivery carriers have been developed and characterized including peptides [167], polymers [168,169], liposomes [170,171], lipids [172,173], and viral vectors [174]. Due to the fundamental drawbacks of viral vectors, such as toxicity and immunogenicity, non-viral vectors have served as an alternative because of their advantage in inducing relatively low toxicity and nearly no immune response [161,162]. Among these non-viral vectors, cell penetrating peptides are being increasingly utilized for gene delivery [163,175,176]. Researchers have proven that cell penetrating peptide MPG, the peptide

derived from both the fusion peptide domain of HIV-1 gp41 protein and the nuclear localization sequence (NLS) -'PKKKRKV'- of SV40, can deliver DNA into the nucleus efficiently. NLS plays an essential role in importing DNA into the nucleus.[177] A single mutation of a lysine residue to a proline residue (PKPKRKV) in NLS, limits its nuclear translocation, but enhances release of the cargo into the cytoplasm, which is helpful for siRNA intracellular localization.[178] Recently, stearylation has proven to be successful in increasing the transfection efficiency of CPPs for DNA delivery [179–185] or that of PEI for siRNA delivery [186]. The increased transfection efficiency is attributed to the enhanced compaction of DNA, increased endosomal escape, and higher cellular uptake, which are all conferred by the stearyl moiety.

Having considered the similarity of siRNA and DNA, a novel type of non-viral siRNA delivery vector was constructed by introducing a stearyl moiety to the N-terminus of the sequence. Three histidine residues serve as a linker between the stearyl moiety and "PKPKRKV". The other reason for using histidine is that it will be helpful for the rapid release of siRNA into the cytosol after intracellular uptake. In this report, the physicochemical and biological characteristics of this new peptide, STR-HK (C_{18}-HHHPKPKRKV-NH_2), was investigated in order to evaluate its potential for siRNA delivery.

6.2 Materials & Methods

6.2.1 Materials

Peptide STR-HK (C_{18}-HHHPKPKRKV-NH_2) with a molecular weight of 1500.9 g/mol, was synthesized by CanPeptide Inc. with a purity >95% (Quebec, CA). The high performance liquid chromatography (HPLC) and liquid chromatography-mass spectrometry (LC-MS) characterization of STR-HK is shown in Figure 6.1 and Figure 6.2. SiRNA targeting the glyceraldehyde 3-phosphate dehydrogenase (GAPDH) gene and Cy3-labeled GAPDH siRNA were purchased from Ambion (Silencer^{TM} GAPDH siRNA kit). The siRNA targeting eGFP gene, GCGACGUAAACGGCCACAAGU, was purchased from Dharmacon, whose antisense sequence is ACUUGUGGCCGUUUACGUCGC and sense sequence is

GACGUAAACGGCCACAAGUUC. The negative control siRNA was purchased from Ambion. Cell counting kit-8 was used for cell viability test and was purchased from Dojindo Molecular Technologies.

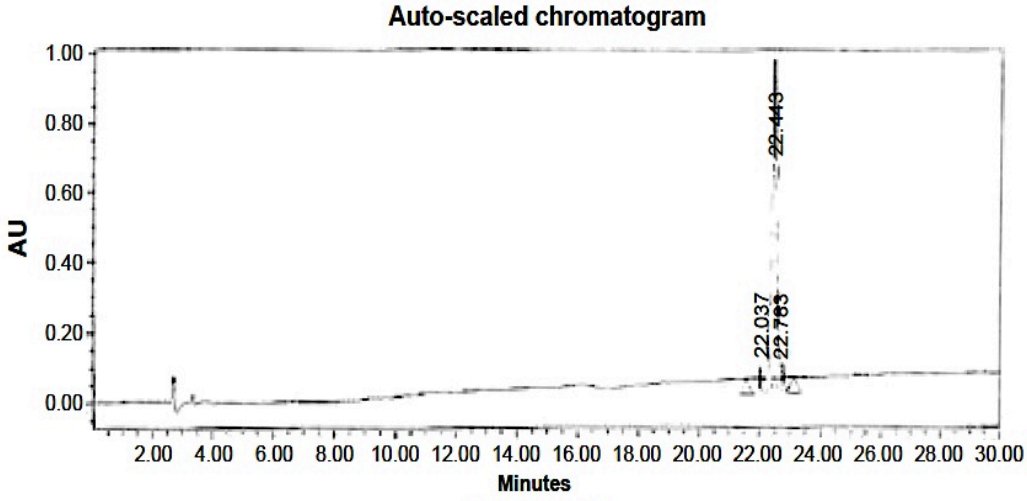

Peak results

	RT (min)	Area µAU*s	Height (µAU)	% area
1	22.037	30,518	2,201	0.31
2	22.443	9617,490	901,710	99.22
3	22.783	45,492	5,771	0.47

Figure 6.1. HPLC data of STR-HK.

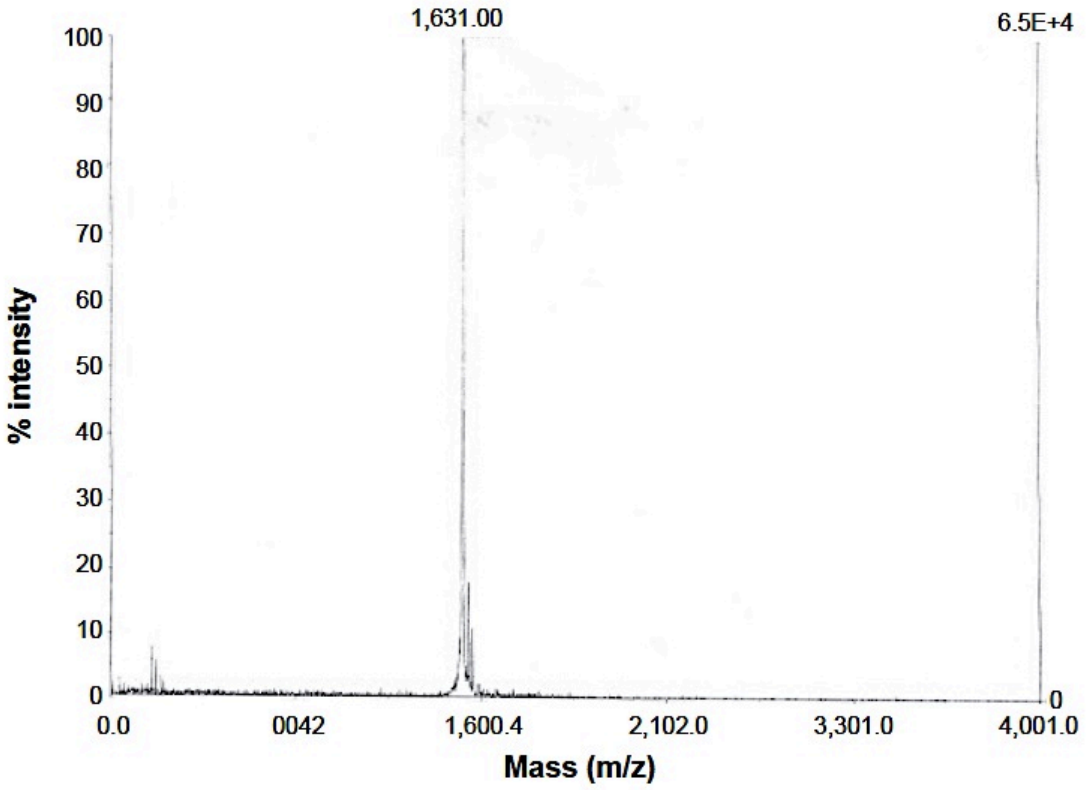

Figure 6.2. LC-MS data of STR-HK.

6.2.2 Methods

6.2.2.1 Cell culture

Human prostate cancer cell line (PC-3) was purchased from the American Type Culture Collection. PC-3 cells were grown in F-12K medium (Thermo Scientific, Ottawa, BC, CA) supplemented with 10% fetal bovine serum (FBS) (Sigma-Aldrich, Oakville, Ontario, CA). The cell line was cultured at 37^{o}C in a 5% CO_2 atmosphere.

6.2.2.2 Preparation of STR-HK-siRNA complexes

The preparation of STR-HK-siRNA complexes in this chapter followed the same procedures as presented in chapter 3.

6.2.2.3 Agarose gel-shift assay

This experiment followed the same procedures as presented in chapter 3.

6.2.2.4 Isothermal titration calorimetry (ITC)

siRNA condensation was evaluated using isothermal titration calorimetry. The experiments were conducted using a Nano-ITC calorimeter (TA Instruments, New Castle, DE, USA). A 500 μM STR-HK peptide solution and a 10 μM siRNA solution were both prepared in RNase-free water. This experiment followed the same procedures as presented in chapter 3.

6.2.2.5 Particle size and zeta potential

This experiment followed the same procedures as presented in chapter 3.

6.2.2.6 Scanning electron microscopy (SEM)

The morphology of STR-HK-siRNA complexes at a molar ratio of 20/1 was observed under SEM. This experiment followed the same procedures as presented in chapter 3.

6.2.2.7 Transmission electron microscopy (TEM)

TEM was utilized to acquire the morphology of STR-HK-siRNA complexes at molar ratio of 20/1 with siRNA concentration of 100 nM. Ten μl of the samples was applied to a 400 mesh Formva coated copper grid (Canemco-Marivac, Canton de Gore, Canada) for 3-5 min. The sample was then washed 5 times with RNase free water and dried over night. Uranyl acetate (Electron Microscopy Sciences, USA) was used to stain the samples. An electron micrograph of the STR-HK-siRNA complexes was acquired using TEM (Philips CM10 TEM, the Netherlands)

6.2.2.8 Circular dichroism (CD) spectroscopy

CD was used to investigate the secondary structure of the peptide and its change after forming a complex with siRNA. This experiment followed the same procedures as presented in chapter 3.

6.2.2.9 Cytotoxicity

The cytotoxicity of peptide-siRNA complexes was determined by the Cell Counting Kit-8 (CCK-8) assay. In brief, cells were seeded at 10,000 cells/well in clear, flat-bottomed, 96-well plates (Costar) 24 h before treatment. After being washed, 100 μl of Opti-MEM that contained peptide-siRNA complexes at different molar ratios was added to the wells and incubated for 4 h. Thereafter, 50 μl of 30% serum containing medium was added, and the cytotoxicity of the relevant reagents was determined by the CCK-8 assay after 24 h and 48 h. Then, the cultures were removed from the incubator and the absorbance at 570 nm was read on a plate reader (BMG, FLUOstar OPTIMA, Germany). The background absorbance of the multiwell plates at 690 nm was determined and subtracted from the 570 nm measurement. The results obtained from triplicate wells were averaged and normalized to the value obtained from the non-treated cells.

6.2.2.10 Cellular uptake

PC-3 cells (80,000/well) were cultured in a 24 well plate 24 h before treatment. The cells were incubated with STR-HK-Cy3-labeled GAPDH siRNA complexes at a molar ratio of 40/1 for 4 h. Lipofectamine 2000-Cy3-labeled GAPDH siRNA complexes was a positive control here. Thereafter, the cells were washed three times with PBS and then fixed by 4% paraformaldehyde (PFA). The nucleus of the cell was stained by DAPI. Images were taken with a fluorescence microscope. To quantify the cellular uptake of peptide-siRNA complexes, PC-3 cells (80,000/well) were cultured in 24-well plates 24 h before treatment. The cells were incubated with peptide-Cy3-labeled GAPDH siRNA complexes at different molar ratios for 4 h. Next, cells were rinsed with PBS and then washed with heparin (10 U/ml). After thorough washing, trypsin-EDTA was added to detach the cells from the plate. The cells were re-suspended in 4% PFA for analysis using fluorescence activated cell sorting (BD Biosciences, BD FACSVantage SE Cell Sorter, CA).

6.2.2.11 *In vitro* transfection

PC-3 cells were seeded at 80,000 cells/well in 24-well plates 24 h before treatment. Cells were treated with peptide-siRNA complexes in 300 μl of Opti-MEM at different molar ratios

for 4h. Thereafter, 300 μl medium containing 20% FBS was added to each well. After incubation of 48 h, cells were washed and collected for qRT-PCR analysis.

Firstly, the total RNA was extracted from the treated cells using the SV Total RNA Isolation System (Promega, Sunnyvale, CA, USA). A Nanodrop (Thermo Scientific, Nanodrop spectrophotometer ND-1000, Ottawa, BC, CA) was used to determine the RNA concentrations. The RNA samples were reverse-transcribed into cDNA using a Bio-Rad iScript cDNA synthesis kit according to the manufacturer's protocol. After the cDNA was synthesized, PCR was performed with Brilliant II fast SYBR Green QPCR Master Mix (Agilent Technologies, Wilmington, DE, USA) using an Mx3005P^{TM} real time PCR System (Agilent Technologies, Santa Clara, CA, USA). The sequences of the primers used for the human GAPDH gene: 5'-GAAATCCCATCACCATCTTCCAG-3' and 5'-GAGCCCCAGCCTTCTCCATG-3' (Sigma-Aldrich, Oakville, ON, CA). Cyclophilin, a housekeeping gene, was used as an internal control to normalize the GAPDH gene expression. Human cyclophilin mRNA was amplified using the following primers: 5'-GGTGATCTTTGGTCTCTTCGG-3' and 5'-TATATGCTCTTTCCTCCTGTG-3' (Sigma, Oakville, Ontario, CA).

6.3 Statistical Analysis

Results were expressed as mean values ± SD. Data were analyzed by two tailed T test and only p-values < 0.05 were considered statistically significant.

6.4 Results

6.4.1 Characterization of Peptide-siRNA Complexes

Agarose gel shift assay was applied to detect the loading capacity of STR-HK. Basic amino acids such as arginine and lysine was protonated and able to interact with the negatively charged phosphate groups on siRNA sugar rings through electrostatic interactions. STR-HK contains four positively charged residues: three arginine and one lysine so as to strongly interact with siRNA. In the agarose gel electrophoresis experiment, when voltage is applied, free siRNA will move towards the positive electrode. As shown in Figure 6.3, the band

produced at higher molar ratio was less dark than band produced by siRNA alone. At molar ratios above 15/1, no free siRNA was detected on the agarose gel, indicating that siRNA molecules were completely complexed with STR-HK. This suggests that at molar ratios higher than 15/1, there is sufficient STR-HK to neutralize the negative charge of siRNA and form complexes with siRNA.

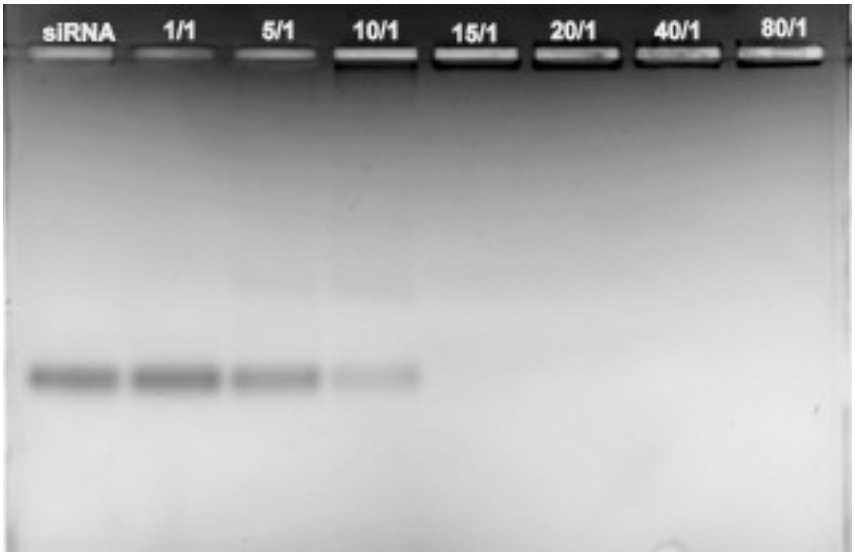

Figure 6.3. Binding ability of siRNA to STR-HK studied by agarose gel-shift assay. The formed STR-HK-siRNA complexes, stained with ehidium bromide, were investigated by electrophoresis on agarose gel (1.2% wt/vol). siRNAs, targeting eGFP gene, were complexed with STR-HK at a series of molar ratios from 1/1 to 80/1. Lane 1 was siRNA control, and lanes 2-8 indicated correlated molar ratios. The amount of siRNA was 300 ng.

To evaluate the stoichiometry between STR-HK and siRNA and the thermodynamic parameters during the condensation process, ITC was employed. As shown in Figure 6.4, the heat exchange during the titration of siRNA by STR-HK (in RNase-free water) was detected by the machine and output as raw data. By fitting the raw ITC data (upper panel of Figure 6.4) to a single-site model (lower panel of Figure 6.4), the thermodynamic parameters of the interaction were obtained and listed in Table 6.1.

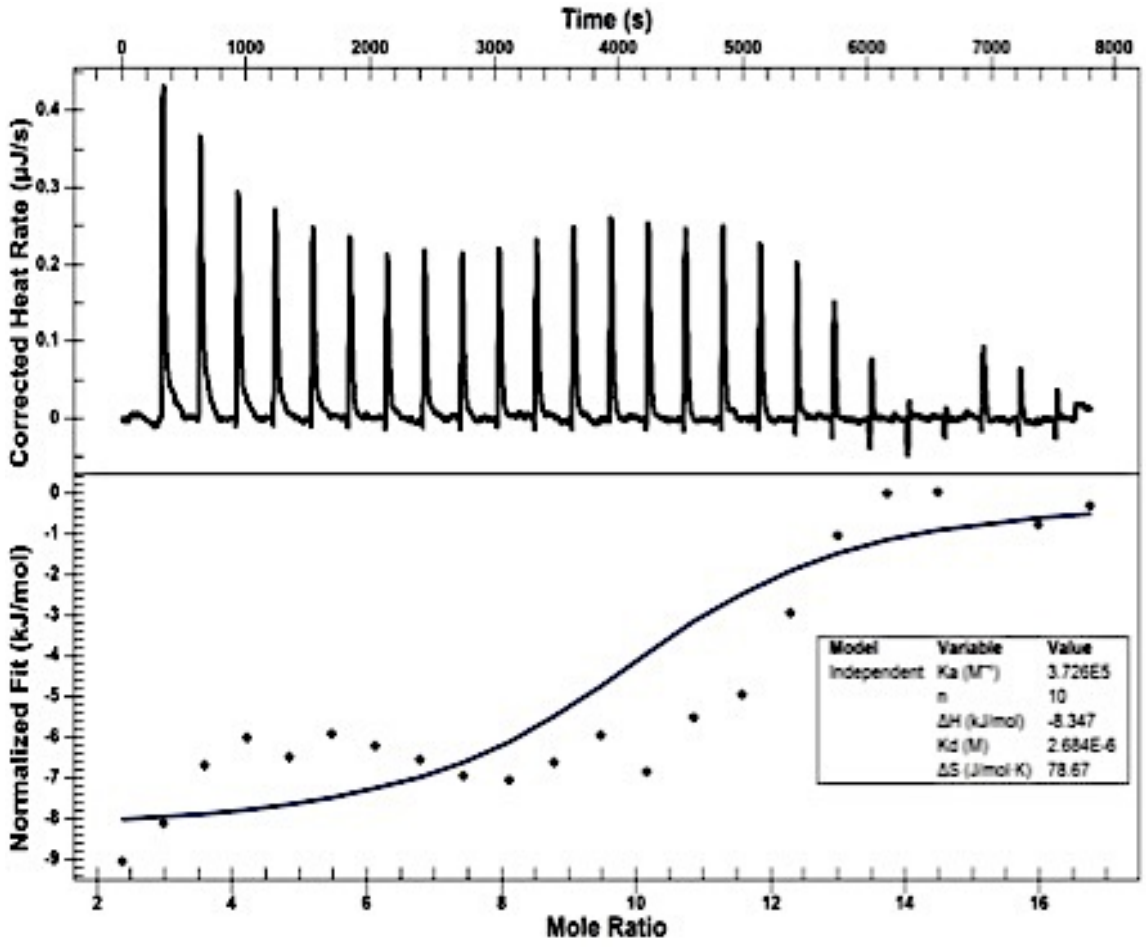

Figure 6.4. Calorimetric titration of siRNA with STR-HK at 25 oC in RNase-free water at pH 6. (a) Corrected thermogram of calorimetric titration of siRNA with STR-HK, (b) Binding analysis of siRNA with STR-HK by fitting the raw data with an independent model. STR-HK concentration was 500 µM and siRNA concentration was 10 µM.

Table 6.1. Thermodynamic parameters when titrating siRNA with STR-HK in water.

Ka (1/M)	ΔH (kJ/mol)	n	K_d (M)	ΔS (J/(mol·K))
$3.726 \cdot 10^5$	-8.347	10	$2.684 \cdot 10^{-6}$	78.67

The obtained molar stoichiometry was 10, which implied that 10 moles of STR-HK could condense 1 mole of siRNA. This number was very close to the theoretical value of 10.5, considering that the STR-HK peptide contains 4 positively charged residues (Arginine and Lysine), and there are 21 pairs of negatively charged nucleotides in the siRNA molecule. With an enthalpy of -8.35 kJ/mol, ΔS of 78.67 J/(mol·K), and entropy of -23.44 kJ/mol, the binding was predominantly entropy-driven. Moreover, ΔG calculated using the equation $\Delta G=\Delta H-T\Delta S$ was equal to -31.79 kJ/mol, which indicated that STR-HK and siRNA assembled spontaneously [102,103].

The particle size and zeta potential of the complexes were measured to gain an understanding of the physicochemical properties of STR-HK-siRNA complexes. As shown in Figure 5a, overall particle sizes remained in the range of 80-160 nm. From a molar ratio 10/1 to 60/1 (peptide/siRNA) particle size increased. However, at a molar ratio of 60/1, particle size slightly decreased and was similar to that of a molar ratio of 40/1. According to the graphs of size distribution by intensity (Figure 6.5), the possible reason for this phenomenon was that at molar ratio of 60/1, excess peptides formed smaller nanoparticles, and thus decreased the average size. However, the wider size distribution at MR 60/1 resulted in a higher variation.

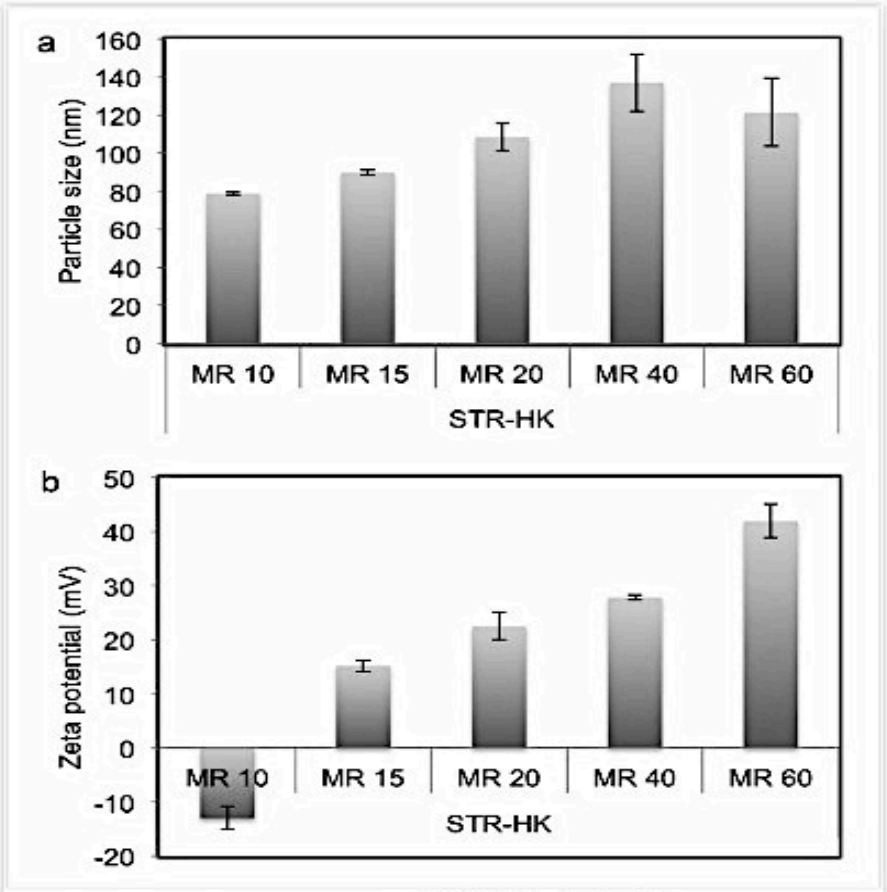
a
Particle size (nm)
160
140
120
100
80
60
40
20
0
MR 10
MR 15
MR 20
MR 40
MR 60
STR-HK
b
Zeta potential (mV)
50
40
30
20
10
0
-10
-20
MR 10
MR 15
MR 20
MR 40
MR 60
STR-HK

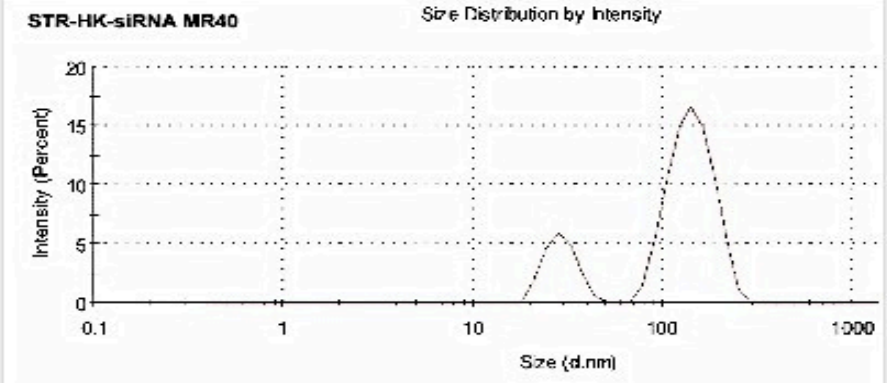
STR-HK-siRNA MR40
Size Distribution by Intensity
Intensity (Percent)
20
15
10
5
0
0.1
1
10
100
1000
Size (d.nm)

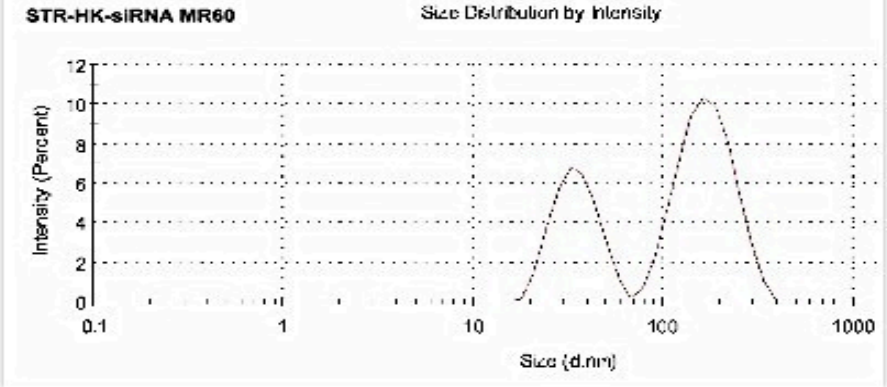
STR-HK-siRNA MR60
Size Distribution by Intensity
Intensity (Percent)
12
10
8
6
4
2
0
0.1
1
10
100
1000
Size (d.nm)

Figure 6.5. (a) The hydrodynamic diameter and (b) zeta potential of the STR-HK-siRNA complexes at different molar ratios were measured by dynamic light scattering (DLS). The lower two graphs are the size distribution by intensity of STR-HK-siRNA complexes at a molar ratio of 40/1 and 60/1. The siRNA concentration was fixed as 100 nM. At different molar ratios, the amount of STR-HK was adjusted. Results are expressed as mean ± standard deviation (n=3). The difference of size distribution at a molar ratio of 40/1 and 60/1 is not statistically significant.

As expected, the zeta potential of complexes increased with increasing molar ratios (Figure 6.5b) due to the addition of excess positively charged peptides. Interestingly, at a molar ratio of 10/1, the surface charge of STR-HK-siRNA complexes was slightly negative (-13 mV), and at a slightly higher molar ratio (15/1), it turned out to be positive (15.2 mV). This interesting phenomenon indicated that siRNA molecules were not fully complexed at a molar ratio of 10/1 but could be so by slightly increasing the molar ratio.

Additionally, a SEM image of the complexes formed by STR-HK with siRNAs at a molar ratio of 20/1 is shown in Figure 6.6a. The graph shows that the STR-HK-siRNA complexes displayed a smooth and spherical shape with the size around 100 nm. The morphology of the complex at molar ratio of 20/1 was also examined by TEM, shown in Figure 6.6c. The electron micrograph exhibited spherical shape with the size of approximately 100 nm. The particle size acquired from SEM and TEM experiments was consistent with the DLS result. More importantly, this morphology indicates that STR-HK could condense siRNA to regular nanoparticles.

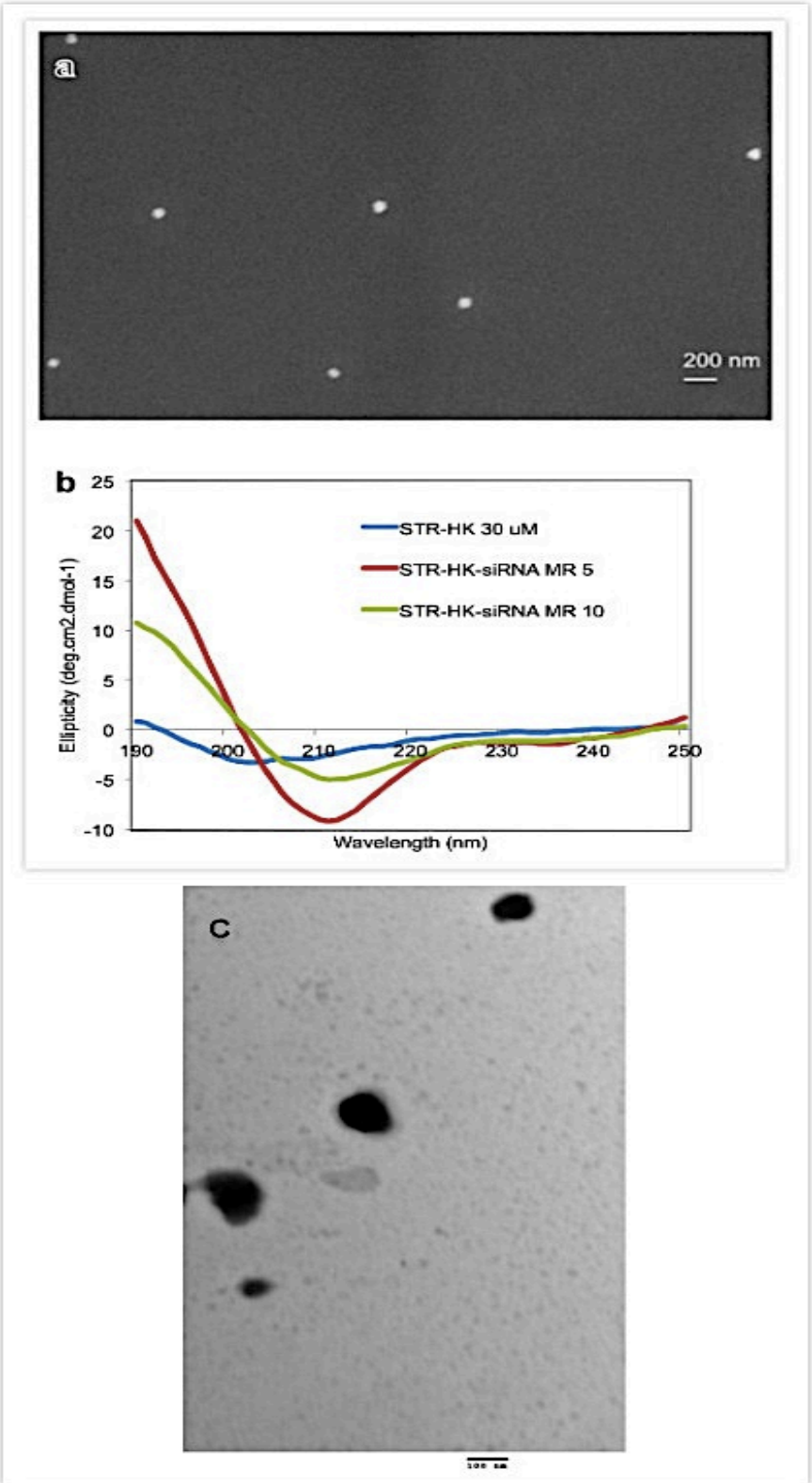
a
200 nm
b
25
20
15
10
5
0
-5
-10
190
200
210
220
230
240
250
Ellipticity (deg.cm2.dmol-1)
Wavelength (nm)
STR-HK 30 uM
STR-HK-siRNA MR 5
STR-HK-siRNA MR 10
C

Figure 6.6. (a) Morphology of STR-HK-siRNA complexes at a molar ratio of 20/1, where siRNA concentration was 100 nM. (b) CD spectra of STR-HK alone and STR-HK-siRNA at different molar ratios. STR-HK concentration was fixed at 30 μM and STR-HK-siRNA complexes were formulated at molar ratios of 5/1 and 10/1. (c) Morphology of STR-HK-siRNA complexes at a molar ratio of 20/1 with siRNA concentration of 100 nM, scale bar: 100 nm.

Furthermore, secondary structure is an important feature of peptides. From the changes of secondary structure, it can prove the interactions of STR-HK and siRNAs at a molecular level. As shown in Figure 6.6b, STR-HK alone in water exhibited a random coil structure with a minimum at 202 nm. After adding siRNAs to the peptide solution to form complexes at a molar ratio of 10/1, a clear conformational change occurred and a minimum at 213 nm was observed, which implied a typical β sheet structure. By adding more siRNAs to attain the molar ratio of 5/1, the absolute values of the minimum spectra at 213 nm and the maximum spectra at 190 nm were increased. The results indicated that upon interaction with siRNAs, STR-HK adopted a more ordered secondary structure-β sheet instead of a randomly folded structure. The conformational change also revealed the flexibility of STR-HK when it formed regular nanoparticles with siRNAs.

6.4.2 Cytotoxicity of STR-HK-siRNA Complexes

The cytotoxicity of peptide-siRNA complexes was evaluated by the CCK-8 assay, and Lipofectamine 2000 (Lipo) was used as the control. As shown in Figure 6.7a, after 24 h of treatment, both peptide alone and Lipo alone caused almost no cytotoxicity. The cytotoxicity of STR-HK-siRNA complexes at molar ratios from 20/1 to 60/1 was less than 5%. However, the cytotoxicity of STR-HK-siRNA complexes was significantly lower than that of Lipo after 24 h of treatment. To evaluate the long-term cytotoxicity of the complexes, cytotoxicity after 48 h of treatment was also studied. Figure 7b shows that the cytotoxicity of each treatment followed a similar trend to that after 24 h of treatment. These results indicated that STR-HK did not cause either short-term or long-term cytotoxicity, which was superior to Lipo in this criterion.

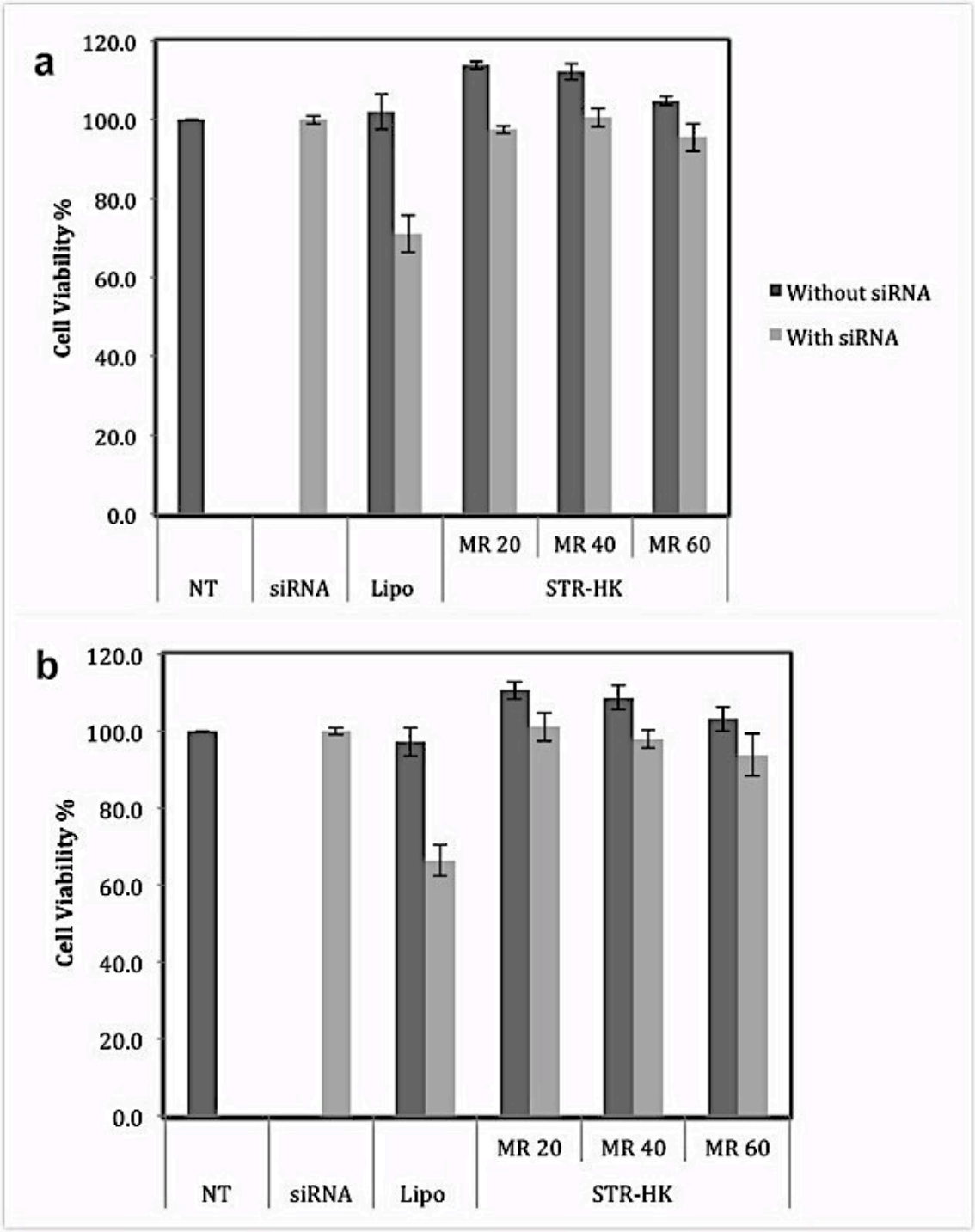

Figure 6.7. Cell viability results of PC-3 cells treated with, peptide-siRNA complexes (siRNA concentration: 100 nM) at different molar ratios or peptide alone at corresponding molar ratio. (NT= Non treated, MR=peptide/siRNA molar ratio, Lipo=Lipofectamine 2000). (a) Cell

viability after 24 h treatment; (b) Cell viability after 48 h treatment. Results are expressed as mean ± standard deviation (n = 3).

6.4.3 Cellular Uptake of STR-HK-siRNA Complexes

The cellular uptake of STR-HK-Cy3-labeled siRNAs complexes was studied with fluorescence microscopy and FACS. As shown in Figure 6.8, most cells treated with Lipofectamine 2000-Cy3-labeled siRNA complexes displayed red dots in their cytosol. In the cells treated with STR-HK-siRNA complexes, siRNAs were localized to regions in close proximity to the nuclear membrane and were distributed in a non-homogeneous pattern at the periphery of the nucleus, which indicated the possibility of endocytotic delivery [107]. More interestingly, the cellular uptake of STR-HK-siRNA complexes was molar ratio dependent and was almost equivalent to that of the Lipo-siRNA complexes at a molar ratio of 60/1 (Figure 6.9). These data indicated that STR-HK could efficiently deliver sufficient Cy3-labeled siRNAs into PC-3 cells.

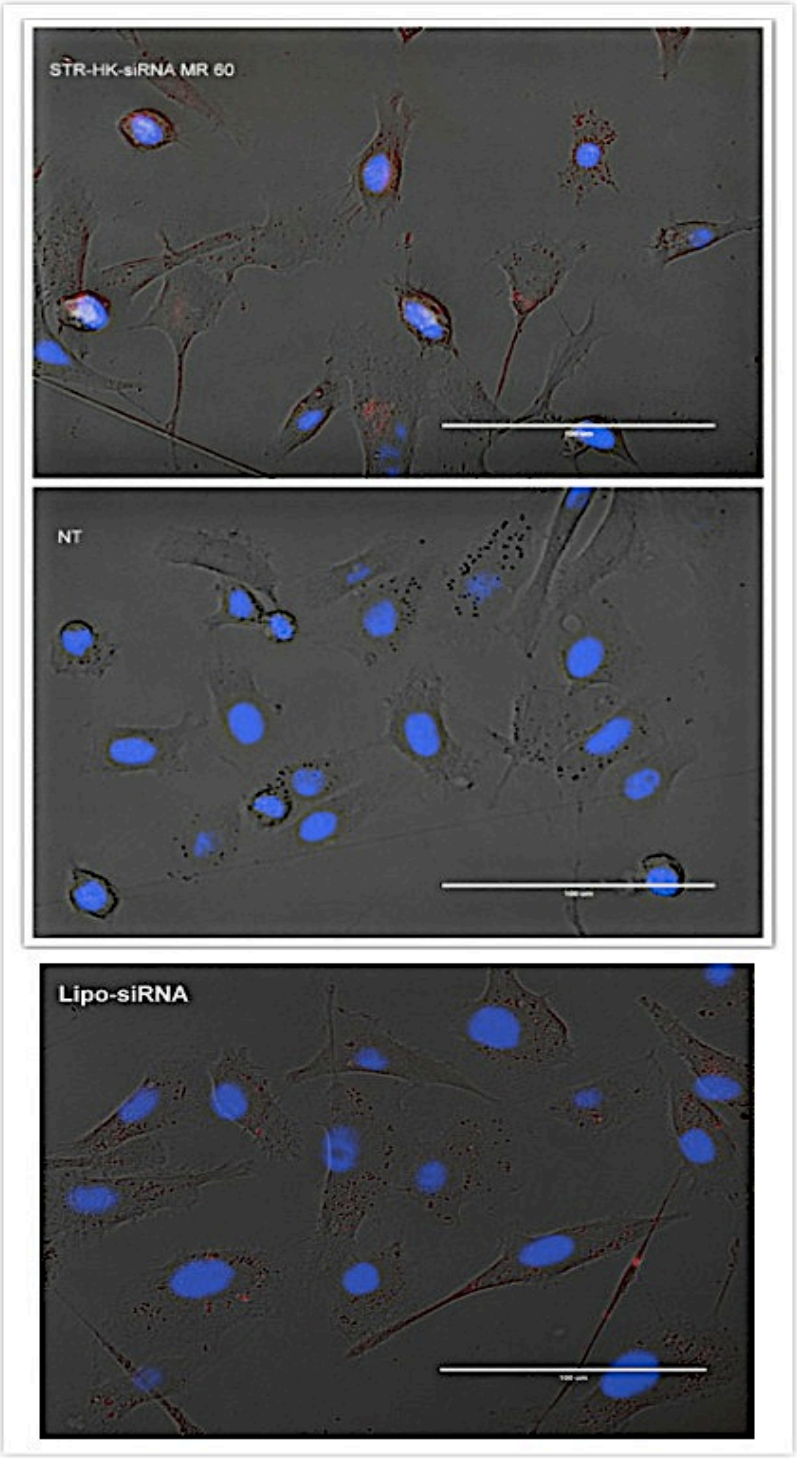

Figure 6.8. Fluorescence microscope image of STR-HK-siRNA complexes at molar ratio 60/1. The red fluorescence indicated Cy3 labeled siRNA, blue fluorescence represented DAPI stained

nuclei. NT was non treated cells, used as a negative control. Cells treated with Lipo-siRNA complexes were a postive control. The scale bar was 100 μm.

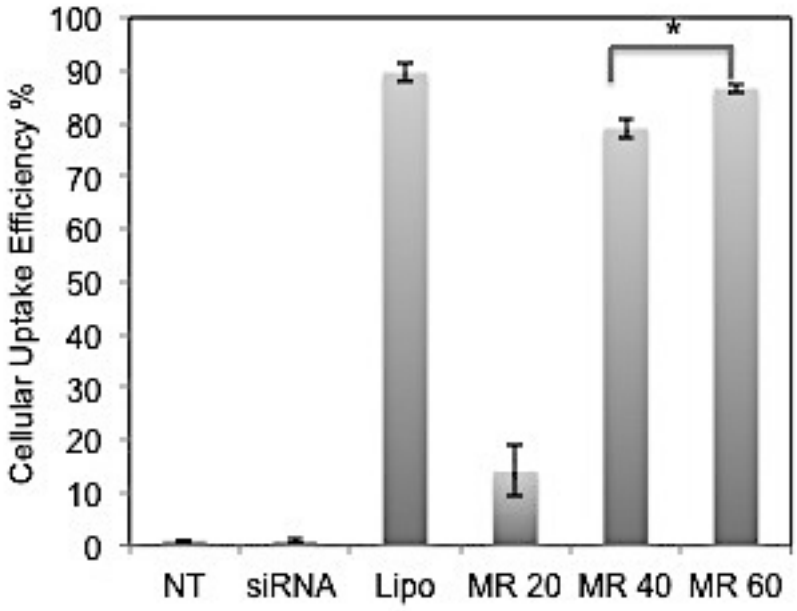

Figure 6.9. FACS results of cellular uptake of siRNA. Non-treated sample was negative control; Lipo-siRNA complexes were positive control. Cy3 labeled GAPDH siRNA was used here. siRNA concentration was 100 nM in both experiments. * P value<0.05, the difference of cellular uptake efficiency of siRNA at a molar ratio of 40/1 and 60/1 is statistically significant.

6.4.4 *In Vitro* Transfection of Peptide-siRNA Complexes

To evaluate the transfection efficiency of STR-HK, PC-3 cells were treated with the complexes formed by STR-HK with GAPDH siRNA at different molar ratios. As shown in Figure 6.10, the transfection efficiency of STR-HK increased with the increasing molar ratios and almost reached the similar level of Lipo at the molar ratio of 60/1.

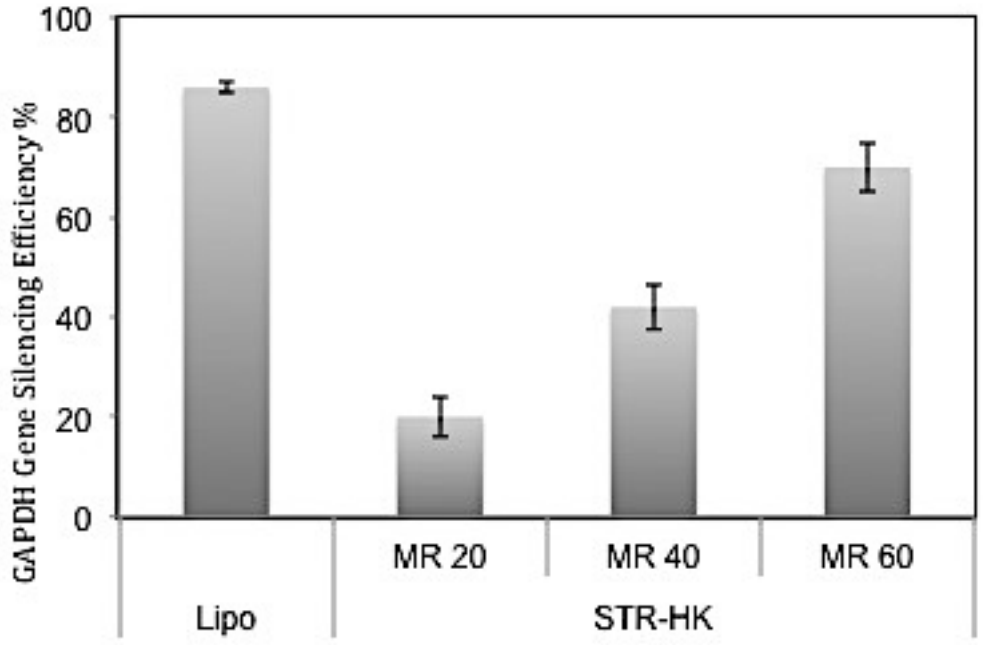

Figure 6.10. Gene silencing efficiency in vitro. Silencing of GAPDH gene in PC-3 cells was evaluated by quantitative real time polymerase chain reaction (qRT-PCR). GAPDH siRNA concentration was 100 nM. Lipo was the positive control, and scrambled siRNA was used as the negative control. Results are expressed as mean ± standard deviation (n = 3).

6.5 Discussion

siRNA molecules hold great therapeutic potential for the development of RNAi based drugs to interfere with various diseases.[179,180,187–189] However, siRNA therapeutics were limited by their low bioavailability due to their physicochemical properties (negative charges, large molecular weight, and size) and instability with plasma half-life of about 10 min [10,111,190], immune stimulation when administered systemically [191], and possible off-target effects due to partial nucleotide sequence match between the siRNA and off-target mRNA [192]. Seeking efficient delivery systems for these molecules is a prerequisite for successful gene therapy. CPPs as one group of nonviral peptide-based delivery vectors have attracted more and more attention due to their high internalization efficiency, low cytotoxicity, and flexible structural design.[187,193,194] Recently, a handful of papers have

shown that stearylation is a successful strategy to enhance the transfection efficiency of CPPs mostly for DNA delivery. Several delivery systems have incorporated this strategy for siRNA delivery [195]. Considering the similarities and differences between DNA/plasmid and siRNA, a novel siRNA delivery vector was constructed by the conjugation of stearic acid to the N-terminus of the sequence ”HHHPKPKRKV”, where “PKPKRKV” is a cytoplasm localization sequence. Our result demonstrated that after cellular uptake, the Cy3-labeled siRNAs were localized in the cytosol and distributed in a heterogeneous pattern (Figure 8), which indicated the possibility of siRNA uptake via an endocytotic pathway [107].

The formation of stable and small nanoparticles for CPP-siRNA complexes is undoubtedly an important feature to mediate high transfection efficiency.[122] The result of Agarose gel shift assay suggested that STR-HK at molar ratios above 15/1 was sufficient to neutralize the negative charge of siRNA and form complexes with siRNA. The high affinity of STR-HK for siRNA (K_d : 2.68E-6 M) is essentially associated with electrostatic interactions involving arginine, lysine residues, and siRNA molecules. Moreover, ITC data revealed that the interaction between STR-HK and siRNA was thermodynamically favored, and the driving forces include hydrophobic interaction among stearyl moieties and hydrogen bonding among amino acid residues when the peptide forms β sheet secondary structure. The conformational change of STR-HK from random coil to β sheet secondary structure upon the formation of STR-HK-siRNA complexes indicated that STR-HK represented a more stable structure when forming complexes with siRNA than peptide alone. Moreover, the stable complexes protect siRNA molecules without affecting their silencing efficiency.

The SEM image and TEM image (Figure 6) showed that STR-HK-siRNA complexes displayed a spherical shape. Ideally, to target tumors, the diameter of CPPs-siRNA particles should not exceed 100 - 300 nm for efficient uptake.[187] In this report, the particle size of STR-HK-siRNA complexes at a molar ratio of >15/1 was in the range of 100 - 160 nm and fulfilled the criteria of size required for an efficient transfection agent. At a molar ratio of 10/1, STR-HK-siRNA complexes displayed a slightly negative surface charge (-13 mV), indicating the surface of the complex was not fully covered by positive charged peptide. At a molar ratio of 15/1, the surface charge of the complex increased to 15 mV, implying that the

surface of the complex was fully covered by peptide; at even a higher molar ratio, the surface charge of the complex increased to 42 mV (at MR 60/1). The net positive surface charge could reduce the aggregation of the complexes and enhance the affinity of the complexes with the negatively charged cell membrane via electrostatic interaction [95], thus, potentially increasing the siRNA delivery efficiency. The quantified cellular uptake of Cy3-labeled siRNA showed that at a molar ratio of 20/1, the uptake of Cy3-labeled siRNA was 14 %, however, at a molar ratio of 40/1, it increased to 79%. This significant change was probably due to the increase of the net positive surface charge and the content of stearyl moiety that enhances the interaction of the complex and the lipid bilayer via hydrophobic force. In addition, at a molar ratio of 60/1, the uptake efficiency increased to 87%, which is similar to that of Lipo but significantly higher than that at a molar ratio of 40/1, implying that optimization of the molar ratio for siRNA delivery is crucial.

After STR-HK-siRNA complexes entered the cytoplasm, the stearyl moiety could disrupt the endosomal membrane through hydrophobic interaction with the lipid bilayer and the histidine residues could induce the proton sponge effect, leading to the rupture of the endosomal membrane to facilitate the endosomal release of siRNA.[87] The results showed that the transfection efficiency was consistent with the cellular uptake efficiency at various molar ratios. At a molar ratio of 60/1, STR-HK achieved a similar transfection level to that obtained with Lipo. The significant difference in GAPDH transfection level at a molar ratio of 40/1 and 60/1 is possibly caused by the significant difference in siRNA uptake and different amount of stearyl moiety and histidine in the complex formulation that affected the endosome release of siRNA. Furthermore, the cytotoxicity of STR-HK was less than 5%, which was significantly lower than that of Lipo. Taken together, a schematic of the uptake of STR-HK-siRNA complex and its endosomal release was proposed (Figure 6.11). Moreover, Effective in vivo RNAi was achieved in a human non-small lung tumor xenograft model through intratumoral injection of the STR-HK-Bcl-2 siRNA complexes (molar ratio: 60/1). STR-HK-Bcl-2 siRNA complexes resulted in a tumor inhibition rate of 63%±3 via downregulation of Bcl-2 protein in mice (data not reported).

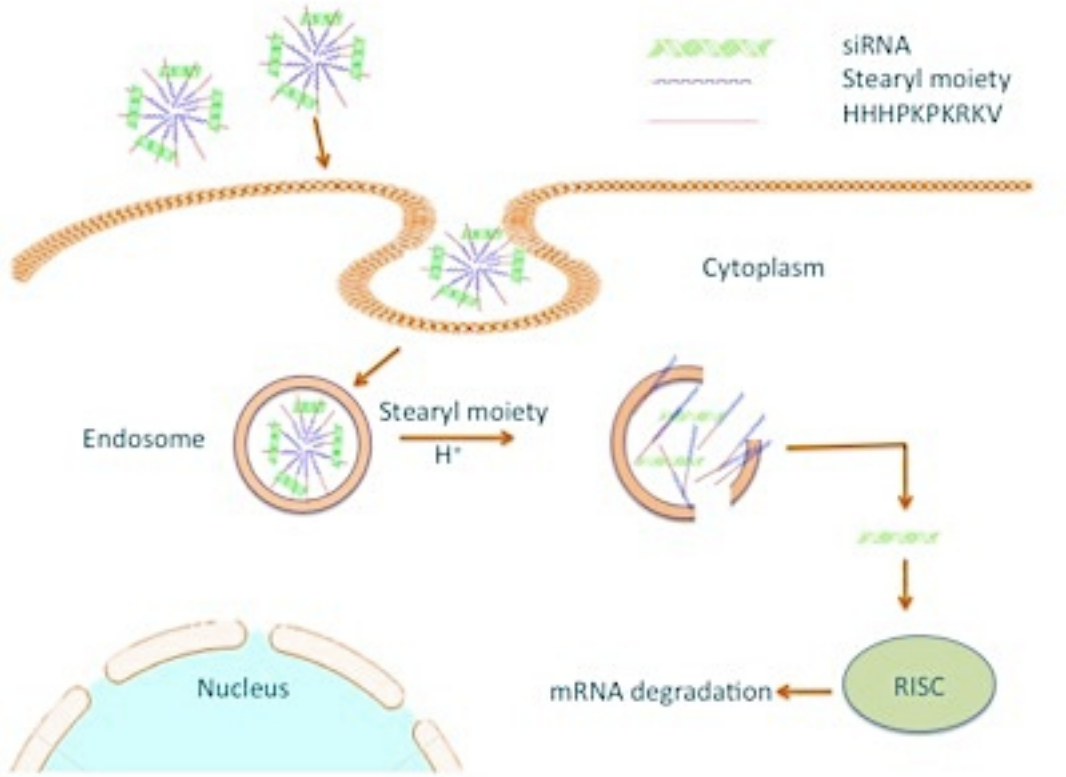

Figure 6.11. The schematic of STR-HK-siRNA complex uptake and endosomal release.

6.6 Conclusions

In this study, a novel siRNA delivery vector was constructed by coupling stearic acid to the N-terminus of "HHHPKPKRKV". Our results demonstrated that STR-HK formed stable complexes with siRNA via non-covalent interactions and mediated efficient delivery of siRNA to PC-3 cells. These results, with the fact that STR-HK induced minimal cytotoxicity while achieving comparable gene silencing efficiency to Lipofectamine 2000, prove that STR-HK is a promising vector for siRNA delivery.

Chapter 7
Original Contributions and Recommendations

7.1 Original Contributions to Research

This thesis focuses on characterization and evaluation of the three newly designed peptides as potential siRNA delivery systems. These three peptides were designed according to the following strategies: (1) modification of the amphipathic, cationic peptide C6 with tryptophan and histidine in the sequence; (2) adoption of parts of peptides CADY and C6M3 along with addition of an amphipilic segment; (3) conjugation of a stearyl moiety to peptide sequence. This thesis includes: (i) characterize physicochemical properties of peptide-siRNA complexes, such as size, charge, secondary structure; (ii) investigate the delivery efficiency, gene silencing effect, and cytotoxicity induced by the peptide-siRNA complexes; (iii) establish multicellular tumor spheroids to examine peptide GL1's potential as siRNA delivery systems; (iv) evaluate siRNA therapeutic effects in an animal xenograft tumor model.

Characterization of a Histidine Containing Amphipathic, Cationic Peptide C6M3 for siRNA Delivery

C6M3, an 18-mer-amphipathic peptide, formed complexes with siRNA exhibiting small particle sizes (<100 nm). C6M3 adopted helical secondary structure in water and became more so upon binding to siRNA. Zeta potential and agarose gel experiments showed the ability of C6M3 to completely encapsulate siRNA at molar ratio of 10/1. ITC data revealed that the stoichiometry between C6M3 and siRNA is 7/1, which is consistent with the theoretical value considering each peptide consists of 6 positive charge residues (R) and siRNA contains 21 negative charge base pairs. However, FACS results revealed that higher molar ratios were required to achieve better siRNA uptake efficiency. Western blot experiment and cell viability data showed that C6M3-siRNA complexes induced 67%

inhibition of GAPDH protein expression with minimal cytotoxicity (<10%). These data demonstrate that C6M3 is a promising carrier for siRNA delivery and the modification strategy is useful.

Design and Characterization of an Amphipathic, Cationic Peptide GL1 for siRNA Delivery in Monolayer Culture

In this study, we have investigated the physicochemical characteristics of the peptide GL1, and evaluated its siRNA delivery efficiency and cellular toxicity on the CHO-K1 cell line. The major conclusions include the following: GL1 could form complexes with siRNA cargo at molar ratio ~10/1 mainly via electrostatic interaction and hydrophobic interaction; GL1 could spontaneously condense siRNA to form spherical particles with sizes on the nanoscale (80-100 nm); GL1 adopted α-helical secondary structure and became more so upon interaction with siRNA molecules to form stable complexes; at molar ratio 40/1, GL1 achieved higher cellular uptake of Cy3-labeled siRNA (95%) than Lipofectamine 2000 in serum free environment and retained the same level of uptake as Lipofectamine 2000 (84%) with the presence of serum; in all the studied molar ratios, GL1 achieved higher cellular viability (>85%) compared to Lipofectamine 2000 (~70%). Therefore, GL1 demonstrated the potential as a vector for siRNA delivery.

Evaluation of the Potential of GL1 Peptide for siRNA Delivery in Multicellular Tumor Spheroids and *In Vivo*

Our studies suggest that MCTS closely mimic the features of tumors in vivo, confirmed through the morphologic characterizations. Utilizing confocal laser scanning microscopy, we observed that GL1-siRNA complexes could penetrate into the deeper layers of MCTS over the time. Taking into account that GL1 achieved marked gene silencing efficiency (50%), compared to the commercial transfection reagent, Lipofectamine 2000 (38%), with minimal cytotoxicity in multicellular tumor spheroids (<10%), and that GL1-Bcl-2 siRNA complexes

enabled significant anti-tumor effects in vivo (52.6%), this indicates that GL1 is a highly promising siRNA delivery vector, both in vitro and in vivo.

Characterization and Investigation of a Stearylated Cationic Peptide STR-HK for siRNA Delivery

In this study, a novel siRNA delivery vector was constructed by coupling stearic acid to the N-terminus of "HHHPKPKRKV". Our results demonstrated that STR-HK formed stable complexes with siRNA via non-covalent interactions and mediated efficient delivery of siRNA to PC-3 cells. These results, with the fact that STR-HK induced minimal cytotoxicity while achieving comparable gene silencing efficiency to Lipofectamine 2000, prove that STR-HK is a promising vector for siRNA delivery.

7.2 Recommendations

Based on the studies carried out in this research, the following recommendations for future studies are proposed:

1. Conjugating cell targeting peptides (CTPs) motifs with these three peptides or their modified versions to determine the targeting efficiency of the complexes *in vitro* and *in vivo*
2. Applying TEM and histology to characterize the internal structure of MCTS and FACS to quantify the uptake of siRNA in MCTS
3. Co-culture the normal cells and cancer cells in 3D to closely mimic the tumor microenvironment and evaluating the efficiency of the complexes in this co-culture MCTS
4. Investigate the biocompatibility and serum stability of these three peptides

Appendix A[†††]

An Amphipathic, Cationic Peptide mediated siRNA Delivery in 3D Culture

Purpose: RNA interference is a natural regulatory process where small, double-stranded RNA molecules (typically 21-25 nucleotides) turn off specific genes in a biological cell. siRNA therapeutic has been hampered by its hydrophilicity, negative charge, and sensitivity to enzyme degradation. Thus, a safe and effective delivery system is mandatory. Our group has designed and characterized an amphipathic, cationic peptide (STR-H16R8), which can achieve pronounced siRNA uptake and gene silencing in monolayer culture. However, due to the lack of characteristics present in live tissues, the preliminary data generated in monolayer cultures may not be predictive as that *in vivo*. Therefore, a 3D cell culture model mimicking the *in vivo* tumors is utilized here to evaluate the cytotoxicity and gene silencing efficiency of STR-H16R8-siRNA complexes.

Methods: The 3D culture model of A549 cells was established using hanging drop method and characterized with light microscopy, confocal microscopy, and scanning electron microscopy. The cytotoxicity and gene silencing efficiency of STR-H16R8-siRNA complexes were quantified with WST-1 assay and qRT-PCR respectively.

Results: A549 cells in 3D culture closely mimicked the properties of tumors proven through microscopic characterizations. STR-H16R8-siRNA complexes induced significant Bcl-2 gene silencing efficiency with minimal cytotoxicity. Note that the complexes achieved lower gene silencing efficiency in 3D than that in 2D, possibly because of the complex microenvironment in 3D culture.

Conclusion: This data provides evidence of the differences in delivering siRNA to 3D cell culture model, comparing to monolayer cell cultures. The simple and reproducible 3D cell culture model introduced here is a useful system for evaluating the future gene delivery systems.

[†††] This Appendix is based on a conference Abstract. Baoling Chen, P. Chen. An Amphipathic, Cationic Peptide mediated siRNA Delivery in 3D culture. Journal of Pharmacy & Pharmaceutical Sciences, 2015, accepted.

Appendix B

GL Family Peptides Screening

CHO-K1 cells were seeded in a 96-well plate with 5,000 cells/well one day before transfection. 24 h later, the peptide/siRNA complexes containing GAPDH siRNA or negative control siRNA were prepared in Opti-MEM and added to each well in quintuplicate giving a final siRNA concentration of 50 nM. After 4 h of incubation at 37°C, equal volume of medium with 20% FBS were added to the cells. After 48 h, the GAPDH enzyme activity was detected using KDalert™ GAPDH assay kit (Life Technologies, Burlington, Canada) according to the manufacturer's protocol.

GAPDH is a tetrameric enzyme, composed of 36 kD protein subunits. It catalyzes the oxidative phosphorylation of glyceraldehyde-3-phosphate (G-3-P) to bisphosphoglycerate (BPG):

$$G-3-P+PO_4^{-2}+NAD^+ \xrightarrow{GAPDH} BPG+NADH+H^+$$

The KDalert GAPDH Assay measures the conversion of NAD+ to NADH by GAPDH in the presence of phosphate and G-3-P. Under the recommended assay conditions, the rate of NADH production is proportional to the amount of GAPDH enzyme present. Thus, this assay can be used to determine the amount of GAPDH protein in a sample. The increase of fluorescence intensity was measured with a FLUOstar OPTIMA microplate reader (BMG Labtech, Ortenberg, Germany) with excitation wavelength at 560 nm and emission wavelength at 590 nm. The GAPDH gene knockdown efficiency was expressed as 100% - the fluorescence intensity of cells treated with GAPDH siRNA/ the cells treated with negative control siRNA. The peptides used here were listed in Table 1. The GAPDH gene silencing efficiency at protein level induced by peptide-siRNA complexes at molar ratio 40/1 with siRNA concentration of 50 nM was shown in Figure 1.

Table 4.2. GL family peptides.

Name	Sequence
GL1	Ac-GLWRAWLWKAFLASNWRRLLRLLR-NH_2
GL2	Ac-GLWRASWLKAWLASNWHKKHRLLR-NH_2
GL3	Ac-GLWGAWFIEGWEGMIDGRRLLRLLR-NH_2
GL4	Ac-GLWRASWLKAFLASNWHKKLHKK-NH_2

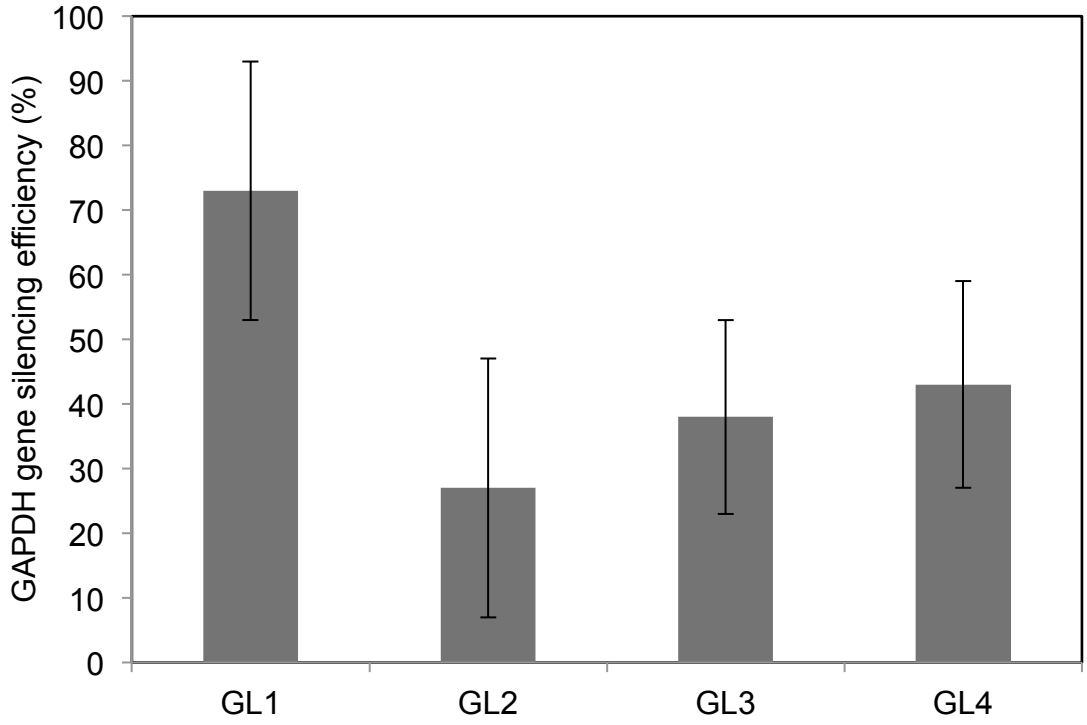

Figure 1. GAPDH gene silencing efficiency at protein level.48 h post transfection, the cells was disrupted in lysis buffer before adding KDalert master mix. The fluorescence intensity was read on a plate reader at 590 nm. The molar ratio used here was 40/1 (peptide/siRNA) with siRNA concentration of 50 nM (n=5).

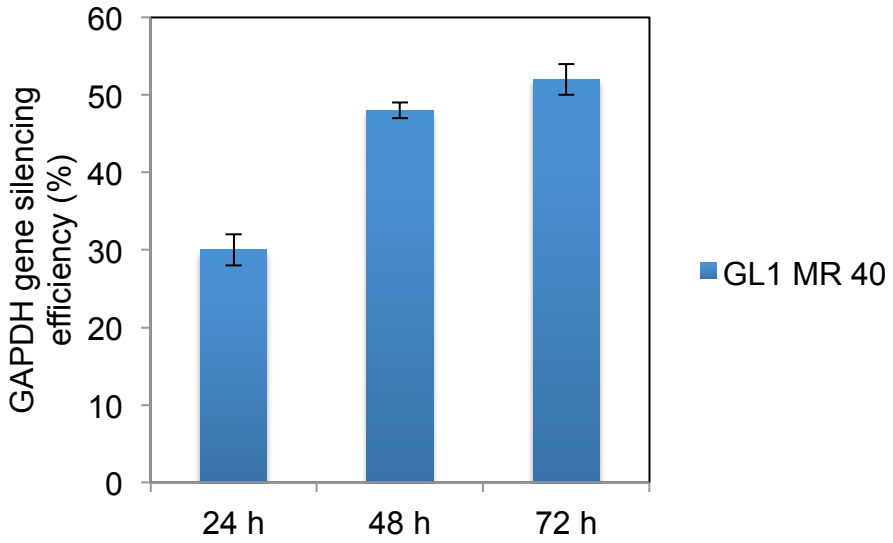

Figure 2. GAPDH gene silencing efficiency at mRNA level determined with real time PCR in CHO cells. GL1-siRNA complexes at molar ratio 40/1 induced gene silencing efficiency at 24 h, 48 h, and 72 h post transcription.

Appendix C

Delivery Efficacy of STR-HK Peptide in CHO-K1 Cells

The detailed procedures are described in sections 4.2.2.8, 4.2.2.9, and 4.2.2.10. The results are shown below.

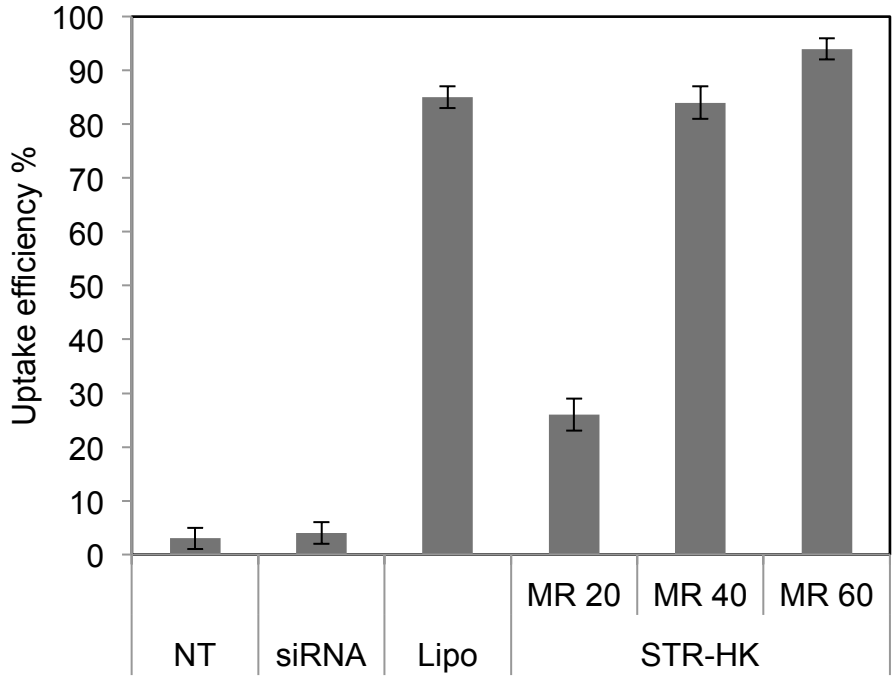

Figure 1. Cellular uptake of siRNA quantified by FACS. Non-treated sample was negative control; Lipo-siRNA complexes were positive control. Cy3 labeled GAPDH siRNA was used here with a concentration of 50 nM. (NT= Non-treated, MR=peptide/siRNA molar ratio, Lipo=Lipofectamine 2000). Results are expressed as mean ± standard deviation (n=3).

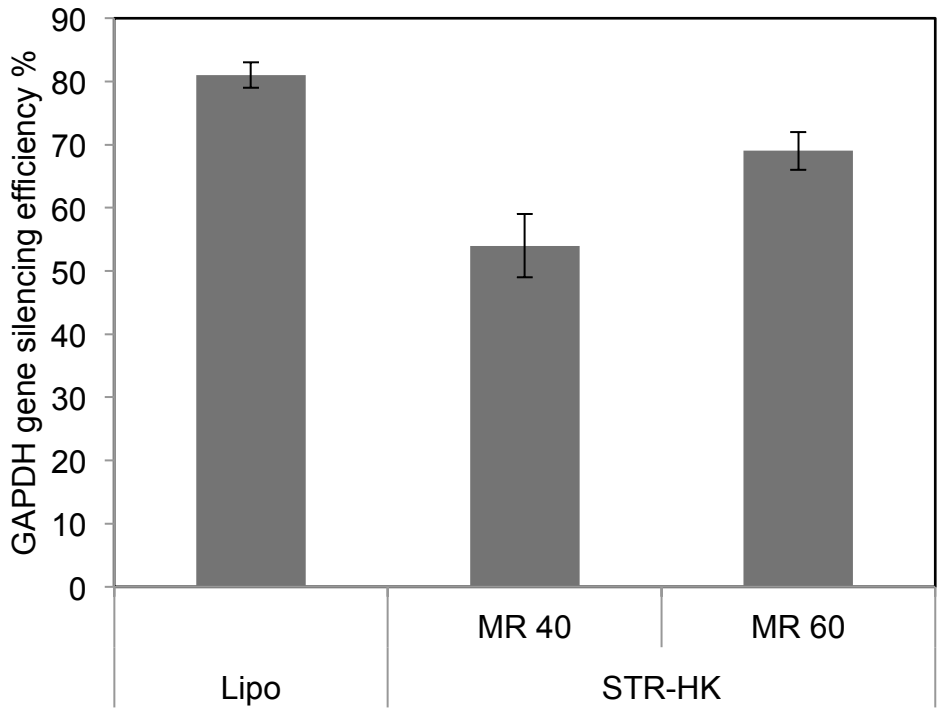

Figure 2. Gene silencing efficiency *in vitro*. Silencing of GAPDH gene in CHO-K1 cells was evaluated by quantitative real time polymerase chain reaction (qRT-PCR). GAPDH siRNA concentration was 50 nM. Lipo was the positive control, and scrambled siRNA was used as the negative control. Results are expressed as mean ± standard deviation (n = 3).

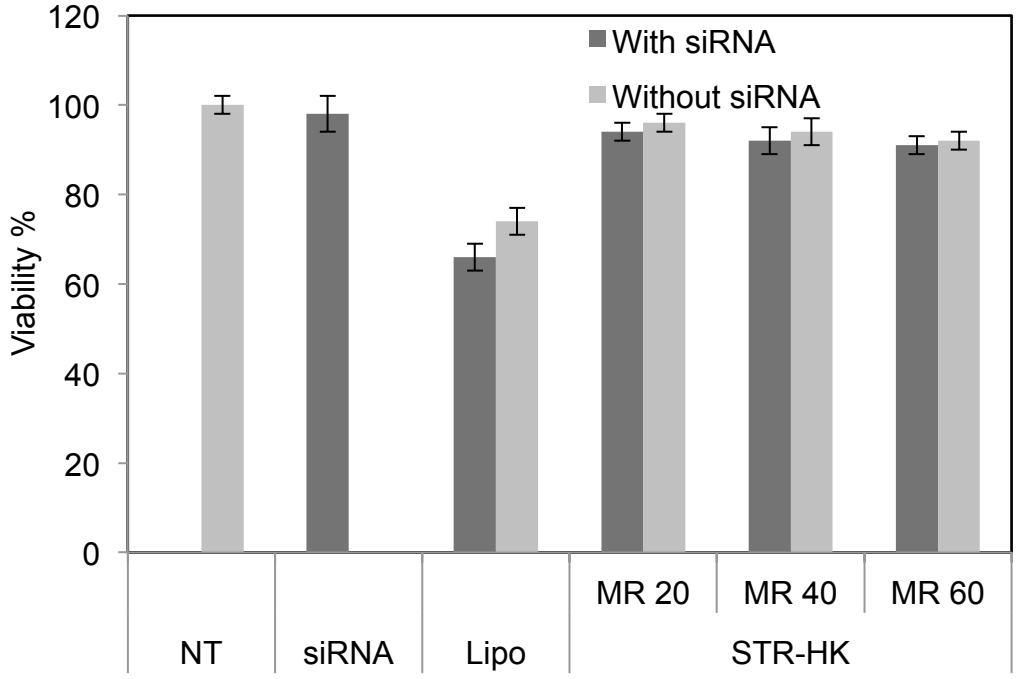

Figure 3. Cell viability results of CHO-K1 cells treated with naked Lipofectamine 2000 or GL1, and the complexes with siRNA (50 nM) at different molar ratios. (NT= Non-treated, MR=peptide/siRNA molar ratio, Lipo=Lipofectamine 2000). Results are expressed as mean ± standard deviation (n=3).

Appendix D

HPLC & LC-MS Data of GL1 Peptide and C6M3 Peptide

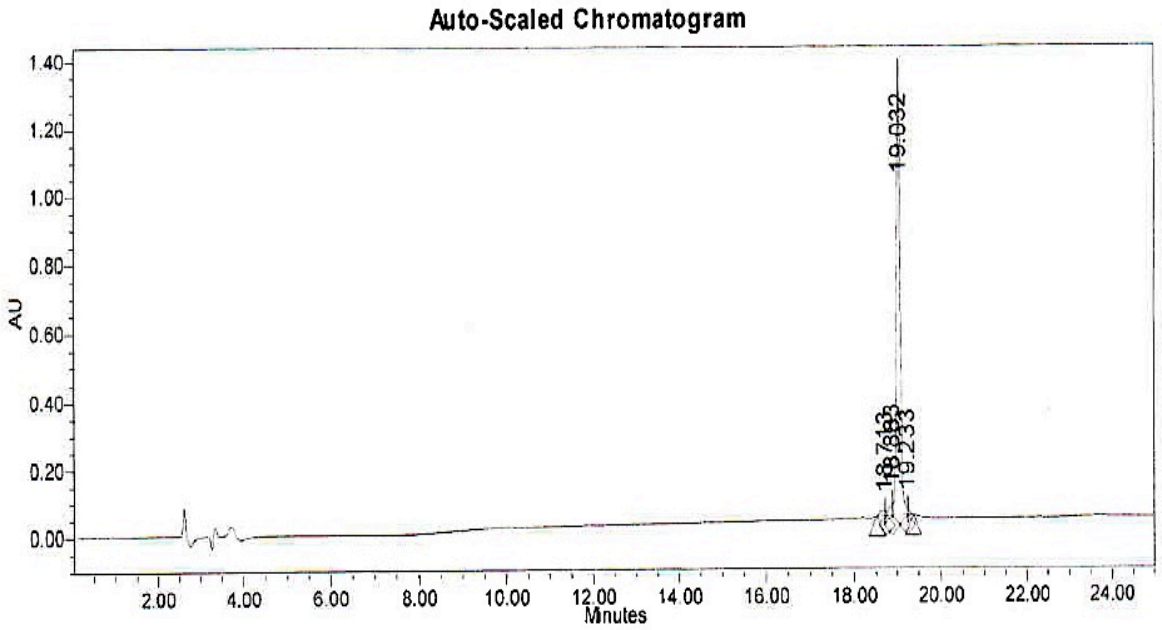

Peak Results

	Name	RT	Area	Height	% Area
1		18.713	128047	13376	1.64
2		18.883	169686	35238	2.18
3		19.032	7432739	1302679	95.45
4		19.233	56309	17436	0.72

Figure 1. HPLC chromatogram of GL1 peptide. HPLC conditions: Waters 600 Multi-Solvent System, solvent A is 0.1% TFA/ACN, solvent B is 0.1% TFA/H_2O, column: Vydac Protein & Peptides C18, 5u, 4.6x250 mm, flow rate: 1 mL/min.

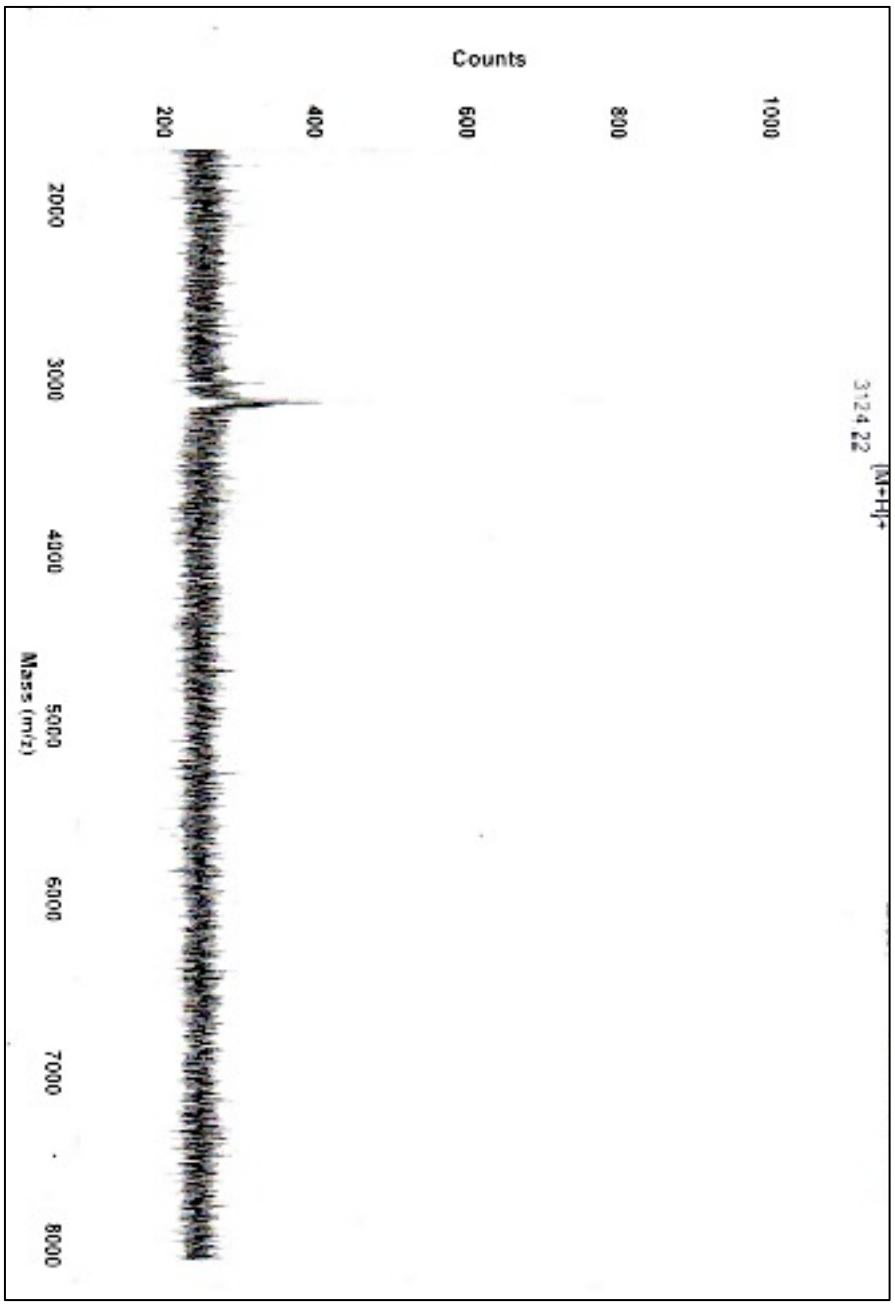

Figure 2. LC-MS data of GL1 peptide. The charge on the ion is 1+. The peak with the highest value for m/z indicates the desired compound (Peptide+H)+ and the value (3124.22) is the relative formula mass of the compound.

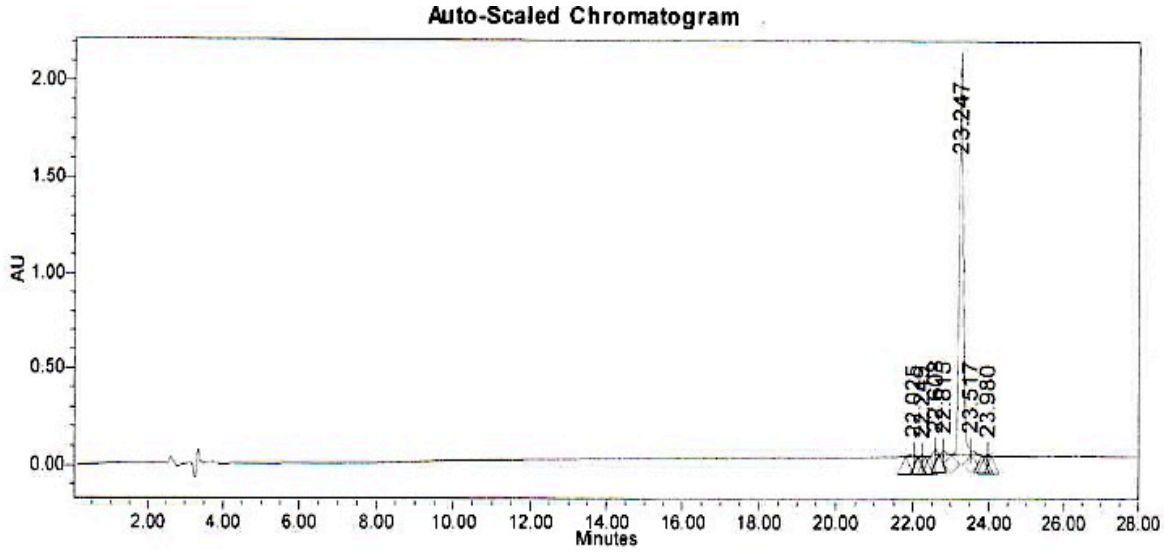

Peak Results

	Name	RT	Area	Height	% Area
1		22.025	122108	11826	0.77
2		22.249	33295	6604	0.21
3		22.608	186491	25757	1.18
4		22.815	154934	20004	0.98
5		23.247	15097996	2052806	95.32
6		23.517	197603	24867	1.25
7		23.980	46144	8410	0.29

Figure 3. HPLC chromatogram of C6M3 peptide. HPLC conditions: Waters 600 Multi-Solvent System, solvent A is 0.1% TFA/ACN, solvent B is 0.1% TFA/H_2O, column: Vydac Protein & Peptides C18, 5u, 4.6x250 mm, flow rate: 1 mL/min.

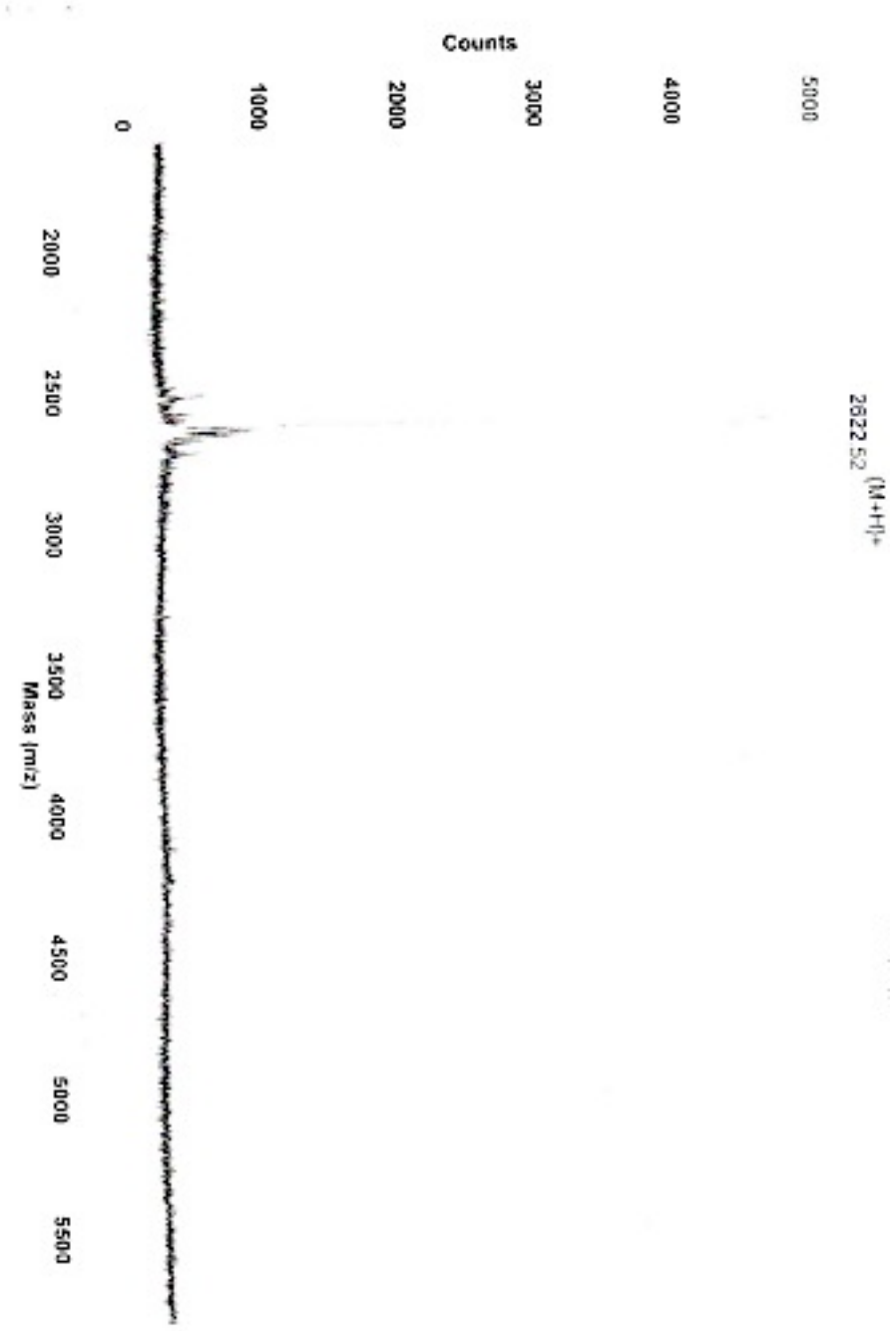

Figure 4. LC-MS data of C6M3 peptide. The charge on the ion is 1+. The peak with the highest value for m/z indicates the desired compound (Peptide+H)+ and the value (2622.52) is the relative formula mass of the compound.

Bibliography

[1] Hannon G. RNA interference. Nat 2002;418:24–6.

[2] Pecot C V, Calin G a, Coleman RL, Lopez-Berestein G, Sood AK. RNA interference in the clinic: challenges and future directions. Nat Rev Cancer 2011;11:59–67.

[3] Manfredsson FP, Lewin a S, Mandel RJ. RNA knockdown as a potential therapeutic strategy in Parkinson's disease. Gene Ther 2006;13:517–24.

[4] Jacque J-M, Triques K, Stevenson M. Modulation of HIV-1 replication by RNA interference. Nat 2002;418:435–8.

[5] Kaiser PK, Symons RCA, Shah SM, Quinlan EJ, Tabandeh H, Do D V, et al. RNAi-based treatment for neovascular age-related macular degeneration by sirna-027. Am J Ophthalmol 2010;150:33–9.

[6] Czech MP, Aouadi M, Tesz GJ. RNAi-based therapeutic strategies for metabolic disease. Nat Rev Endocrinol 2011;7:473–84.

[7] Xu H, Wilcox D, Nguyen P, Voorbach M, Smith H, Brodjian S, et al. Hepatic knockdown of stearoyl-CoA desaturase 1 via RNA interference in obese mice decreases lipid content and changes fatty acid composition. Front Biosci a J Virtual Libr 2007;12:3781–94.

[8] Hibbitt O, Agkatsev S, Owen C, Cioroch M, Seymour L, Channon K, et al. RNAi-mediated knockdown of HMG CoA reductase enhances gene expression from physiologically regulated low-density lipoprotein receptor therapeutic vectors in vivo. Gene Ther 2012;19:463–7.

[9] Courties G, Presumey J, Duroux-Richard I, Jorgensen C, Apparailly F. RNA interference-based gene therapy for successful treatment of rheumatoid arthritis. Expert Opin Biol Ther 2009;9:535–8.

[10] Takahashi Y, Nishikawa M, Takakura Y. Nonviral vector-mediated RNA interference: its gene silencing characteristics and important factors to achieve RNAi-based gene therapy. Adv Drug Deliv Rev 2009;61:760–6.

[11] Zhen G, Hinton TM, Muir BW, Shi S, Tizard M, McLean KM, et al. Glycerol monooleate-based nanocarriers for siRNA delivery in vitro. Mol Pharm 2012;9:2450–7.

[12] Wang J, Lu Z, Wientjes MG, Au JL-S. Delivery of siRNA therapeutics: barriers and carriers. AAPS J 2010;12:492–503.

[13] Meade BR, Dowdy SF. Exogenous siRNA delivery using peptide transduction domains/cell penetrating peptides. Adv Drug Deliv Rev 2007;59:134–40.

[14] Kanasty R, Dorkin JR, Vegas A, Anderson D. Delivery materials for siRNA therapeutics. Nat Mater 2013;12:967–77.

[15] Maria Alsina, Tabemero Josep, Shapiro Geoffrey, Burris Howard, Infante Jeffrey R., Weiss Glen J. C-RA et al. Open-label extension study of the RNAi therapeutic ALN-VSP02 in cancer patients responding to therapy. J. Clin. Oncol., vol. 30, 2012.

[16] Khan A, Benboubetra M, Sayyed PZ, Ng KW, Fox S, Beck G, et al. Sustained polymeric delivery of gene silencing antisense ODNs, siRNA, DNAzymes and ribozymes: in vitro and in vivo studies. J Drug Target 2004;12:393–404.

[17] Katas H, Cevher E, Alpar HO. Preparation of polyethyleneimine incorporated poly(D,L-lactide-co-glycolide) nanoparticles by spontaneous emulsion diffusion method for small interfering RNA delivery. Int J Pharm 2009;369:144–54.

[18] Nafee N, Taetz S, Schneider M, Schaefer UF, Lehr C-M. Chitosan-coated PLGA nanoparticles for DNA/RNA delivery: effect of the formulation parameters on complexation and transfection of antisense oligonucleotides. Nanomedicine 2007;3:173–83.

[19] Patil Y, Panyam J. Polymeric nanoparticles for siRNA delivery and gene silencing. Int J Pharm 2009;367:195–203.

[20] Murata N, Takashima Y, Toyoshima K, Yamamoto M, Okada H. Anti-tumor effects of anti-VEGF siRNA encapsulated with PLGA microspheres in mice. J Control Release 2008;126:246–54.

[21] Gonzalez H, Hwang SJ, Davis ME. New class of polymers for the delivery of macromolecular therapeutics. Bioconjug Chem 1999;10:1068–74.

[22] Hu-Lieskovan S, Heidel JD, Bartlett DW, Davis ME, Triche TJ. Sequence-specific knockdown of EWS-FLI1 by targeted, nonviral delivery of small interfering RNA inhibits tumor growth in a murine model of metastatic Ewing's sarcoma. Cancer Res 2005;65:8984–92.

[23] Pun SH, Bellocq NC, Liu A, Jensen G, Machemer T, Quijano E, et al. Cyclodextrin-modified polyethylenimine polymers for gene delivery. Bioconjug Chem 2004;15:831–40.

[24] Pun SH, Davis ME. Development of a nonviral gene delivery vehicle for systemic application. Bioconjug Chem 2002;13:630–9.

[25] Hwang SJ, Bellocq NC, Davis ME. Effects of structure of beta-cyclodextrin-containing polymers on gene delivery. Bioconjug Chem 2001;12:280–90.

[26] Popielarski SR, Mishra S, Davis ME. Structural effects of carbohydrate-containing polycations on gene delivery. 3. Cyclodextrin type and functionalization. Bioconjug Chem 2003;14:672–8.

[27] Davis ME. The first targeted delivery of siRNA in humans via a nanoparticle : from concept to clinic 2009;6:659–68.

[28] Mishra S, Heidel JD, Webster P, Davis ME. Imidazole groups on a linear, cyclodextrin-containing polycation produce enhanced gene delivery via multiple processes. J Control Release 2006;116:179–91.

[29] Bartlett DW, Su H, Hildebrandt IJ, Weber W a, Davis ME. Impact of tumor-specific targeting on the biodistribution and efficacy of siRNA nanoparticles measured by multimodality in vivo imaging. Proc Natl Acad Sci U S A 2007;104:15549–54.

[30] Bartlett DW, Davis ME. Impact of tumor-specific targeting and dosing schedule on tumor growth inhibition after intravenous administration of siRNA-containing nanoparticles 2008;99:975–85.

[31] Fire, A., Xu, S.Q., Montgomery, M.K., Kostas, S.A., Driver, S.E., Mello CC. Potent and specific genetic interference by double-stranded RNA in Caenorhabditis elegans. Nat 1998;391:806–11.

[32] Svenson S. Dendrimers as versatile platform in drug delivery applications. Eur J Pharm Biopharm 2009;71:445–62.

[33] Tseng Y-C, Mozumdar S, Huang L. Lipid-based systemic delivery of siRNA. Adv Drug Deliv Rev 2009;61:721–31.

[34] Hatakeyama H, Ito E, Akita H, Oishi M, Nagasaki Y, Futaki S, et al. A pH-sensitive fusogenic peptide facilitates endosomal escape and greatly enhances the gene silencing of siRNA-containing nanoparticles in vitro and in vivo. J Control Release 2009;139:127–32.

[35] Semple SC, Akinc A, Chen J, Sandhu AP, Mui BL, Cho CK, et al. Rational design of cationic lipids for siRNA delivery. Nat Biotechnol 2010;28:172–6.

[36] Bao Y, Jin Y, Chivukula P, Zhang J, Liu Y, Liu J, et al. Effect of PEGylation on biodistribution and gene silencing of siRNA/lipid nanoparticle complexes. Pharm Res 2013;30:342–51.

[37] Belliveau NM, Huft J, Lin PJ, Chen S, Leung AK, Leaver TJ, et al. Microfluidic synthesis of highly potent limit-size lipid nanoparticles for in vivo delivery of siRNA. Mol Ther Nucleic Acids 2012;1:e37.

[38] Kolli S, Wong S-P, Harbottle R, Johnston B, Thanou M, Miller AD. pH-triggered nanoparticle mediated delivery of siRNA to liver cells in vitro and in vivo. Bioconjug Chem 2013;24:314–32.

[39] Lin S-Y, Zhao W-Y, Tsai H-C, Hsu W-H, Lo C-L, Hsiue G-H. Sterically polymer-based liposomal complexes with dual-shell structure for enhancing the siRNA delivery. Biomacromolecules 2012;13:664–75.

[40] Akinc A, Querbes W, De S, Qin J, Frank-Kamenetsky M, Jayaprakash KN, et al. Targeted delivery of RNAi therapeutics with endogenous and exogenous ligand-based mechanisms. Mol Ther 2010;18:1357–64.

[41] Wan K, Ebert B, Voigt J, Wang Q, Dai Y, Haag R, et al. In vivo tumor imaging using a novel RNAi-based detection mechanism. Nanomedicine 2012;8:393–8.

[42] Yoshizawa T, Hattori Y, Hakoshima M, Koga K, Maitani Y. Folate-linked lipid-based nanoparticles for synthetic siRNA delivery in KB tumor xenografts. Eur J Pharm Biopharm 2008;70:718–25.

[43] Feng C, Wang T, Tang R, Wang J, Long H, Gao X, et al. Silencing of the MYCN gene by siRNA delivered by folate receptor-targeted liposomes in LA-N-5 cells. Pediatr Surg Int 2010;26:1185–91.

[44] Sahay G, Querbes W, Alabi C, Eltoukhy A, Sarkar S, Zurenko C, et al. Efficiency of siRNA delivery by lipid nanoparticles is limited by endocytic recycling. Nat Biotechnol 2013;31:653–8.

[45] Love KT, Mahon KP, Christopher G, Whitehead KA, Querbes W, Robert J, et al. Lipid-like materials for low-dose, in vivo gene silencing. Proc Natl Acad Sci 2010;107:1864–9.

[46] Akinc A, Zumbuehl A, Goldberg M, Leshchiner ES, Busini V, Hossain N, et al. A combinatorial library of lipid-like materials for delivery of RNAi therapeutics. Nat Biotechnol 2008;26:561–9.

[47] Rozema DB, Lewis DL, Wakefield DH, Wong SC, Klein JJ, Roesch PL, et al. Dynamic PolyConjugates for targeted in vivo delivery of siRNA to hepatocytes. Proc Natl Acad Sci U S A 2007;104:12982–7.

[48] Rensen PCN, van Leeuwen SH, Sliedregt L a JM, van Berkel TJC, Biessen E a L. Design and synthesis of novel N-acetylgalactosamine-terminated glycolipids for targeting of lipoproteins to the hepatic asialoglycoprotein receptor. J Med Chem 2004;47:5798–808.

[49] Biessen E a, Beuting DM, Roelen HC, van de Marel G a, van Boom JH, van Berkel TJ. Synthesis of cluster galactosides with high affinity for the hepatic asialoglycoprotein receptor. J Med Chem 1995;38:1538–46.

[50] Lee H, Lytton-Jean AKR, Chen Y, Love KT, Park AI, Karagiannis ED, et al. Molecularly self-assembled nucleic acid nanoparticles for targeted in vivo siRNA delivery. Nat Nanotechnol 2012;7:389–93.

[51] Vivès E, Schmidt J, Pèlegrin A. Cell-penetrating and cell-targeting peptides in drug delivery. Biochim Biophys Acta 2008;1786:126–38.

[52] Lewin M, Carlesso N, Tung CH, Tang XW, Cory D, Scadden DT, et al. Tat peptide-derivatized magnetic nanoparticles allow in vivo tracking and recovery of progenitor cells. Nat Biotechnol 2000;18:410–4.

[53] Chiu Y, Ali A, Chu C, Cao H, Rana T. Visualizing a correlation between siRNA localization, cellular uptake, and RNAi in living cells. Chem Biol 2004;11:1165–75.

[54] Deshayes S, Heitz A, Morris MC, Charnet P, Divita G, Heitz F. Insight into the mechanism of internalization of the cell-penetrating carrier peptide Pep-1 through conformational analysis. Biochemistry 2004;43:1449–57.

[55] Simeoni F, Morris MC, Heitz F, Divita G. Insight into the mechanism of the peptide-based gene delivery system MPG: Implications for delivery of siRNA into mammalian cells. Nucleic Acids Res 2003;31:2717–24.

[56] D'Andrea LD, Del Gatto A, Pedone C, Benedetti E. Peptide-based molecules in angiogenesis. Chem Biol Drug Des 2006;67:115–26.

[57] Press P. Opioid agonist and antagonist bivalent ligands as receptor probes. J Life Sci 1982;31:1283–6.

[58] Ye Y, Bloch S, Xu B, Achilefu S. Design, synthesis, and evaluation of near infrared fluorescent multimeric RGD peptides for targeting tumors. J Med Chem 2006;49:2268–75.

[59] Xiong JP, Stehle T, Diefenbach B, Zhang R, Dunker R, Scott DL, et al. Crystal structure of the extracellular segment of integrin alpha Vbeta3. Science 2001;294:339–45.

[60] Dijkgraaf I, Kruijtzer J a W, Liu S, Soede AC, Oyen WJG, Corstens FHM, et al. Improved targeting of the alpha(v)beta (3) integrin by multimerisation of RGD peptides. Eur J Nucl Med Mol Imaging 2007;34:267–73.

[61] Dijkgraaf I, Liu S, Kruijtzer J a W, Soede AC, Oyen WJG, Liskamp RMJ, et al. Effects of linker variation on the in vitro and in vivo characteristics of an 111In-labeled RGD peptide. Nucl Med Biol 2007;34:29–35.

[62] Chen X., Tohme M., Park R., Hou Y., Bading J.R. CPS. Micro-PET imaging of alphavbeta3-integrin expression with 18F-labeled dimeric RGD peptide. Mol Imaging 2004;3:96–104.

[63] Harris TD, Cheesman E, Harris AR, Sachleben R, Edwards DS, Liu S, et al. Radiolabeled divalent peptidomimetic vitronectin receptor antagonists as potential tumor radiotherapeutic and imaging agents. Bioconjug Chem 2007;18:1266–79.

[64] Handl H.L., Sankaranarayanan R., Josan J.S., Vagner J., Mash E.A., Gillies R.J. HVJ. Synthesis and evaluation of bivalent NDP-alpha-MSH(7) peptide ligands for binding to the human melanocortin receptor 4 (hMC4R). Bioconjug Chem 2007;18:1101–19.

[65] Janssen M.L., Oyen W.J., Dijkgraaf I., Massuger L.F., Frielink C., Edwards D.S., Rajopadhe M., Boonstra H., Corstens F.H. BOC. Tumor targeting with radiolabeled alpha(v)beta(3) integrin binding peptides in a nude mouse model. Cancer Res 2002;62:6146–51.

[66] Dromi S, Frenkel V, Luk A, Traughber B, Angstadt M, Bur M, et al. Pulsed-high intensity focused ultrasound and low temperature-sensitive liposomes for enhanced targeted drug delivery and antitumor effect. Clin Cancer Res 2007;13:2722–7.

[67] Duncan Ruth, Cable Hazel C., Lloyd John B., Rejmanova Pavla KJ. Degradation of sidechains of N-(2-hydroxypropyl)methacrylamide copolymers by lysosomal thiolproteinases. Biosci Rep 1982;2:1041–6.

[68] Friend DS, Papahadjopoulos D, Debs RJ. Endocytosis and intracellular processing accompanying transfection mediated by cationic liposomes. Biochim Biophys Acta 1996;1278:41–50.

[69] Zuhorn IS, Kalicharan R, Hoekstra D. Lipoplex-mediated transfection of mammalian cells occurs through the cholesterol-dependent clathrin-mediated pathway of endocytosis. J Biol Chem 2002;277:18021–8.

[70] Conner SD, Schmid SL. Regulated portals of entry into the cell. Nature 2003;422:37–44.

[71] Khalil I, Kogure K, Akita H, Harashima H. Uptake pathways and subsequent intracellular trafficking in nonviral gene delivery. Pharmacol Rev 2006;58:32–45.

[72] Takei K, Haucke V. Clathrin-mediated endocytosis: membrane factors pull the trigger. Trends Cell Biol 2001;11:385–91.

[73] Maxfield FR, McGraw TE. Endocytic recycling. Nat Rev Mol Cell Biol 2004;5:121–32.

[74] Kolli S, Wong SP, Harbottle R, Johnston B, Thanou M, Miller AD. PH-triggered nanoparticle mediated delivery of siRNA to liver cells in vitro and in vivo. Bioconjug Chem 2013;24:314–32.

[75] Matveev S, Li X, Everson W, Smart EJ. The role of caveolae and caveolin in vesicle-dependent and vesicle-independent trafficking. Adv Drug Deliv Rev 2001;49:237–50.

[76] Ferrari a. Caveolae-Mediated internalization of extracellular HIV-1 tat fusion proteins visualized in real time. Mol Ther 2003;8:284–94.

[77] Matsui H, Johnson LG, Randell SH, Boucher RC. Loss of binding and entry of liposome-DNA complexes decreases transfection efficiency in differentiated airway epithelial cells. J Biol Chem 1997;272:1117–26.

[78] Subtil a, Hémar A, Dautry-Varsat A. Rapid endocytosis of interleukin 2 receptors when clathrin-coated pit endocytosis is inhibited. J Cell Sci 1994;107:3461–8.

[79] Perales JC, Grossmann G a, Molas M, Liu G, Ferkol T, Harpst J, et al. Biochemical and functional characterization of DNA complexes capable of targeting genes to hepatocytes via the asialoglycoprotein receptor. J Biol Chem 1997;272:7398–407.

[80] Horth M, Lambrecht B, Khim MC, Bex F, Thiriart C, Ruysschaert JM, et al. Theoretical and functional analysis of the SIV fusion peptide. EMBO J 1991;10:2747–55.

[81] Wiley DC, Skehel JJ. The Structure and Function Of The Hemagglutinin Membrane Glycoprotein Of Influenza Virus. Biochemistry 1987;56:365–94.

[82] Nishiyama N, Arnida, Jang W-D, Date K, Miyata K, Kataoka K. Photochemical enhancement of transgene expression by polymeric micelles incorporating plasmid DNA and dendrimer-based photosensitizer. J Drug Target 2006;14:413–24.

[83] Prasmickaite L, Høgset a, Berg K. Evaluation of different photosensitizers for use in photochemical gene transfection. Photochem Photobiol 2001;73:388–95.

[84] Berg K, Selbo PK, Prasmickaite L, Tjelle TE, Sandvig K, Moan J, et al. Photochemical internalization : a novel technology for delivery of macromolecules into cytosol. Cancer Res 1999;59:1180–3.

[85] Moreira C, Oliveira H, Pires LR, Simões S, Barbosa M a, Pêgo a P. Improving chitosan-mediated gene transfer by the introduction of intracellular buffering moieties into the chitosan backbone. Acta Biomater 2009;5:2995–3006.

[86] Pack DW, Putnam D, Langer R. Design of imidazole-containing endosomolytic biopolymers for gene delivery. Biotechnol Bioeng 2000;67:217–23.

[87] Jenssen H, Hamill P, Hancock REW. Peptide antimicrobial agents. Clin Microbiol Rev 2006;19:491–511.

[88] Kim WJ, Kim SW. Efficient siRNA delivery with non-viral polymeric vehicles. Pharm Res 2009;26:657–66.

[89] Whitehead K a, Langer R, Anderson DG. Knocking down barriers: advances in siRNA delivery. Nat Rev Drug Discov 2009;8:129–38.

[90] Yao Y, Wang C, Varshney RR, Wang D-A. Antisense makes sense in engineered regenerative medicine. Pharm Res 2009;26:263–75.

[91] Saghir Akhtar IFB. Nonviral delivery of synthetic siRNAs in vivo. J Clin Inverstigation 2007;117:3623–32.

[92] Krebs MD, Alsberg E. Localized, targeted, and sustained siRNA delivery. Chemistry 2011;17:3054–62.

[93] Monaghan M, Pandit A. RNA interference therapy via functionalized scaffolds. Adv Drug Deliv Rev 2011;63:197–208.

[94] Krebs MD, Jeon O, Alsberg E. Localized and sustained delivery of silencing RNA from macroscopic biopolymer hydrogels. J Am Chem Soc 2009;131:9204–6.

[95] Jafari M, Xu W, Naahidi S, Chen B, Chen P. A new amphipathic, amino-acid-pairing (AAP) peptide as siRNA delivery carrier: physicochemical characterization and in vitro uptake. J Phys Chem B 2012;116:13183–91.

[96] Reithmeier R a F. Characterization and modeling of membrane proteins using sequence analysis. Curr Opin Struct Biol 1995;5:491–500.

[97] Von Heijne G. Membrane proteins: from sequence to structure. Annu Rev Biophys Biomol Struct 1994;23:167–92.

[98] Landolt-Marticorena C, Williams KA, Deber CM, Reithmeier RAF. Non-random distribution of amino acids in the transmembrane segments of human type I single span membrane proteins. J Mol Biol 1993;229:602–8.

[99] Yau WM, Wimley WC, Gawrisch K, White SH. The preference of tryptophan for membrane interfaces. Biochemistry 1998;37:14713–8.

[100] Zimenkov Y, Dublin SN, Ni R, Tu RS, Breedveld V, Apkarian RP, et al. Rational design of a reversible pH-responsive switch for peptide self-assembly. J Am Chem Soc 2006;128:6770–1.

[101] Lee ES, Oh KT, Kim D, Youn YS, Bae YH. Tumor pH-responsive flower-like micelles of poly(l-lactic acid)-b-poly(ethylene glycol)-b-poly(l-histidine). J Control Release 2007;123:19–26.

[102] Ladbury JE, Chowdhry BZ. Sensing the heat: the application of isothermal titration calorimetry to thermodynamic studies of biomolecular interactions. Chem Biol 1996;3:791–801.

[103] Pierce MM, Raman CS, Nall BT. Isothermal titration calorimetry of protein-protein interactions. Methods 1999;19:213–21.

[104] Lehto T, Simonson OE, Mäger I, Ezzat K, Sork H, Copolovici D-M, et al. A peptide-based vector for efficient gene transfer in vitro and in vivo. Mol Ther 2011;19:1457–67.

[105] Conner SD, Schmid SL. Regulated portals of entry into the cell. Nat 2003;422:37–44.

[106] Pujals S, Fernández-Carneado J, López-Iglesias C, Kogan MJ, Giralt E. Mechanistic aspects of CPP-mediated intracellular drug delivery: relevance of CPP self-assembly. Biochim Biophys Acta 2006;1758:264–79.

[107] Veldhoen S, Laufer SD, Trampe A, Restle T. Cellular delivery of small interfering RNA by a non-covalently attached cell-penetrating peptide: quantitative analysis of uptake and biological effect. Nucleic Acids Res 2006;34:6561–73.

[108] Samir, El-andaloussi, Henrik, J.Johansson, Potus, Lundberg, Ulo L. Induction of splice correction by cell-penetrating peptide nucleic acids. J Gene Med 2006;8:1262–73.

[109] Wadia JS, Stan R V, Dowdy SF. Transducible TAT-HA fusogenic peptide enhances escape of TAT-fusion proteins after lipid raft macropinocytosis. Nat Med 2004;10:310–5.

[110] Xu W, Pan R, Zhao D, Chu D, Wu Y, Wang R, et al. Design and Evaluation of Endosomolytic Biocompatible Peptides as Carriers for siRNA Delivery. Mol Pharm 2015;12:56–65.

[111] Whitehead KA, Langer R, Anderson DG. Knocking down barriers: advances in siRNA delivery. Pharm Res 2009;26:129–38.

[112] Hannon GJ. RNA interference. Nat 2002;418:24–6.

[113] Wagner E. Biomaterials in RNAi therapeutics: quo vadis? Biomater Sci 2013;1:804–9.

[114] Elbashir SM, Harborth J, Lendeckel W, Yalcin A, Weber K, Tuschl T. Duplexes of 21-nucleotide RNAs mediate RNA interference in cultured mammalian cells. Nat 2001;411:494–8.

[115] Behlke M a. Progress towards in vivo use of siRNAs. Mol Ther 2006;13:644–70.

[116] Sung M, Poon GMK, Gariépy J. The importance of valency in enhancing the import and cell routing potential of protein transduction domain-containing molecules. Biochim Biophys Acta 2006;1758:355–63.

[117] Lindgren M, Hällbrink M, Prochiantz a, Langel U. Cell-penetrating peptides. Trends Pharmacol Sci 2000;21:99–103.

[118] Dietz GPH, Bähr M. Delivery of bioactive molecules into the cell: the Trojan horse approach. Mol Cell Neurosci 2004;27:85–131.

[119] Snyder EL, Dowdy SF. Recent advances in the use of protein transduction domains for the delivery of peptides, proteins and nucleic acids in vivo. Expert Opin Drug Deliv 2005;2:43–51.

[120] Chan DI, Prenner EJ, Vogel HJ. Tryptophan- and arginine-rich antimicrobial peptides: structures and mechanisms of action. Biochim Biophys Acta 2006;1758:1184–202.

[121] Ohmori N, Niidome T, Kiyota T, Lee S, Sugihara G, Wada A, et al. Importance of hydrophobic region in amphiphilic structures of a-helical peptides for their gene transfer-ability into cells. Biochem Biophys Res Commun 1998;245:259–65.

[122] Nyunt MT, Dicus CW, Cui Y-Y, Yappert MC, Huser TR, Nantz MH, et al. Physico-chemical characterization of polylipid nanoparticles for gene delivery to the liver. Bioconjug Chem 2009;20:2047–54.

[123] Bishop NE. An update on non-clathrin-coated endocytosis. Med Virol 1997;7:199–209.

[124] Oupický D, Carlisle RC, Seymour LW. Triggered intracellular activation of disulfide crosslinked polyelectrolyte gene delivery complexes with extended systemic circulation in vivo. Gene Ther 2001;8:713–24.

[125] Convertine AJ, Benoit DSW, Duvall CL, Hoffman AS, Stayton PS. Development of a novel endosomolytic diblock copolymer for siRNA delivery. J Control Release 2009;133:221–9.

[126] Grayson ACR, Doody AM, Putnam D. Biophysical and structural characterization of polyethylenimine-mediated siRNA delivery in vitro. Pharm Res 2006;23:1868–76.

[127] Ziegler A, Seelig J. Binding and clustering of glycosaminoglycans: a common property of mono- and multivalent cell-penetrating compounds. Biophys J 2008;94:2142–9.

[128] Ezzat K, Helmfors H, Tudoran O, Juks C, Lindberg S, Padari K, et al. Scavenger receptor-mediated uptake of cell-penetrating peptide nanocomplexes with oligonucleotides. FASEB J 2012;26:1172–80.

[129] Jafari M, Karunaratne DN, Sweeting CM, Chen P. Modification of a designed amphipathic cell-penetrating peptide and its effect on solubility, secondary structure, and uptake efficiency. Biochemistry 2013;52:3428–35.

[130] Kawasaki H. Short hairpin type of dsRNAs that are controlled by tRNAVal promoter significantly induce RNAi-mediated gene silencing in the cytoplasm of human cells. Nucleic Acids Res 2003;31:700–7.

[131] Billy E, Brondani V, Zhang H, Müller U, Filipowicz W. Specific interference with gene expression induced by long, double-stranded RNA in mouse embryonal teratocarcinoma cell lines. Proc Natl Acad Sci U S A 2001;98:14428–33.

[132] Zeng Y, Cullen BR. RNA interference in human cells is restricted to the cytoplasm. RNA 2002;8:855–60.

[133] Mäe M, Andaloussi S El, Lehto T, Langel U. Chemically modified cell-penetrating peptides for the delivery of nucleic acids. Expert Opin Drug Deliv 2009;6:1195–205.

[134] Dass CR, Walker TL, Burton MA. Liposomes containing cationic dimethyl dioctadecyl ammonium bromide: formulation , quality control , and lipofection efficiency. Drug Deliv 2002;9:11–8.

[135] Van Asbeck AH, Beyerle A, McNeill H, Bovee-Geurts PHM, Lindberg S, Verdurmen WPR, et al. Molecular parameters of siRNA-cell penetrating peptide nanocomplexes for efficient cellular delivery. ACS Nano 2013;7:3797–807.

[136] Simeoni F, Morris MC, Heitz F, Divita G. Insight into the mechanism of the peptide-based gene delivery system MPG: Implications for delivery of siRNA into mammalian cells. Nucleic Acids Res 2003;31:2717–24.

[137] Veldhoen S, Laufer SD, Trampe A, Restle T. Cellular delivery of small interfering RNA by a non-covalently attached cell-penetrating peptide: Quantitative analysis of uptake and biological effect. Nucleic Acids Res 2006;34:6561–73.

[138] Crombez L, Aldrian-Herrada G, Konate K, Nguyen QN, McMaster GK, Brasseur R, et al. A new potent secondary amphipathic cell-penetrating peptide for siRNA delivery into mammalian cells. Mol Ther 2009;17:95–103.

[139] García-Sosa AT, Tulp I, Langel K, Langel Ü. Peptide-ligand binding modeling of siRNA with cell-penetrating peptides. Biomed Res Int 2014;Article ID:1–7.

[140] Elbashir SM, Harborth J, Lendeckel W, Yalcin A, Weber K, Tuschl T. Duplexes of 21 - nucleotide RNAs mediate RNA interference in cultured mammalian cells. Nat 2001;411:494–9.

[141] Jain KK. Drug delivery systems - an overview. Drug Deliv. Syst., 2008, p. 1–50.

[142] Mark SW. Drug delivery: engineering principles for drug therapy. 2001.

[143] Torchilin VP. Passive and active drug targeting: drug delivery to tumors as an example. Drug Deliv., 2010, p. 3–54.

[144] Karunaratne D. Nedra, Silverstein Peter S., Vasandani Veena, Young Amber M., Rytting Erik, Yops Bradley AKL. Cell culture models for drug transport studies. Drug Deliv. Princ. Appl., 2005, p. 103–24.

[145] J.W. H. 3D cell culture: a review of current approaches and techniques. Methods Mol Biol 2011;695:1–15.

[146] Mehta G, Hsiao AY, Ingram M, Luker GD, Takayama S. Opportunities and challenges for use of tumor spheroids as models to test drug delivery and efficacy. J Control Release 2012;164:192–204.

[147] Tung Y-C, Hsiao AY, Allen SG, Torisawa Y, Ho M, Takayama S. High-throughput 3D spheroid culture and drug testing using a 384 hanging drop array. Analyst 2011;136:473–8.

[148] Hsiao Amy Y., Tung Yi-Chung, Kuo Chuan-Hsien, Mosadegh Bobak, Bedenis Rachel, Pienta Kenneth J. TS. Micro-ring structures stabilize microdroplets to enable long term spheroid culture in 384 hanging drop array plates. Biomed Mircrodevices 2012;29:997–1003.

[149] Hsiao AY, Tung YC, Qu X, Patel LR, Pienta KJ, Takayama S. 384 hanging drop arrays give excellent Z-factors and allow versatile formation of co-culture spheroids. Biotechnol Bioeng 2012;109:1293–304.

[150] Ho WY, Yeap SK, Ho CL, Rahim RA, Alitheen NB. Development of multicellular tumor spheroid (MCTS) culture from breast cancer cell and a high throughput screening method using the MTT assay. PLoS One 2012;7:e44640.

[151] Jorgen C, Helmut A. Relations between pH , oxygen partial pressure and growth in cultured cell spheroids. Int J Cancer 1988;42:715–20.

[152] Rosai J, Ackerman L V. The pathology of tumors part II : diagnostic techniques. CA Cancer J Clin 1979;29:22–39.

[153] Judah F. Tumor aniogenesis: a possible control point in tumor growth. Ann Intern Med 1975;82:96–100.

[154] Ma H, Jiang Q, Han S, Wu Y, Tomshine JC, Wang D, et al. Multicellular tumor spheroids as an in vivo – like tumor model for three-dimensional imaging of chemotherapeutic and nano material cellular penetration. Mol Imaging 2012;11:487–98.

[155] Kim B, Han G, Toley BJ, Kim C-K, Rotello VM, Forbes NS. Tuning payload delivery in tumour cylindroids using gold nanoparticles. Nat Nanotechnol 2010;5:465–72.

[156] Carver K, Ming X, Juliano RL. Multicellular tumor spheroids as a model for assessing delivery of oligonucleotides in three dimensions. Mol Ther Nucleic Acids 2014;3:e153.

[157] Konishi M, Kawamoto K, Izumikawa M, Kuriyama H, Yamashita T. Gene transfer into guinea pig cochlea using adeno-associated virus vectors. J Gene Med 2008;10:610–8.

[158] Tang L, Gabrielson NP, Uckun FM, Fan TM, Cheng J. Size-dependent tumor penetration and in vivo efficacy of monodisperse drug-silica nanoconjugates. Mol Pharm 2013;10:883–92.

[159] Popović Z, Liu W, Chauhan VP, Lee J, Wong C, Greytak AB, et al. A nanoparticle size series for in vivo fluorescence imaging. Angew Chem Int Ed Engl 2010;49:8649–52.

[160] Xu Shuyun, Bian Rulian CX. 药理实验方法学. 2002.

[161] McManus MT, Sharp P a. Gene silencing in mammals by small interfering RNAs. Nat Rev Genet 2002;3:737–47.

[162] Hannon GJ, Rossi JJ. Unlocking the potential of the human genome with RNA interference. Nat 2004;431:371–8.

[163] Caplen NJ, Parrish S, Imani F, Fire a, Morgan R a. Specific inhibition of gene expression by small double-stranded RNAs in invertebrate and vertebrate systems. Proc Natl Acad Sci U S A 2001;98:9742–7.

[164] Verma UN, Surabhi RM, Schmaltieg A, Becerra C, Gaynor RB. Small Interfering RNAs Directed against β -Catenin Inhibit the in Vitro and in Vivo Growth of Colon Cancer Cells. J Clin Cancer Res 2003;9:1291–300.

[165] Soutschek J, Akinc A, Bramlage B, Charisse K, Constien R, Donoghue M, et al. Therapeutic silencing of an endogenous gene by systemic administration of modified siRNAs. Nat 2004;432:173–8.

[166] Oliveira, S., Storm, G., Schiffelers RM. Targeted delivery of siRNA. J Biomed Biotechnol 2006;2006:1–9.

[167] Mok H, Park TG. Self-crosslinked and reducible fusogenic peptides for intracellular delivery of siRNA. Biopolymers 2008;89:881–8.

[168] Kim SH, Mok H, Jeong JH, Kim SW, Park TG. Comparative evaluation of target-specific GFP gene silencing efficiencies for antisense ODN, synthetic siRNA, and siRNA plasmid complexed with PEI-PEG-FOL conjugate. Bioconjug Chem 2006;17:241–4.

[169] Urban-Klein B, Werth S, Abuharbeid S, Czubayko F, Aigner a. RNAi-mediated gene-targeting through systemic application of polyethylenimine (PEI)-complexed siRNA in vivo. Gene Ther 2005;12:461–6.

[170] Landen CN, Chavez-Reyes A, Bucana C, Schmandt R, Deavers MT, Lopez-Berestein G, et al. Therapeutic EphA2 gene targeting in vivo using neutral liposomal small interfering RNA delivery. Cancer Res 2005;65:6910–8.

[171] Zimmermann TS, Lee ACH, Akinc A, Bramlage B, Bumcrot D, Fedoruk MN, et al. RNAi-mediated gene silencing in non-human primates. Nat 2006;441:111–4.

[172] Santel a, Aleku M, Keil O, Endruschat J, Esche V, Durieux B, et al. RNA interference in the mouse vascular endothelium by systemic administration of siRNA-lipoplexes for cancer therapy. Gene Ther 2006;13:1360–70.

[173] Yano J, Hirabayashi K, Nakagawa S, Yamaguchi T, Nogawa M, Kashimori I, et al. Antitumor Activity of Small Interfering RNA / Cationic Liposome Complex in Mouse Models of Cancer Antitumor Activity of Small Interfering RNA / Cationic Liposome Complex in Mouse Models of Cancer. Clin Cancer Res 2004;10:7721–6.

[174] Grimm D, Streetz KL, Jopling CL, Storm T a, Pandey K, Davis CR, et al. Fatality in mice due to oversaturation of cellular microRNA/short hairpin RNA pathways. Nat 2006;441:537–41.

[175] Jeong JH, Kim SW, Park TG. Molecular design of functional polymers for gene therapy. Prog Polym Sci 2007;32:1239–74.

[176] Dorsett Y, Tuschl T. siRNAs: applications in functional genomics and potential as therapeutics. Nat Rev Drug Discov 2004;3:318–29.

[177] Morris MC, Vidal P, Chaloin L, Heitz F, Divita G. A new peptide vector for efficient delivery of oligonucleotides into mammalian cells. Nucleic Acids Res 1997;25:2730–6.

[178] Simeoni F. Insight into the mechanism of the peptide-based gene delivery system MPG: implications for delivery of siRNA into mammalian cells. Nucleic Acids Res 2003;31:2717–24.

[179] Futaki S, Ohashi W, Suzuki T, Niwa M, Tanaka S, Ueda K, et al. Stearylated arginine-rich peptides: a new class of transfection systems. Bioconjug Chem 2001;12:1005–11.

[180] Tönges L, Lingor P, Egle R, Dietz GPH, Fahr A. Stearylated octaarginine and artificial virus-like particles for transfection of siRNA into primary rat neurons Stearylated octaarginine and artificial virus-like particles for transfection of siRNA into primary rat neurons. RNA 2006;12:1431–8.

[181] Mäe M, El Andaloussi S, Lundin P, Oskolkov N, Johansson HJ, Guterstam P, et al. A stearylated CPP for delivery of splice correcting oligonucleotides using a non-covalent co-incubation strategy. J Control Release 2009;134:221–7.

[182] El-Sayed A, Masuda T, Khalil I, Akita H, Harashima H. Enhanced gene expression by a novel stearylated INF7 peptide derivative through fusion independent endosomal escape. J Control Release 2009;138:160–7.

[183] Lehto T, Abes R, Oskolkov N, Suhorutsenko J, Copolovici D-M, Mäger I, et al. Delivery of nucleic acids with a stearylated (RxR)4 peptide using a non-covalent co-incubation strategy. J Control Release 2010;141:42–51.

[184] Wang H-Y, Chen J-X, Sun Y-X, Deng J-Z, Li C, Zhang X-Z, et al. Construction of cell penetrating peptide vectors with N-terminal stearylated nuclear localization signal for targeted delivery of DNA into the cell nuclei. J Control Release 2011;155:26–33.

[185] Veiman K-L, Mäger I, Ezzat K, Margus H, Lehto T, Langel K, et al. PepFect14 peptide vector for efficient gene delivery in cell cultures. Mol Pharm 2013;10:199–210.

[186] Alshamsan A, Haddadi A, Incani V, Samuel J, Lavasanifar A, Uludag H. Formulation and Delivery of siRNA by Oleic Acid and Stearic Acid Modified Polyethylenimine. Mol Pharm 2008;6:121–33.

[187] Hoyer JAN, Neundorf I. Peptide vectors for the nonviral delivery of nucleic acids. Acc Chem Res 2012;45:1048–56.

[188] Meyer M a. Malignant gliomas in adults. N Engl J Med 2008;359:494–507.

[189] Pulkkanen KJ, Yla-Herttuala S. Gene therapy for malignant glioma: current clinical status. Mol Ther 2005;12:585–98.

[190] Grimm D. Small silencing RNAs: state-of-the-art. Adv Drug Deliv Rev 2009;61:672–703.

[191] Judge AD, Bola G, Lee ACH, MacLachlan I. Design of noninflammatory synthetic siRNA mediating potent gene silencing in vivo. Mol Ther 2006;13:494–505.

[192] Jackson AL, Burchard J, Schelter J, Chau BN, Cleary M, Lim LEE, et al. Widespread siRNA off-target transcript silencing mediated by seed region sequence complementarity. RNA 2006;12:1179–87.

[193] Bolhassani A. Potential efficacy of cell-penetrating peptides for nucleic acid and drug delivery in cancer. Biochim Biophys Acta 2011;1816:232–46.

[194] Nakase I, Akita H, Kogure K, Graslund A, Langel Ü, Harashima H, et al. Efficient intracellular delivery of nucleic acid pharmaceuticals using cell-penetrating peptides. Acc Chem Res 2012;45:1132–9.

[195] Tönges L, Lingor P, Egle R, Dietz GPH, Fahr A. Stearylated octaarginine and artificial virus-like particles for transfection of siRNA into primary rat neurons. RNA 2006;12:1431–8.